UNIVERSITÉ DU QUÉBEC

THÈSE PRÉSENTÉE À
L'UNIVERSITÉ DU QUÉBEC À TROIS-RIVIÈRES

COMME EXIGENCE PARTIELLE
DU DOCTORAT EN BIOPHYSIQUE

PAR
MEIMEI GAO

REVERSIBILITY OF ANESTHETIC-INDUCED CONFORMATIONAL AND FUNCTIONAL CHANGES IN THE PURPLE MEMBRANE

MARCH 2004

ACKNOWLEDGEMENTS

First, I wish to thank Mr. Claude Gicquaud for allowing me to use the Differential Scanning Calorimeter. Next, my special thanks goes to Dr. Nathalie Hauet of the Université Paris XI for her X-ray diffraction measurements.

I also wish to thank my laboratory colleagues – Michel Déry, Bandoin Normand, Nathalie Hauet, Isabelle Cloutier and Danny Létournant – for their generous assistance.

Finally, I am deeply grateful to Mr. François Boucher, my advisor, for stimulating discussions, helpful suggestions and, most of all, his enthusiastic support for this project.

Résumé

La bactériorhodopsine est une pompe à proton de nature protéique qui utilise son chromophore rétinien pour convertir le rayonnement électromagnétique en gradient électrochimique de protons. Le siège de cette activité est la membrane pourpre de certaines bactéries halophiles du genre *Halobacterium*. Cette membrane spécialisée tient son nom de la couleur qui lui est conférée par sa grande concentration de bactériorhodopsine. L'état natif de la bactériorhodopsine étant un réseau hexagonal de trimères, la membrane pourpre est donc un cristal bidimensionnel dont la taille peut atteindre le micromètre.

L'introduction d'anesthésiques généraux halogénés volatils dans la membrane pourpre induit l'apparition d'un équilibre acido-basique entre deux formes de bactériorhodopsine. Ainsi, en présence de différentes molécules appartenant à cette famille de xénobiotiques, comme l'enflurane, le maximum d'absorption de la bactériorhodopsine passe réversiblement de 570 à 480 nm. Cette transition spectrale réversible (bR_{570} $\Leftrightarrow$ bR_{480}) est accompagnée de transitions structurales et fonctionnelles qui, elles, ne sont pas forcément réversibles. La précision du caractère irréversible de changements induits par les anesthésiques dans ces membranes constitue l'objet de cette thèse.

La transition spectrale induite par la présence des anesthésiques possède une forte coopérativité. Toutefois, les concentrations d'anesthésiques requises pour induire la transition dépendent de l'histoire de l'échantillon. Selon toute vraisemblance, il est impossible de retirer les traces restantes d'anesthésique d'un échantillon préalablement traité par ces derniers, en dépit de leur grande volatilité. Un comportement identique, tant du point de vue de l'équilibre des formes spectrales que de la dépendance du pH, est observé quand, au lieu de traiter un échantillon avec un anesthésique, on le soumet à des températures supérieures à 70 °C. Les anesthésiques induisent donc, à la température de la pièce, une transition qui, autrement ne se produirait qu'à des températures beaucoup plus élevées. L'analyse de ce

phénomène par calorimétrie différentielle à balayage indique qu'une modification irréversible du réseau cristallin serait en jeu.

Les anesthésiques inhibent complètement l'activité de pompage de protons par la bactériorhodopsine et ils modifient la cinétique de son cycle photochimique. Nos mesures en photolyse éclair indiquent que la forme bR_{480} de la bactériorhodopsine se caractérise par une accélération de l'étape de déprotonation du chromophore (déclenchement du pompage de proton) et un ralentissement de sa reprotonation. Dépendant de la quantité d'anesthésique ajouté aux échantillons, ces modifications peuvent être importantes; cependant, elles conservent toutes un caractère d'irréversibilité, petit mais significatif, qui, lui, est indépendant de la quantité d'anesthésique ajouté.

Par ailleurs, nous avons examiné la modification structurale des membranes par plusieurs de méthodes physiques. Ainsi, on a pu observer qu'en présence d'anesthésique, la structure quaternaire de la bactériorhodopsine passait réversiblement de la forme trimère à la forme monomère, à en juger par les spectres de dichroïsme circulaire. Les indications d'altération possible de la structure cristalline qui nous venaient des mesures en calorimétrie différentielle ont été confirmées par diffraction des rayons X. En fait, les anesthésiques détruisent complètement et irréversiblement le réseau hexagonal cristallin de la bactériorhodopsine. Toutefois, l'analyse des mêmes membranes par microscopie à force atomique montre clairement que si la cristallinité originale est perdue, il persiste néanmoins un certain degré d'organisation des trimères de bactériorhodopsine.

Du point de vue de la structure secondaire, des mesures d'échange isotopique et de spectroscopie FTIR révèlent des modifications mineures mais réversibles. Ces changements surviennent surtout autour des groupements CH_3 des chaînes carbonées des lipides.

Enfin, nous avons aussi réalisé des expériences avec un modèle plus simple: des vésicules lipidiques de dipalmitoyl phosphatidyl choline. Elles confirment le caractère irréversible et l'énergie importante des interactions entre les anesthésiques généraux et certaines régions de la membrane, notamment la partie immédiatement adjacente aux têtes polaires des lipides. Ces dernières mesures appuient ainsi nos conclusions quant à la force d'interaction particulière des anesthésiques avec les régions des architectures macromoléculaires qui possèdent un fort gradient de polarité.

ABSTRACT

Bacteriorhodopsin, a retinal protein, is a light-activated proton pump that converts directly electromagnetic energy into electrochemical energy. In its native form, it exists as a hexagonal array of protein trimers known as the purple membrane. Anesthetics induce a pH-dependent equilibrium between two spectral forms of bacteriorhodopsin. In the presence of the halogenated general anesthetic enflurane, the maximal absorption of bacteriorhodopsin reversibly changes from 570 nm to 480 nm. This is accompanied by a structural and functional transition. But, structural and functional changes of the purple membrane do not recover completely. Irreversible effects are found, both in the structure of purple membranes and the photochemistry of proton pumping.

The absorption changes as a function of anesthetic concentration show a very strong cooperativity among the bacteriorhodopsin molecules. However the concentration that induces absorption transition depends on the history of the sample. Samples that have been treated with anesthetics may retain part of previously added anesthetics. Besides anesthetics, high temperatures (~70 °C) induce the same reversible pH-dependent absorption transition of bacteriorhodopsin. This suggests that anesthetics induce, at room temperature, a transition that otherwise, would only occur above 70 °C. Analysis of this phenomenon by calorimetry indicates that this transition is strongly related to the crystalline array.

Anesthetics inhibit the bR proton pumping activity and change the kinetics of the bR photocycle. The photocycle of bR_{480} is characterized by a fast deprotonation and a slow reprotonation of its chromophore, corresponding to a fast rise and a slow decay of its intermediate M. The decay of intermediate M is split into two components, a fast one and a slow one, which can be detected even in the presence of a very small amount of anesthetic. Comparing the decay of intermediate M in the presence of different concentrations of anesthetics to that of the native bR, we find that bR photochemistry does not

completely recover after anesthetic-treatment and that the remaining effect of anesthetic is not due to an excess amount added to the sample.

The structure of purple membranes was also examined by several physical techniques. Circular dichroism spectroscopy of the purple membrane in the presence of anesthetics shows that bR trimers change to monomers. After removal of anesthetics, most of bR monomers recover their trimeric structure. Differential scanning calorimetry measurement indicates lost of organization of the crystalline lattice, while x-ray diffraction and atomic force microscopy reveal that the crystalline array is seriously damaged after anesthetic removal from the sample.

On the other hand, bR secondary and tertiary structures were examined by Fourier transform infrared spectroscopy. The changes of bR secondary structure are very small and reversible but the change in the lipid seems not to be completely reversible. The asymmetric bands corresponding to CH_3 groups prove that. In addition, H/D exchange measurements show that the change of bR tertiary structure occurs at the surface region of the membrane.

Experiments with simple DPPC lipid membranes provide additional evidence that the effect of anesthetics at the surface of the membrane is not as easily removed as that in the core of the membrane. We thus conclude that the irreversible effect of anesthetics, namely the irreversible modification of the crystal array may be due to strong interactions of anesthetics and polar groups of the membrane surface.

CONTENTS

TABLES

FIGURES

ABBREVIATIONS

PM: purple membrane

bR: bacteriorhodopsin

CD: circular dichroism

DSC: differential scanning calorimetry

AFM: atomic force microscopy

FTIR: Fourier transform infrared spectroscopy

DPPC: dipalmitoylphosphatidylcholine

MAC: minimum alveolar concentration

CHAPTER 1

INTRODUCTION

Anesthetics are drugs that induce loss of sensation and usually consciousness without loss of vital functions. In 1769, an English chemist named Joseph Priestley discovered the first recognized anesthetic, nitrous oxide. It wasn't until 1844 that nitrous oxide was first put to use during a dentistry procedure by an American dentist, Horace Wells. Since that time, the number and popularity of anesthetics have increased. Of these, a general anesthetic is that which causes a complete loss of sensation and consciousness and mainly affects synaptic transmission. Thus, analysis of their effects has been focused on nerve membranes and, in particular, neuronal ligand-gated ion channels such as glutamate receptors, nicotinic acetylcholine receptors (nAchR) and $GABA_A$ receptors.

The next issue is where general anesthetics are located in these receptors to change the function of the ion channels. At the molecular level, it is not known whether anesthetics act on the membranes of neural cells through the lipid phase, the protein phase or the lipid-protein interface. The answer remains unclear because the structures of these receptors are too complicated to determine the molecular events involved in the presence of commonly used anesthetics. Other systems are used in research, including water-soluble proteins and lipid bilayers. Researches on these models provide additional information on the relationship between anesthetics with proteins and the changes in the character of lipid bilayers. These models, however, cannot represent the complete structure of membranous ligand-gated ion channels. Recently, the purple membrane of halobacterium was used in this kind of research. Its structure is simple and well documented.

To better understand why purple membranes were chosen to study the mechanism of action of anesthetics, we will return to the structure of the ligand-gated ion channels in the nerve membrane, the

hypothesis on the mechanism of action of general anesthetics, the structure and function of the purple membrane, as well as the effects of general anesthetics on the purple membrane.

1.1 COMMON MOLECULAR ARCHITECTURES OF EXCITABLE MEMBRANES

Excitable membranes are those able to change their potential rapidly in response to a stimulus. They are located in the nerve membranes and muscle membranes in which the ligand-gated ion channels are found. Stimuli may be electrical or chemical, such as neurotransmitters in the nerve system. When a neurotransmitter molecule binds to the receptor, the channel opens. An ion-flow across the membrane produces a rapid change in the membrane potential. The nicotinic acetylcholine receptor (nAchR) is the most thoroughly studied receptor, because it is easy to obtain in large amounts and its role in the central nervous system is well understood. The nAChR shares several structural and functional properties with other ligand-gated ion channel receptors, namely the γ-aminobutyric acid ($GABA_A$ and $GABA_C$ type), the glycine, and the 5-hydroxytryptane (5-HT3 type) receptor[1, 2, 3]. The receptors consist of five subunits: 2α, β, δ, γ. Each receptor subunit crosses the lipid membrane four times, forming the transmembrane (hydrophobic) domain M1-M4 (Fig. 1.1). The M2 sequences from each subunit combine to form the wall of the receptor-associated ion channel. In cation-selective channels, the M2 sequences contain negatively charged residues, whereas residues in the M2 sequences in anion-selective channels are positively charged. The other transmembrane domains of the AChR, M1, M3, and M4, have been shown to be in close contact with the lipid phase.

With respect to the surface of the nAChR in intimate contact with the lipid binding regions, two well-differentiated lipid-binding regions have been identified - the annular lipid domain and the non-annular lipid domain[4]. The annular lipid domain is surrounded by a lipid belt abutting the intramembranous perimeter of the nAChR[5, 6]. The non-annular lipid binding sites are close to the hydrophilic portions[7]. It is

evident that structural analysis of changes in such a complex structure upon addition of anesthetics is very difficult since the desensitization[8] that they induce may be mediated by subtle structural modifications.

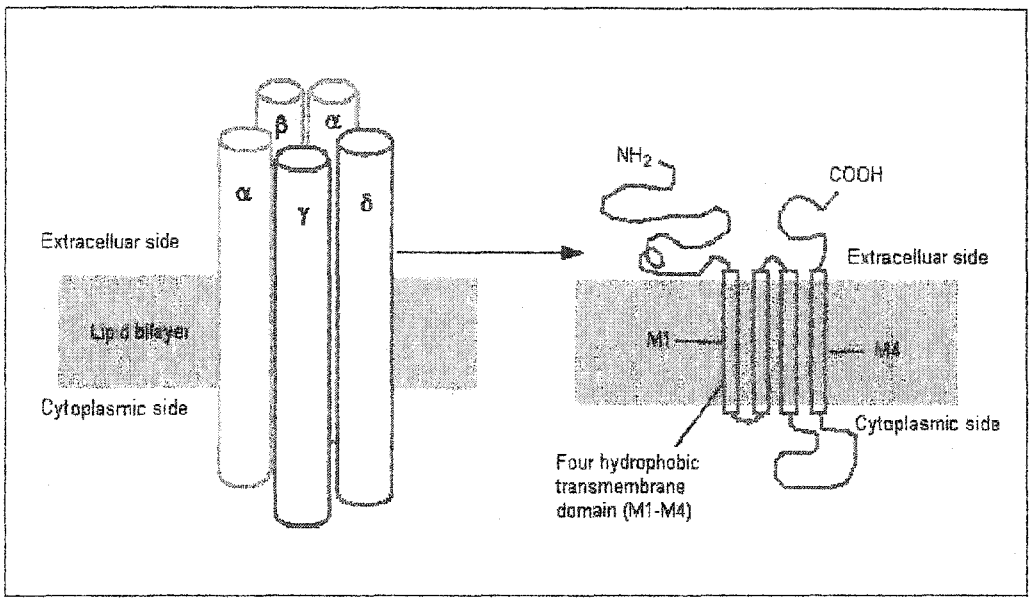

Figure 1. 1 Diagram of the nicotinic acetylcholine receptor. The receptor consists of five subunits, 2α. β, δ, γ (left). Four transmembrane (hydrophobic) domains M1-M4 of each subunit are embedded in the lipid bilayer (right). The N- and C- termini are located in the extracellular side.

1.2 POSSIBLE MECHANISMS OF ACTION OF ANESTHETICS IN EXCITABLE MEMBRANES

An anesthetic blocks a receptor-associated ion channel reaction towards a stimulus, causing anesthesia. A wide variety of substances may induce anesthesia; these range from aliphatic hydrocarbons to alcohols, ethers, and halogenated compounds. They lack common chemical structures except for the fact that they are all more or less hydrophobic molecules. Such a large amount of chemicals with different structures makes it difficult to understand their mechanism of action from their structural properties.

Despite many investigations, the action site of anesthetics on the membrane has not been ascertained. Two opposing mechanisms have been proposed to account for the action of anesthetics on their target membranes: the first involves an alteration of the phospholipid bilayer properties by these agents, resulting in a modulation of membrane protein function while the second is based on a direct interaction between anesthetics and membrane proteins[9, 10]. The lipid mechanism was based originally on the observation that there is a direct correlation between anesthetic potency and the solubility of an anesthetic in the lipid bilayer (Fig. 1.2).

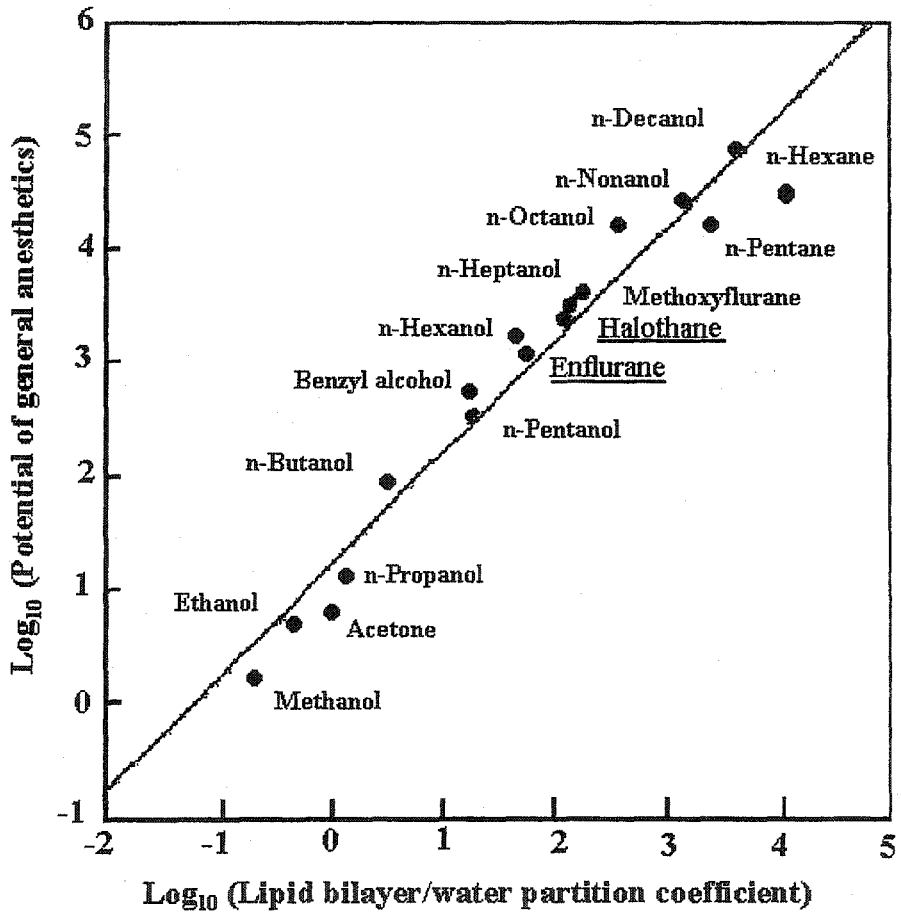

Figure 1. 2 Log-log plot of the potential of general anesthetics and their lipid bilayer/water partition coefficient.

At the turn of the 20th century, Meyer[11] and Overton[12] independently observed that the anesthetic potency of general anesthetics correlates with their solubility in a solvent representing the hydrophobic interior of the cell membrane. For example, when we compare enflurane and halothane, two common inhalational general anesthetics, we find that halothane, with a shorter hydrocarbon chain, is more soluble in the lipid membrane and that it is also more potent as an anesthetic (Fig. 1.3).

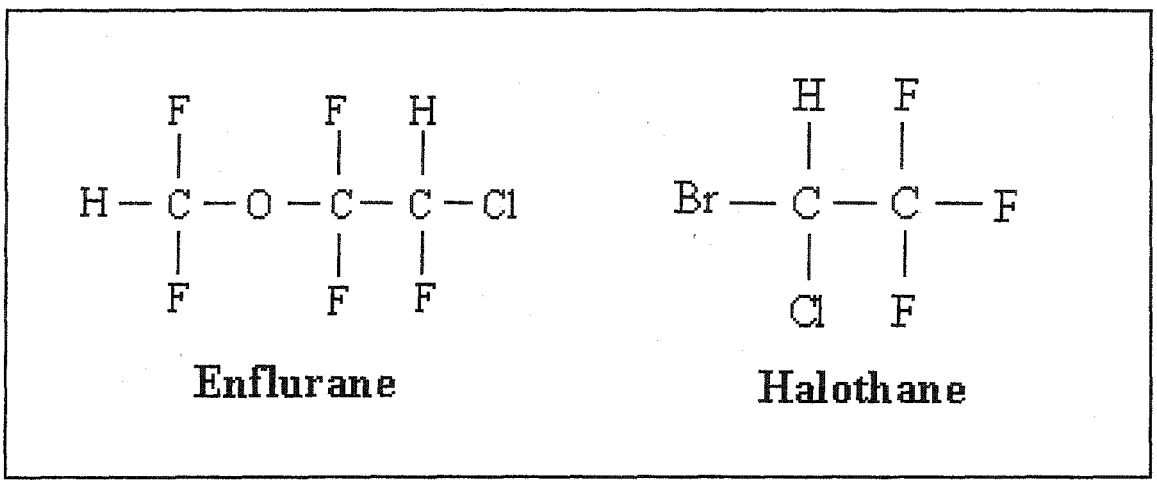

Figure 1. 3 Molecular structures of enflurane and halothane.

The theories derived from the Meyer-Overton rule, which localizes the primary target of anesthetics in the lipid part of the membrane, explain the molecular mechanism of anesthetics by an effect on lipid fluidity or its phase transition[13]. The membrane fluidity measured by probe molecules represents the property of the microenvironment where the probe molecules reside. The depression in phase transition temperature indicates a transition from solid-gel domains to the liquid-crystal structure. Applying high pressure on the lipid system may reverse the effects of anesthetics by recovery of the membrane order[14]. However, lipid bilayer theories have two weaknesses: membrane perturbations are relatively small at

clinical anesthetic concentrations, which can often be duplicated by small variations in different properties (e. g., a temperature increase of 1 °C) that do not induce anesthesia[15]. Exceptions such as the cutoff in the potency for long n-alkanols as well as the anomalously low potency of perfluorinated hydrocarbons and the lighter inert gases also remain unexplained[16, 17, 18].

Specific binding to a receptor protein has been suggested to replace the traditional concept of nonspecificity of the anesthetic action on the lipid part of the membrane[19, 20, 21]. The principal findings in support of this theory affirm that 1) the photon emission from firefly luciferase, a water-soluble protein, can be inhibited by a variety of general anesthetics at their respective clinical concentration[16], 2) some important ligand-gated ion channels, e.g., nicotinic acetylcholine (Ach) receptors[22], and γ-aminobutyric acid ($GABA_A$) receptors[23], are sensitive to volatile anesthetics at clinical concentrations, and 3) bovine serum albumin (BSA), another water-soluble protein, contains a limited number of saturable binding sites for volatile anesthetics such as halothane and isoflurane[24].

There are three ways in which anesthetics may bind to proteins: 1) General anesthetics may compete with endogenous ligands for a receptor site. According to this postulate, general anesthetics bind to a recognition site on a receptor and thereby competitively interfere with the binding of an endogenous neurotransmitter or, alternatively, mimic the effect of the transmitter; 2) General anesthetics may bind to nonannular hydrophobic domains in membrane proteins. In this case general anesthetics bind to a receptor protein in a position that is allosteric to the agonist recognition site. These allosteric sites are selective in that they are inaccessible to membrane phospholipids. They may be embedded in the lipid domain, or they may be in nonmembranous protein segments directly in contact with the aqueous phase. 3) The third possible binding site of general anesthetics is associated with the protein – lipid interface. This postulated site is related to the lipid bilayer site. Rather than changing a macroscopic property of the bilayer, however, anesthetics would associate with the protein – lipid domain and interfere with localized interactions

between annular lipids and proteins that are crucial for protein function. Thus, minor effects of the lipid bilayer may translate into physiologically significant changes at the protein – lipid interface [25, 26].

Anesthetics have been used for almost 150 years, and many hypotheses have been proposed for elucidating the mechanisms by which they act on excitable membranes. This is in part because a diversity of chemical materials may cause anesthesia, but also because a variety of models are used in research. Models are too simple to represent an entire excitable membrane with proteins and lipids. However, a membrane containing ion channels or receptors involves too many events and prevents researchers from identifying actual anesthetic effects during signal transmission and ion transportation.

1.3 JUSTIFICATION OF THE EXPERIMENTAL MODEL

Ligand-gated ionic channels isolated from some part of the nervous system are used as models for researches on the mechanism of action of anesthetics, since that they are likely sites of anesthetic action. The purple membrane is a bacterial membrane functioning as a proton pump. At first glance, it may not appear a relevant model for studying the molecular mechanism of anesthetics, since a bacterial membrane cannot be compared to a nerve membrane. To justify the use of the purple membrane as a relevant model, one should first examine its structure and reaction to anesthetics.

Bacteriorhodopsin, bR, in the purple membrane is the smallest and best-characterized transmembrane protein, from its primary to quaternary structure[27]. It is a one-peptide-chain protein, but it has a structure similar to that of the receptor-associated ion channel in the nerve membrane. In the lipid bilayer, bR is coiled into α-helices, forming a channel. The α-helices are connected by loops and β-structure at both sides of the membrane - cytoplasmic and extracellular. Bacteriorhodopsin works like an ion channel. By absorbing a photon, bacteriorhodopsin transfers a proton from the inside to outside of the membrane, producing a change in the membrane potential. Such a simple, well-defined system enables us to detect

small structural changes occurring in the protein and lipids by means of different physical and chemical techniques, and to obtain information that cannot easily be found on more complicated systems.

The purple membrane is widely used in the researches on energy transduction, membrane transport, protein folding and stabilization, and dynamic simulation[28, 29, 30, 31], because it is easily obtained in a very pure form. The special relationship between bacteriorhodopsin and the surrounding lipids [32] clearly shows how the function and conformation of the protein depend on the lipid properties[33, 34].

The first research on the effects of anesthetics on the purple membrane dated from 1985. Nishimura et al. [35] measured the absorption spectrum and circular dichroism spectrum of purple membranes with the general anesthetics halothane, enflurane and methoxyflurane. Results indicated that volatile anesthetics act directly on the bacteriorhodopsin and induce changes in its conformation. Indeed, general anesthetics shift the absorption band of bR from 570 to 480 nm. This effect of halogenated anesthetics on the spectrum of purple membranes is reversed under high pressure, as has already been observed on models generally used in the researches on the mechanism of anesthesia. In 1993, Messaoudi et al.[36] observed the effects of several solvents sharing few chemical properties on the spectral forms of the purple membrane. They estimated the extent of the transition from bR_{570} to bR_{480} as a function of organic solvent concentration, the latter being expressed as its molar ratio to bacteriorhodopsin (solvent:bR). In the case of ethanol, half spectral transition is attained when the ethanol:bR ratio is approximately 50 000. Other solvents such as methanol, propanol, butanol and acetone, as well as the general anesthetics, enflurane and halothane were shown to induce this spectral shift. The amount of these chemical agents required to complete the transition decreases with the water miscibility. Figure 1.4 shows a log-log plot of the molar ratio needed to convert half of the bR570 to bR480 as a function of the lipid/buffer partition coefficients of the solvents. The linear relation that is observed follows the Meyer-Overton rule, which predicts that the anesthetic potency of a given molecule directly correlates with its membrane solubility.

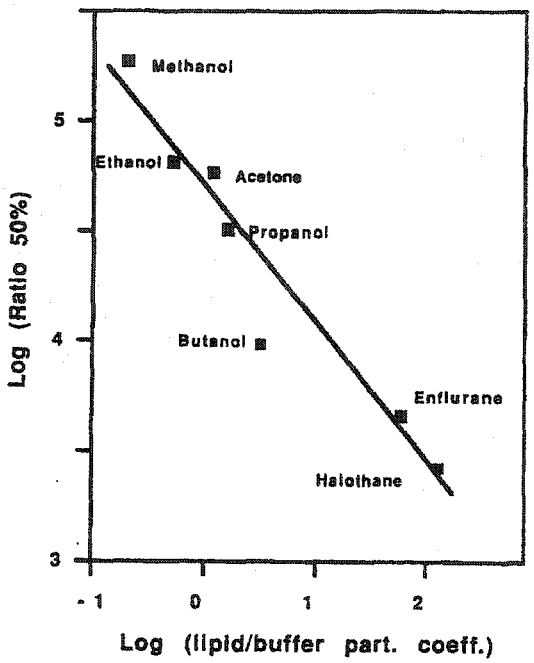

Figure 1. 4 Log-log plot of different solvents:bR molar ratios needed to convert half of the bR_{570} to bR_{480} (Ratio 50%) as a function of the lipid/buffer partition coefficient of the solvent (Messaoudi S[36]).

Additional researches on the interaction of general anesthetics and the structural and functional perturbation in the purple membrane[37] proved that the purple membrane is a good model for researches on the action mechanism of anesthetics.

1.4 DESCRIPTION OF THE EXPERIMENTAL MODEL

1.4.1 Halobacteria

Halobacterium is very much like a bacterium, but it belongs to the Archaea, a group different from the eubacteria and the eukaryotes. None of these three groups is ancestral to the others; each shares certain features with the others and has unique characteristics of its own as well. Archaeans include inhabitants of

some of the planet's most extreme environments. Some live near rift vents in the deep sea at temperatures well over 100 °C. Others live in hot springs, in extremely alkaline or acid water, or in extremely saline water. Since most of them live in an extreme environment, Archaeans developed a special system to produce energy for living. For example, Halobacterium uses a pigment protein very similar to the light-detecting pigment rhodopsin found in the vertebrate retina as an energy capturer, instead of the photosystems based on chlorophylls found in plants and eubacteria. Bacteriorhodopsin is very effective and has a high capacity to transform light energy to a chemical gradient used for ATP formation when the oxygen concentration is too low for conducting a normal respiration in the Halobacterium.

1.4.2 The Purple Membrane and Bacteriorhodopsin

Purple membranes are purple patches in the cell membrane of the Halobacterium. They contain a single protein, bacteriorhodopsin, (bR)[38]. In Halobacteria, purple membranes are over-expressed under low oxygen conditions to generate the proton electrochemical gradient necessary for ATP formation and other metabolic processes[39].

In the purple membrane, bacteriorhodopsin molecules are clustered within a two-dimensional hexagonal lattice of trimers. This 2-D crystalline structure contains few lipids, forming no more than one lipid layer around each protein molecule. It confers a unique rigid characteristic to the overall architecture.

The natural crystalline character of the purple membrane has allowed for an early structural analysis using electron diffraction methods[40, 41] and, more recently, the X-ray diffraction of micro 3-D crystals [42]. While earlier attempts gave mainly a precise picture of the crystalline lattice and an average picture of the protein tertiary structure, most recent data make it possible to show a 3.0 Å resolution picture of the purple membrane architecture. Figure 1.5 illustrates an X-ray diffraction pattern of a purple membrane pellet. Peak intensity and spacing are characteristic of a hexagonal crystal with a lattice constant of 62 to 63 Å. Such measurements established the crystalline nature of the purple patches as early as 1978. An atomic

force microscope image of the purple membrane is also reproduced on the same figure and shows clearly the regular organization of the membrane components.

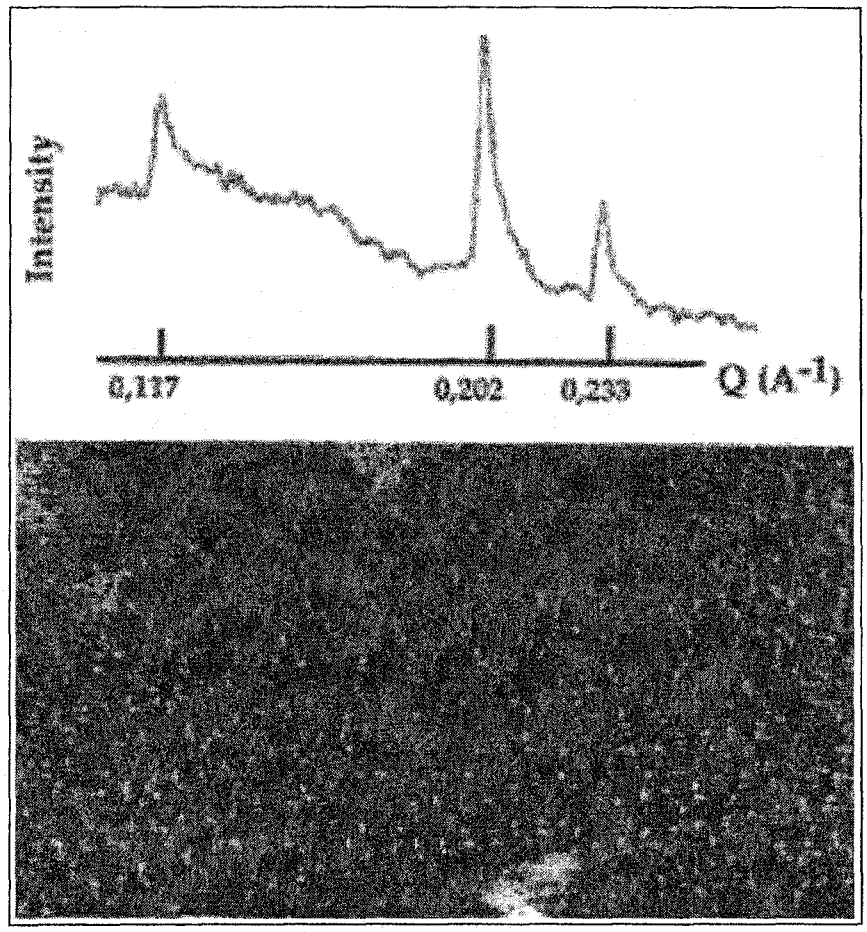

Figure 1. 5 Top: Small angle X-ray scattering intensity profile of the purple membrane pelletted in a capillary. The intensity (relative) is plotted against Q (=2π/d). The figure shows only the first three diffraction orders, but the sample allows for measurement up to the 13th order. Measurement was done at L. U. R. E. in Orsay. Bottom: AFM scan of the purple membrane sample deposited on mica sheet. Measurement was done using the AFM set up of Professor H. E. Gaub in Munich.

The structural information obtained from electron diffraction measurements makes it possible to locate the transmembrane sections of the protein in relation to each other. Figure 1.6 shows such an electron density map. The relative position of the individual bR monomer within the trimer is easily seen, together with the relative position of the transmembrane helices. It is noteworthy that even when such maps achieve a respectable resolution within the plane of the membrane, they do not allow for the precise positioning of individual amino acid residues in the plane perpendicular to it. In fact, the less than 4 Å resolution of Figure 1.6 applies only to the X-Y plane, since the resolution in the Z plane is less than 10 Å.

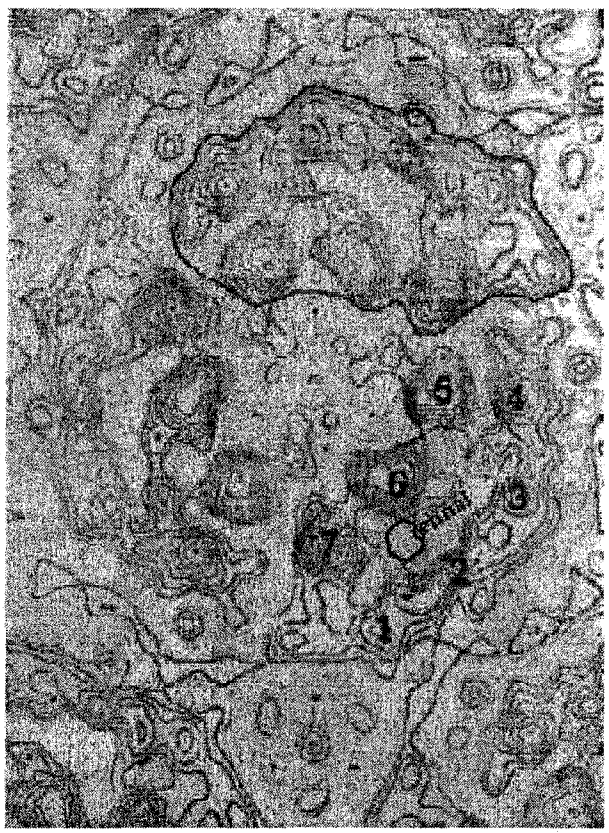

Figure 1. 6 Electron density (3.7 Å resolution) map established from electron diffraction of the purple membrane (viewed from the cytoplasmic side). One trimer is centered in the figure. The upper monomer of this trimer is circled in black. On the right monomer, the electron density attributed to the transmembrane α-helical segments is numbered from 1 to 7. The position of the retinal is also shown (Stoeckenius W. and Bogomolni R. [43]).

Very recently, however, 3-D microcrystals of bacteriorhodopsin were obtained, and the 3-D structure of the protein is now known to a resolution of 2.5 Å[42]. The average structure is shown in Figure 1.7. The 248 amino acid residues are shown from residue 7 to 227. They consist of 7 transmembrane helices connected by short loops. The hydrophobic amino acid content goes as high as 70% and the protein contains neither histidine nor cysteine. The C- and N-terminal sides are on the cytoplasmic and extracellular sides, respectively[44]. Retinal, the chromophore of the bacteriorhodopsin, is covalently linked to the Lys216 via a Schiff base linkage (Fig. 1.8).

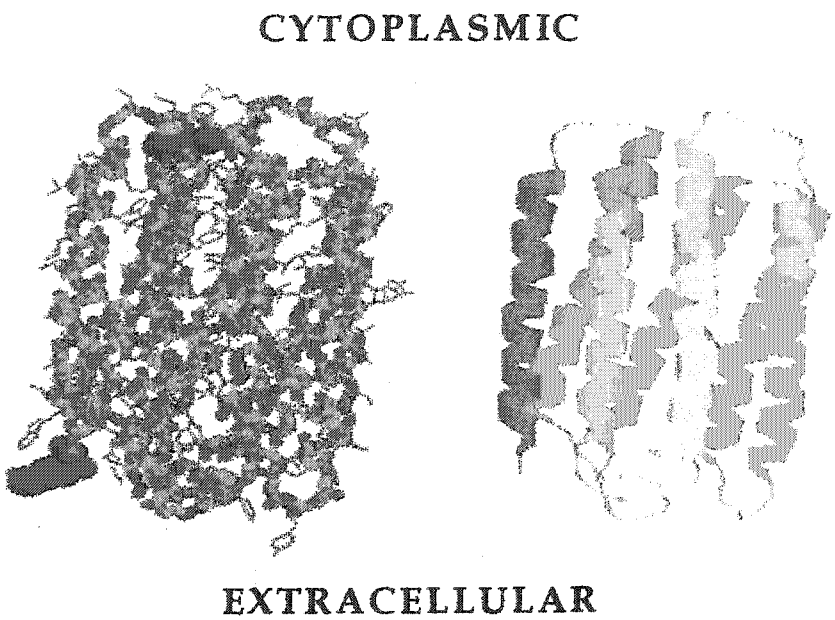

Figure 1. 7 3-D representation of bacteriorhodopsin. The left picture shows an enlarged peptidic backbone with thinner side chains. The right picture represents a cartoon of the transmembrane helices connected by cytoplasmic and extracellular loops. The amino acid residues represented as VdW spheres are #7 to #227. (Grigorieff et al. [45]).

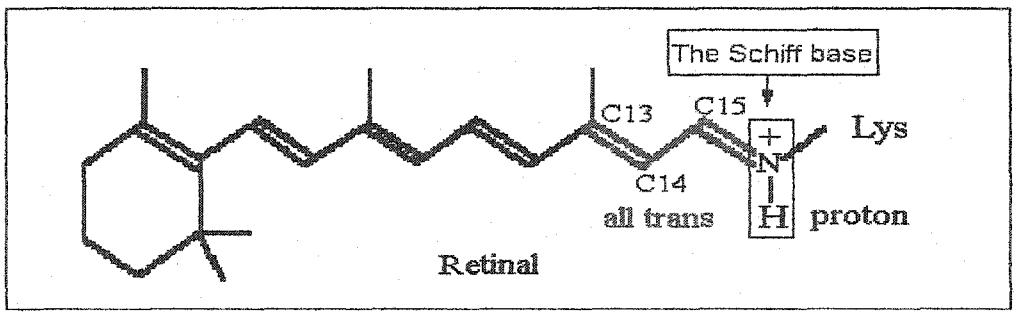

Figure 1. 8 Structural formula of the all-*trans* retinal bound to the protein via a protonated Schiff base.

1.4.3 Lipids of the Purple Membrane

The crystalline organization of bacteriorhodopsin within the purple membrane leaves little space for lipid components. Indeed, electron density maps like the one presented in Figure 1.6 show that most of the membrane surface is occupied by bacteriorhodopsin itself. In fact, purple membrane lipids only make up about 10% of the membrane's dry weight. There is currently no exact determination of their positions. The structure presented in Figure 1.9, however, was predicted by molecular dynamics calculations. Its features include 42% of the gauche conformation of the acyl chain, which makes it possible for sufficient conformational disorder to fit the rough surface of the bR molecule. Figure 1.10 represents all lipid molecules as being diphytanyl phosphatidyl glycerophosphate. Their actual structures are quite different. Lipids of the purple membrane are composed, approximately, of 60% phospholipids, 30% glycolipids and 10% neutral lipids, primarily squalene (Fig. 1.9)[46]. Polar lipids are unique in that their glycerol or triglycosyl groups are attached by ether linkages to two phytanyl chain moieties, consisting of saturated palmityl chains with branched methyl groups every four carbons[47]. The phospholipids in the purple membrane are phosphatidylglycerophosphate (PGP), phosphatidylglycerosulfate (PGS) and phosphatidyl

glycerol (PG) appearing as minor membrane components. The glycolipids are predominately composed of glycolipid sulfate (GLS)[48]. There are about 10 lipids per bR[49].

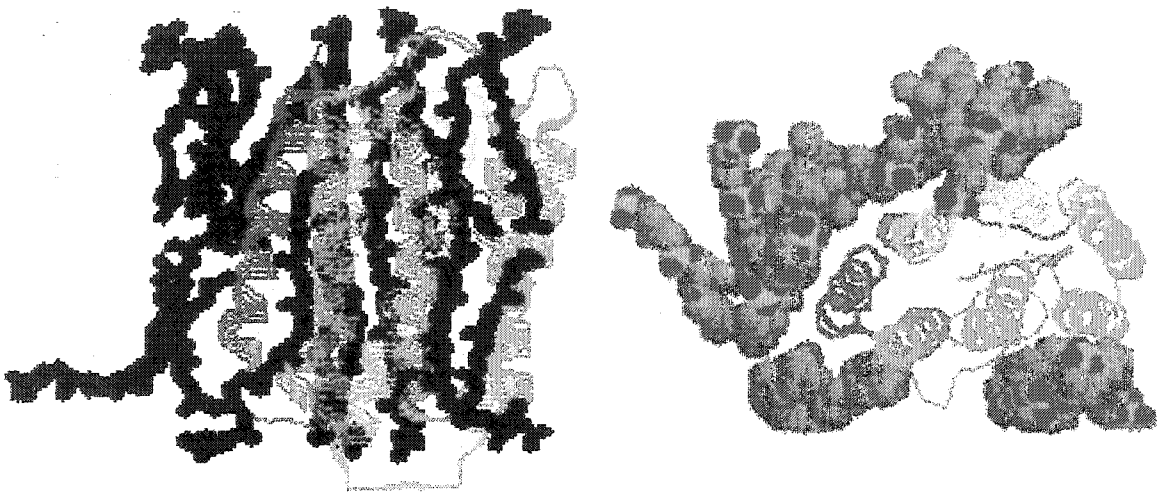

Figure 1. 9 Putative organization of the lipids of the purple membrane. The left part shows the lipid backbone in black and the peptidic helical backbone in transparency. The membrane is viewed from the side. The right part shows the membrane viewed from the top. Lipids are represented as VdW spheres, surrounding the 7 transmembrane helices (from Edholm et al.[50]).

Furthermore, lipids are not symmetrically distributed on each membrane side. Indeed, if an equal number of lipids on each membrane side is assumed, 2.5 GLS, 0.5 PGP, 0.5 PGS, 0.5 PG and one squalene would be found on the N-terminal side. The C-terminal side consists mainly or entirely of phospholipids, e.g. 5 PGPs per bR[51]. It is noteworthy that the purple membrane possesses a permanent dipole moment (~4 X 10^{24} C/M)[52]. However, it is not clear whether this dipole originates from an asymmetric lipid distribution only or from asymmetrically distributed charges of amino acids.

Lipids of purple membranes are closely associated with proteins. They form a highly regular crystalline structure and are crucial for the properties of purple membranes. Partial removal of lipids by mild detergent treatment affects photocycle kinetics. Wild-type kinetics can be restored by adding back halobacterial lipids, whereas phospholipids lacking the ether-linked dihydrophytanyl side chains are not effective, suggesting a specific role for the lipids in maintaining bR functionality[53].

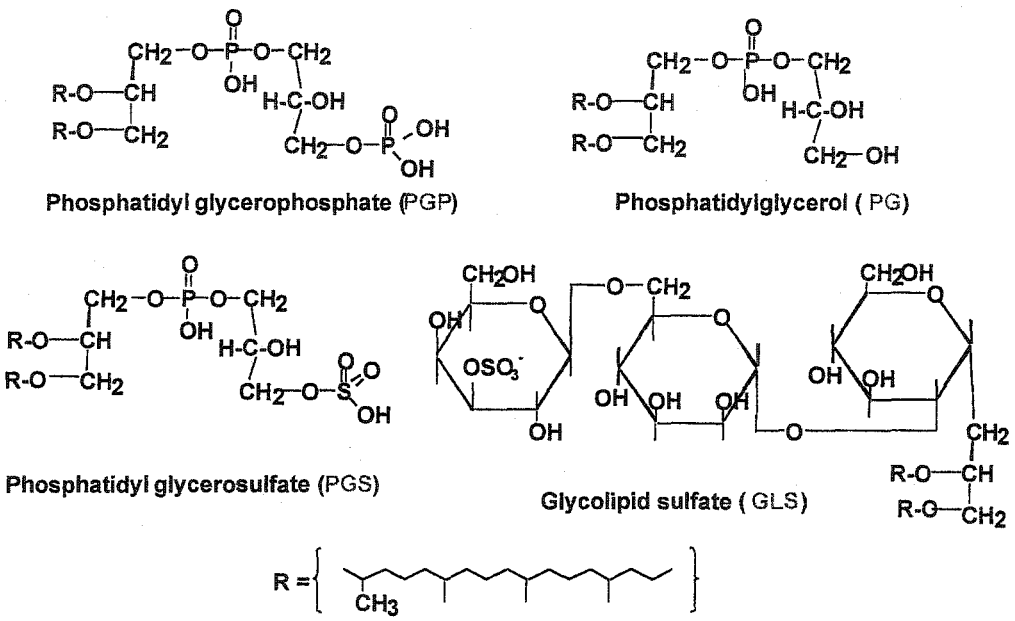

Figure 1. 10 Structure of the major lipids of the purple membrane.

Delipidated bacteriorhodopsin exists in equilibrium between a red and a purple form depending on the pH; the apparent pKa of this equilibrium is 7.3. When pH is higher than pKa, bR appears as red (λ_{max}=480 nm), while at a pH lower than 7.3, bR is mostly in its purple form (λ_{max}=570 nm). On

combining delipidated bR into a lipid bilayer containing minute amounts of tetramethyl pentadecane, bR remains in purple color and the $bR_{570} \Leftrightarrow bR_{480}$ disappears. But if the lipid vesicles contain pentadecane instead of tetramethyl pentadecane, bR can be titrated again in a mild pH range. These results suggest that in lipid vesicles with pentadecane without methyl side groups, bR is more accessible, while lipid vesicles with tetramethyl pentadecane mimic the native lipids, i.e. they 'protect' the 'titratable group' of the chromophore. The methyl side groups of the purple membrane alkyl chain thus play a specific structural role in the maintenance of the native lipid-protein interaction[32].

Using reconstitution technology, Joshi[54] et al. proved the importance of specific native lipids in the photocycle of bacteriorhodopsin. Reconstructing delipidated bR with different combinations of purple membrane lipids, they found a synergistical effect between PGP and SQ. The addition of SQ to suboptimal levels of PGP and the addition of a small amount of PG to SQ also induces a complete reconstitution. A SQ-PGP lipid complex may thus be essential for normal bR activity.

1.4.4 Proton Transportation Channel

Retinal is the aldehyde form of vitamin A. The isolated retinal does not absorb light in the visible range but in a broad band near 380 nm. In bR, the all-*trans* retinal lies in the interhelical area nearly parallel to the membrane plane. It is flanked by the proton acceptor and donor, Asp85 and Asp96, on its extracellular and cytoplasmic sides, respectively, the former being in its immediate vicinity and the latter at an approximate distance of 12 Å.

The extracellular side of the proton-pathway contains the hydrophilic residues Asp85, Asp212, Arg82, Glu194, Glu204, Glu9, Thr205, Tyr83, Tyr57, Tyr185, and Trp86. Among these, Asp212, Arg82, Glu194, Glu204 and seven water molecules form a hydrogen-bond network around the retinal (Fig. 1.11). The reprotonation pathway in the cytoplasmic half of the channel includes Asp96, Thr49, and Asp38. On the cytoplasmic side, only two water molecules are found in functionally relevant positions. Asp104,

Asp102, Asp36 and lipid head groups are involved in proton capture and guidance on the cytoplasmic surface.

We now have a clear picture of the deprotonation half of the pathway in the extracellular region. The active site comprises water402 that receives a hydrogen bond from the protonated Schiff base and donates hydrogen bonds to the side-chain carboxyl oxygen of the anionic Asp85 and Asp212. This arrangement together with additional hydrogen bonds of Asp85 to water401 and Thr89, and of Asp212 to Tyr185, Tyr57, and through water406 to Arg82, stabilizes the separated charges in this buried location.

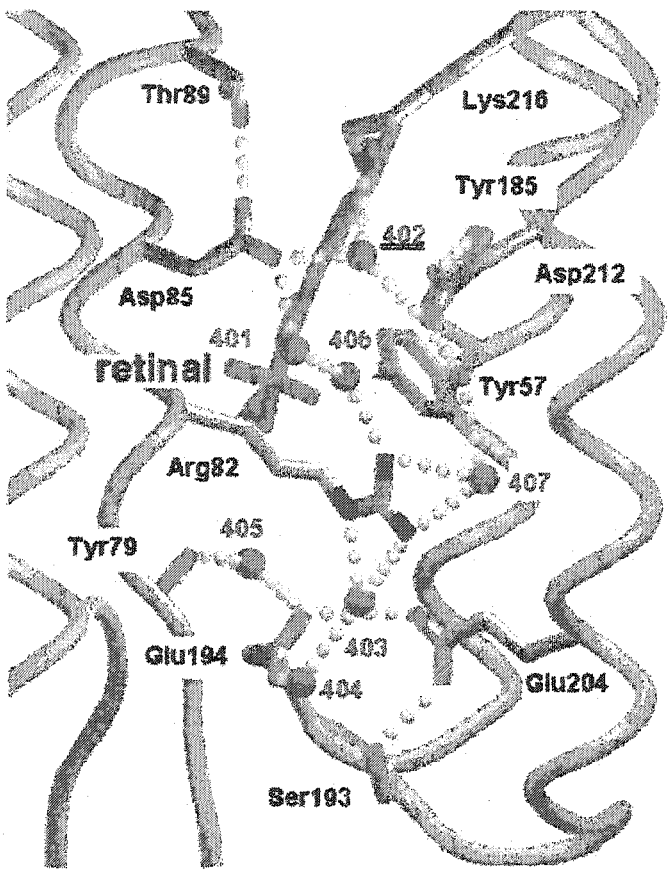

Figure 1. 11 Structure of the extracellular region of bacteriorhodopsin. The extracellular membrane surface is toward the bottom. View is from the direction of helix C. Hydrogen bonds visible from this angle are drawn as dotted lines. Water molecules are numbered from 401 to 407 (Luecke, H.[55]).

On the cytoplasmic side, water501 is hydrogen-bonded to the peptide C=O of Ala215 on one hand, and the indole N of Trp182 on the other. Water502 is hydrogen-bonded to the peptide C=O of Lys216 and to the peptide C=O of Thr46. The participation of Ala215 and Lys216 in these bonds imparts a kink, in the form of a π-bulge, to helix G where the retinal is bound. This arrangement may provide a mechanism for the long-range coupling between Asp96 and the retinal in the cytoplasmic region that occurs in the photocycle[56].

1.4.5 Photochemical Cycle

Proton absorption by the light-adapted bR triggers a photochemical cycle (Fig. 1.12) that includes a series of intermediates termed bR, J, K, L, M, N and O. Each intermediate has its own lifetime and spectral characteristic[57, 58]. The photocycle of bacteriorhodopsin begins with the formation of intermediate J_{610}, (subscript indicates the absorbance maximum), with a time constant of 0.5 ps[59, 60]. J_{610} stores the light energy by a rapid change of the Schiff base, irreversibly inducing the formation of intermediate K_{600}, L_{550}, M_{412}, N_{560} and O_{630} at times of ~5 ps, ~1.5 μs, ~80 μs, ~3 ms, ~5 ms and 2 ms respectively after excitation[61, 62]. M_{412} is the key intermediate in the proton pumping activity. It forms when the Schiff base is deprotonated and recovers its original state by the reprotonation of the Schiff base.

The proton transportation that accompanies the formation of intermediates is divided into five steps (Fig. 1.13)

(1): Deprotonation of the Schiff base and protonation of Asp85, the transition from bR to J, K, L and M.

Before deprotonation of the Schiff base, it is a process for preparing the deprotonation of bR and the expulsion of a proton to the extracellular side. From bR_{570} to the intermediate J_{610}, the retinal undergoes a

very rapid isomerization, a partial rotation of C_{13}=C_{14}[63, 64, 65], which induces the redistribution of electronic density in the retinal, decreasing the electrostatic interactions of the Schiff base.

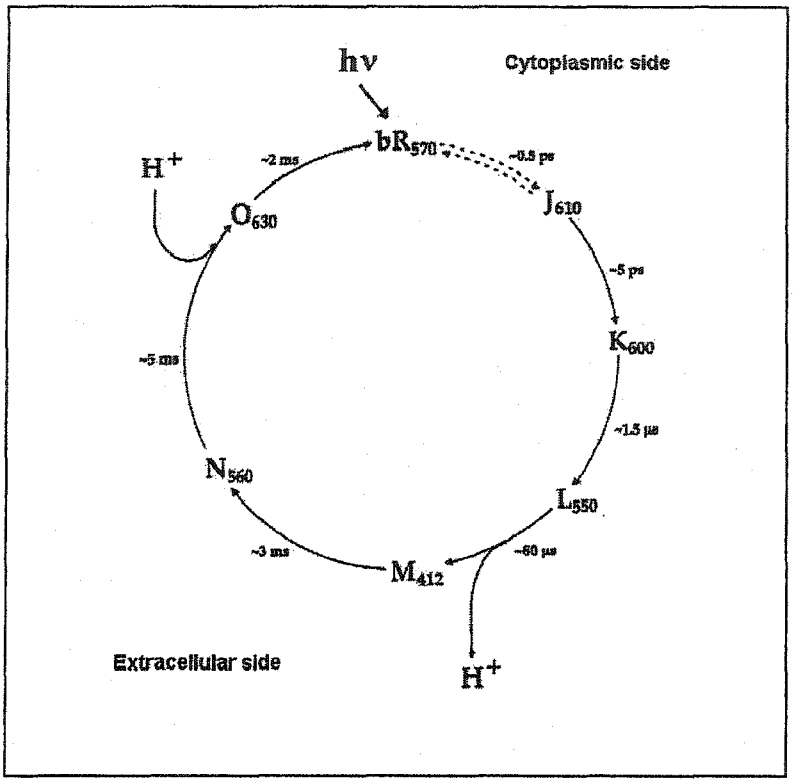

Figure 1. 12 Simplified unbranched photocycle of light-adapted bacteriorhodopsin. The intermediates include J, K, L, M, N, O. The subscript for each intermediate is the absorbance maximum (Trissl, H W. [66]).

J_{610} converts to the intermediate K_{590} with a full conversion of an all-*trans* to a 13-*cis* retinal. This conformational distortion of the retinal results in the separation of the cationic charge of the Schiff base from the anionic charge (counterion group) distributed over several amino acids, Asp85, Asp212, Arg82 and Tyr7 as well as water molecules[63, 65, 66]. The intermediate K is assumed to play a key role in energy

conversion, since the transition of J $\rightarrow$K is an irreversible photochemical reaction. By the isomerization of the Schiff base, at least 16 kcal/mol are conserved in the intermediate K.

The formation of the intermediate L is a relaxation process for the energy stored in K. There is no essential configurational change between the K- and L-intermediates; therefore, changes in the charge of other groups in the vicinity of the retinal should occur. FTIR data show that an aspartic acid group is deprotonated during the K $\rightarrow$ L transition[58]. The intermediate L converts to M by transferring one proton from the Schiff base to Asp85 in the vicinity of the retinal [65, 66, 67]. The Schiff base is deprotonated.

(2): Expulsion of a proton to the extracellular side.

One proton near the surface of the membrane is released to the extracellular side of the membrane through a protonated group, which may consist of Arg82, Tyr57 and other polar amino acids in the extracellular domain[65, 66]. The FTIR spectroscopic analysis points to a three-step model: $M_1 \rightarrow M_2 \Leftrightarrow M_N$, while $M_1 \rightarrow M_2$ is irreversible. At the M_1 state, the Schiff base proton is transferred to Asp85 without large conformational changes. Protonation of Asp85 is linked to the release of a proton to the extracellular surface [68, 69], and at a pH well above the pK for the release (pK5-6) of protons, the protonation equilibrium undergoes a major shift towards full deprotonation of the Schiff base. Thus, the release of the proton to the extracellular side of the membrane shifts the next step, the M_1 to M_2 transition, toward M_2[70]. In M_N, the protein has adopted the conformation typical for the N intermediate, but the Schiff base is still deprotonated.

(3): Reprotonation of the Schiff base: transition of M $\rightarrow$ N

One of the events occurring during the intermediate M $\rightarrow$ N is the reprotonation of the Schiff base. The reprotonation of the Schiff base could be done by increasing the proton affinity of the Schiff base[65], modifying the orientation of the Schiff base and its proton accessibility from the cytoplasmic domain of

bR. Large-scale conformational changes in the cytoplasmic region[71, 72, 73] causes both the lowering of the pK of Asp96 and the establishment of a proton conductive pathway from Asp96 to the Schiff base, so as to reprotonate the Schiff base in M_2 to N reaction.

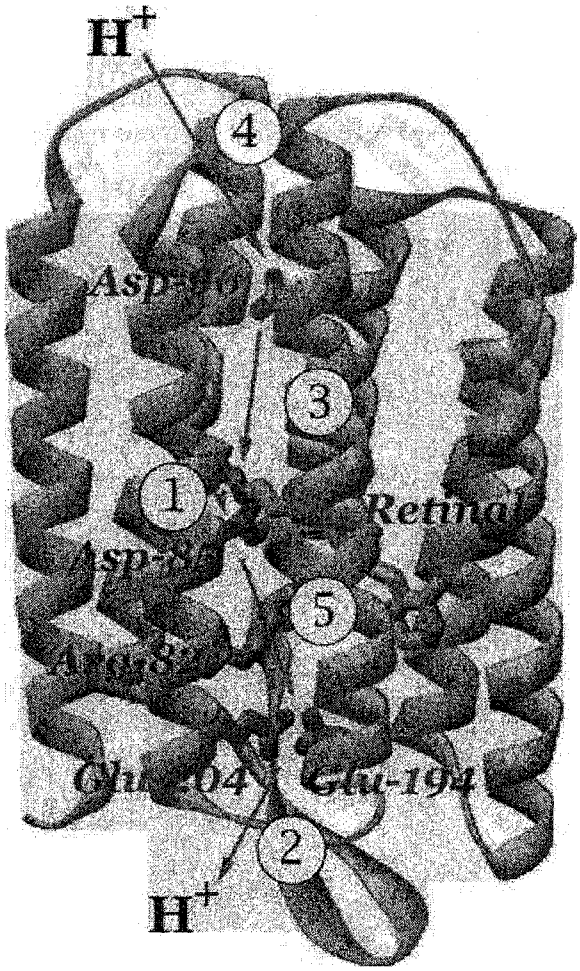

Figure 1. 13 Overall view of bacteriorhodopsin, shown with the retinal and residues directly implicated in the proton transport. Top, the cytoplasmic side. Arrows indicate proton transfer steps during the photochemical cycle. Numbers refer to the sequential order: (1) deprotonation of the Schiff base, protonation of Asp85; (2) proton release to the extracellular surface; (3) reprotonation of the Schiff base, deprotonation of Asp96; (4) reprotonation of Asp96 from the cytoplasmic surface; and (5) deprotonation of Asp85, reprotonation of the proton release site (Luecke H.[74]).

(4): Reprotonation of Asp96 from the cytoplasmic surface, from the intermediate N to O

The pK of Asp96 increases as a proton is transferred to the Schiff base[66] inducing the reprotonation of Asp96 from the cytoplasmic surface during its lifetime. The protonation of the Schiff base removes a large barrier to the rotation of the C_{13}=C_{14} double bond[75]. The thermal reisomerization converts the retinal from 13-*cis* to a twisted all-*trans* configuration. After reprotonation of Asp96, the 13-*cis* to all-*trans* isomerization shifts the retinal in the environment of a protonated Asp85.

(5). Deprotonation of Asp85, reprotonation of the release site, and recovery of bR from the intermediate O

Re-establishment of the initial state at the Schiff base occurs in the O to bR reaction, when Asp85 dissociates and releases the proton of Asp85 to an extracellular site that has released the proton. The retinal chain then relaxes to a non-strained all-*trans* configuration[76, 77].

1.4.6 bR Structural Changes during Proton Pumping

Light-induced changes are detected at the cytoplasmic end of helices A to G. At the beginning of the photocycle, the retinal is hit by a photon and changes its configuration from the all-*trans* to the 13-*cis*. A small movement of helix C brings the side chain of Asp85 closer to the nitrogen atom of the Schiff base[78]. The nitrogen atom moves upwards towards the cell interior, pushing against some bulky residues on helix F. The cytoplasmic side of helix F swings out in late M while helix G moves partly into its place. The movement of helices F and G opens a narrow channel through which the Asp96 is reprotonated (Fig. 1.14). In the N to O transition, the proton is released to the outside of the membrane. Asp85 transfers its proton through a network of hydrogen bonds and water molecules to the outside medium, past Arg82, which has moved slightly. Finally, the retinal relaxes to the all-*trans* form, helices F and G swing back to their original position, and another proton-pumping cycle can begin.

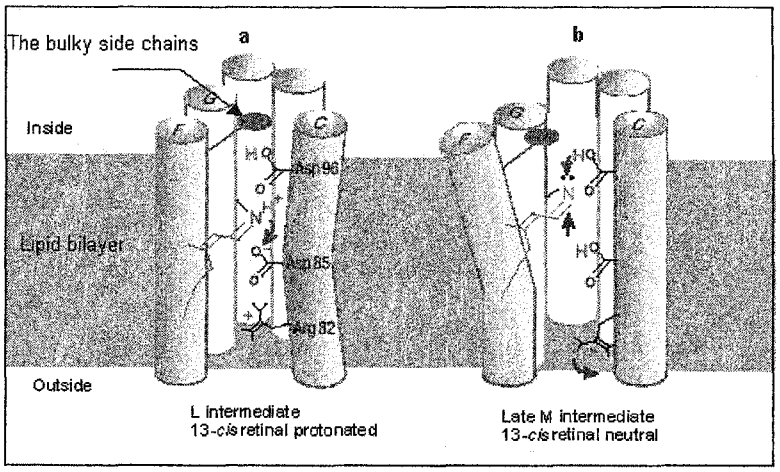

Figure 1. 14 Structural changes during proton transportation. (a), In the L state, aspartate 85 gets close to the nitrogen atom, aided by a slight movement of helix C. (b), In the M state, the deprotonated retinal (yellow) straightens, pushing against helix F and causing it to tilt. Red arrows, proton movements; blue arrows, movements by groups of atoms. Helices D and E are omitted for clarity. The 'paddle' attached to helix F represents the bulky side chains, which move to open the cytoplasmic proton channel (Kuhlbrandt W.[79]).

Since the purple membrane functions as a light-driven proton pump, it is obvious that the function of purple membranes is affected by pH. High temperatures, detergents, organic solvents and anesthetics also affect the function of the purple membrane. The following section presents a detailed discussion of the effects of general anesthetics on the purple membrane.

1.5 THE PURPLE MEMBRANE AS AN EXPERIMENTAL MODEL IN THE SEARCH FOR THE MECHANISM OF ACTION OF ANESTHETICS

1.5.1 The Equilibrium of Three Chromophoric States of Bacteriorhodopsin

Bacteriorhodopsin has a visible maximal absorption at 570 nm in the light-adapted state, called bR_{570}. The maximal absorbance depends on the state of protonation of the Schiff base and the distribution of

charges or dipoles around the chromophore, which are maintained by the interaction of the apoprotein with the retinal. Once this interaction is disturbed by the detergents used for the isolation of proteins or by anesthetics, the purple color changes due to a redistribution of the electronic state around the Schiff base. Therefore, the color change of purple membranes is a good indicator of the conformational changes of bacteriorhodopsin.

Lipid-protein interactions are important in stabilizing the purple chromophore[80]. A blue shift occurs upon solubilization of completely delipidated bacteriorhodopsin by detergents; its maximal absorbance is at 480 nm, named bR_{480}. bR_{480} can be reversibly titrated with an apparent pKa ranging from 2.5 to 12, depending on the detergent used for dispersion. In a detergent with a longer hydrophobic tail, the apparent pKa is higher, since detergents with a long hydrophobic tail are very similar to the lipids, playing a stabilizing role for the environment around the chromophore. A relatively high pH favors the formation of the red chromophore[81]. bR_{480} may also form in the presence of general anesthetics, such as enflurane and halothane. The light-adapted bacteriorhodopsin is more sensitive to anesthetics than the dark-adapted one. The rate of transformation to bR_{480} for the dark-adapted bacteriorhodopsin is similar to that of 13-*cis* to all-*trans* thermal equilibration, indicating that the anesthetics only interact with all-*trans* bacteriorhodopsin. This is further proved by the fact that all the dark-adapted bacteriorhodopsin transfer to all-*trans* form after being treated by anesthetics[82]. bR_{480} changes to bR_{380} when anesthetics remain in the membrane for a long time at a high pH. bR_{380} can be recovered to bR_{480}, and then to bR_{570}, provided it does not remain in the 380 nm form for more than one hour[36]. Figure 1.15 shows the equilibrium among these three spectral species in the presence of 0.2% (v/v) enflurane, pH=11. This pH favors the formation of the red form of bacteriorhodopsin, even of its yellow form. The maximal absorbance of bacteriorhodopsin shifts to 480 nm as shown by spectra 2 and 3 which were obtained 5 and 10 minutes respectively after the addition of enflurane. Next, spectra 3 through 13 show the progressive conversion of bR_{480} to bR_{380}. The reverse process is not shown, but it is worth mentioning that at the point where

spectrum 13 is obtained, a pH jump produced by the rapid addition of diluted HCl sufficient to lower the pH to 9 causes the bR_{480} to reappear, and then recover to the bR_{570} [36].

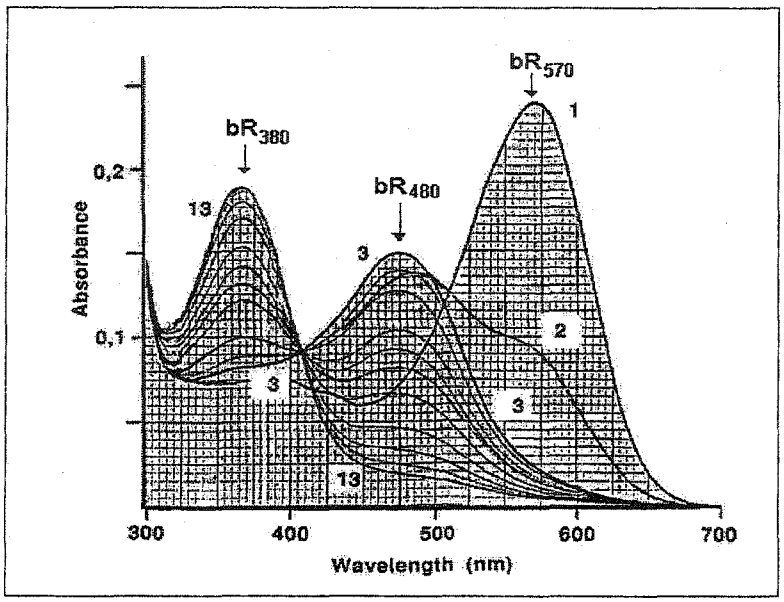

Figure 1. 15 Three spectral species observed upon addition of 0.2% (v/v) enflurane to the purple membrane suspended in 10 mM carbonate buffer (pH=11). Spectra 1 to 13 were measured at 5-minute intervals (Messaoudi S. et al. [36]).

The equilibrium between bR_{570}, enflurane-induced bR_{480} and bR_{380} is also pH dependent (Fig. 1.16). In the presence of enflurane, bR_{570} and bR_{480} coexist between pH=5 to 7. When pH is higher than 7 and lower than 10, all bR_{570} rapidly turn to bR_{480}. The yellow form bR_{380} exists only when pH is higher than 10 or lower than 5. Low halothane concentrations gave results comparable to those observed with enflurane, except that the alkaline bR_{380} appears only at pH 12, or lower than 6.

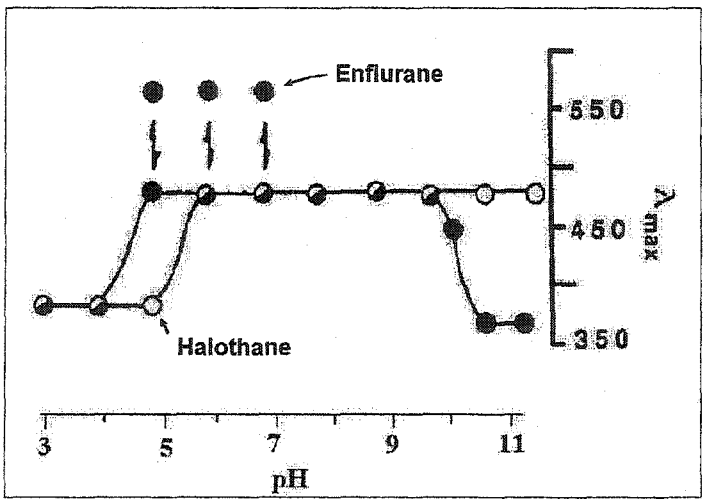

Figure 1. 16 Acid-base equilibrium between the different spectral forms of bacteriorhodopsin in the presence of 1% (v/v) enflurane (black dots) or 0.3% (v/v) halothane (open dots) (Messaoudi S. et al.[36]).

1.5.2 Structural Features of Enflurane-Treated Purple Membranes

1.5.2.1 Circular Dichroïsm Spectroscopy of the Purple Membrane in the Presence of Enflurane

The delipidated bR_{480} is found as monomers, what is proved by its circular dichroism spectrum[83]. Indeed, an excitonic coupling between the chromophores in the native bR trimer is thought to be responsible for the bilobed CD spectrum of the pigment. The visible CD spectra of the purple membrane are bilobed though asymmetric, consisting of a positive band around 520 nm and a negative band around 605 nm (Fig. 1.17, curve 1)[84]. In the presence of 4 mM halothane, the negative band decreases more drastically than the positive band does (Fig. 1.17, curve 2), and at 8 mM halothane the positive band shifts to around 480 nm (Fig. 1.17, curve 3). At 16 mM halothane, the visible CD spectrum disappears (Fig. 1.17 curve 4). These results indicate that enflurane breaks the connection between bR molecules and induces the change from trimers into monomers [35].

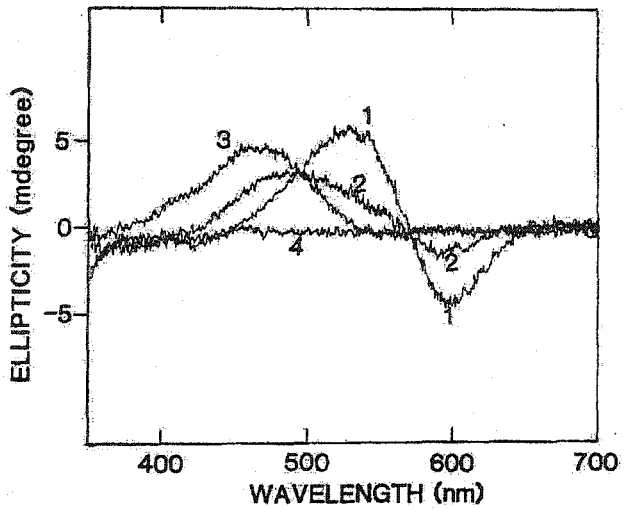

Figure 1. 17 Visible CD spectra of bacteriorhodopsin in the purple membrane. The ellipticity of 15.9 μM bacteriorhodopsin is given with and without halothane: (1) control, (2) 4 mM, (3) 8 mM, (4) 16 mM (Nishimura S. et al. [35]).

1.5.2.2 Effects of Enflurane on the bR Tertiary Structure

The effects of enflurane on the structure of bR apoprotein have been examined by FT-IR spectroscopy [85]. The structural changes in the protein could be observed in the region from 1650 to 1500 cm^{-1}. The bands at 1660 and 1547 cm^{-1} are referred to as the amide I and II, respectively. Of the bR helices, three are almost perpendicular to the plane of the membrane, while the other four are tilted 10° to 20° from this orientation. bR helices are α_{II}-helices. A particular α_{II}-structure is almost the same as a normal α_I-structure, but the N-H bonds in the amide peptide groups point more toward the helical axis. A weak and bent hydrogen bond forms between the N-H bond and C=O bond, resulting in stronger C=O bonds in accordance with a higher frequency for the amide I mode in α_{II}-helices. As a result, the amide I band in the α_{II}-helix is located at 1659 cm^{-1} instead of 1655 cm^{-1} for the normal α-helices. Due to the photoselection effect, the tilted N-H bond gives rise to an amide II band as intense as the amide I band (Fig. 1.18, upper spectrum on the left). In the presence of enflurane, few differences are observed in the

frequencies of protein structural indicators - the bands at 1660 and 1547 cm^{-1} - between the native purple membrane and the membrane containing enflurane. This means that enflurane does not affect the bR secondary structure. However, there are differences in the amide II/I intensity ratios (Fig. 1.18, bottom). The ratio of the amide II/I drops from 1 in the bR_{570} to 0.94 in bR_{480}, upon addition of enflurane.

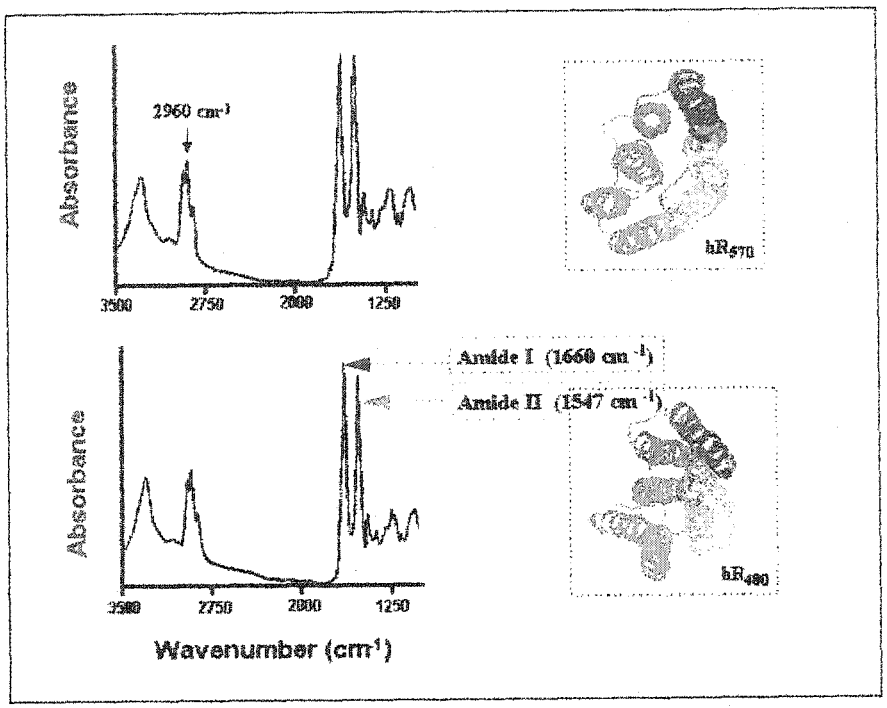

Figure 1. 18 FT-IR spectra of oriented purple membrane film in the form of bR_{570} (top) and bR_{480} (bottom) (Messaoudi S. et al. [85]). The helices of bR_{570} (top) and bR_{480} (bottom) are shown on the right.

This effect was interpreted as a relaxation of the helical orientations with respect to each other (Fig. 1.18, right). By comparison with the intensity of the band at 2960 and 2860 cm^{-1} (Fig. 1.18, left), we can see that the C-H/amide II intensity ratios are the same (within 4%) in the 570 and 480 nm bacteriorhodopsin. It is the amide I intensity that increases when the pigment is converted from bR_{570} to bR_{480}. This indicates that enflurane induces a relaxation of the helical orientations with respect to each other.

1.5.3 Uncoupling of the Photochemical Reaction from Proton Pumping Activity in the Presence of Anesthetics

The enflurane-induced bR_{480} has full photochemical activity with its intermediate M at 380 nm, called M_{380}. The kinetic analysis shows that the photocycle of M_{380} is characterized by a rapid M rise and a slow M decay [81]. Figure 1.19 at left shows the photocycle of the native bR. One third of the M is back to the original bR through the intermediate O, and the rest follows a branched cycle (bypassing 'O'). The numbers indicate the time constants (s^{-1}) of M rise and decay. A high time constant means a rapid rise or decay. In the presence of enflurane (Fig. 1.19, right), the time constant of the M rise is higher than that of the native bR. The time constant of its decay is low when M is back to bR through O but is high through the direct pathway (bypassing 'O'). That suggests a fast phase and a slow phase during the M decay. Therefore, the M rise of bR_{480} is fast and its decay is slow due to the slow phase.

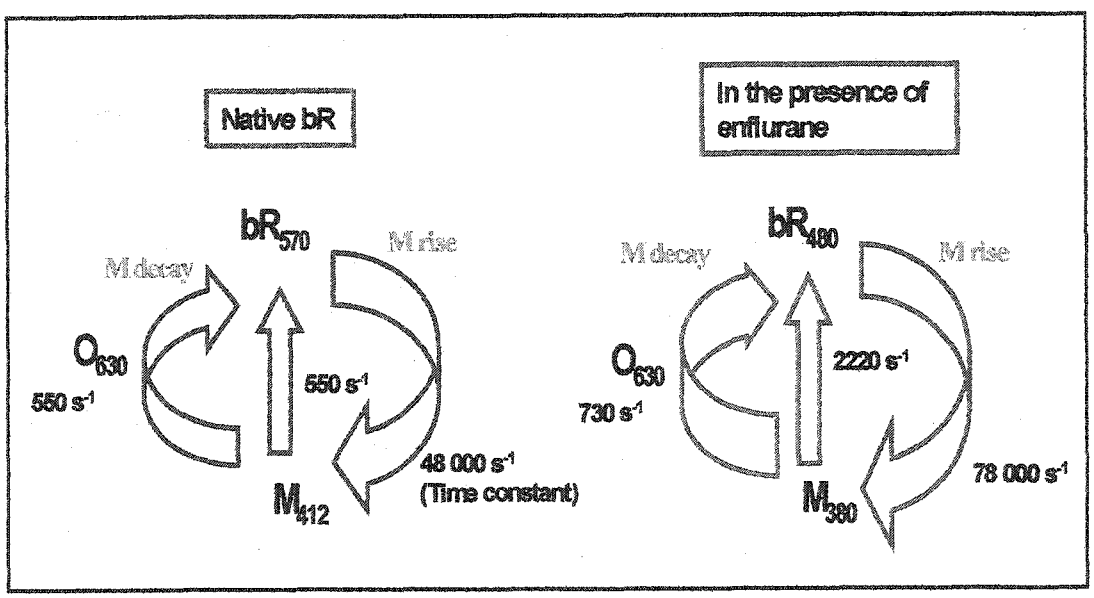

Figure 1. 19 Photocycles of the native bR (left) and the enflurane-containing bR (right).

Although it has a photochemical cycle, bR_{480} has no proton-pumping activity. In Figure 1.20 (right) the function of the bR proton pump is shown as the relative pH changes when the samples are irradiated

with monochromatic light. The maximal pH change of the native sample is at 570 nm, which agrees with the absorbance spectrum. In the presence of enflurane (0.3% v/v), the maximal absorbance is at 480 nm (Fig. 20, left), and there are very little or no pH changes at 480 nm for the red form of bR. The maximum in the action spectrum is still at 570 nm owing to the residual bR_{570} in the sample (Fig. 1.20 right). In addition, photoelectrical analysis shows an acceleration of the deprotonation and a deceleration of the reprotonation, which results in little or no proton pumping activity in the bR_{480} sample [81]. Finally, the proton pumping activity recovers after removal of enflurane under a mild vacuum (Fig. 1.20, inset).

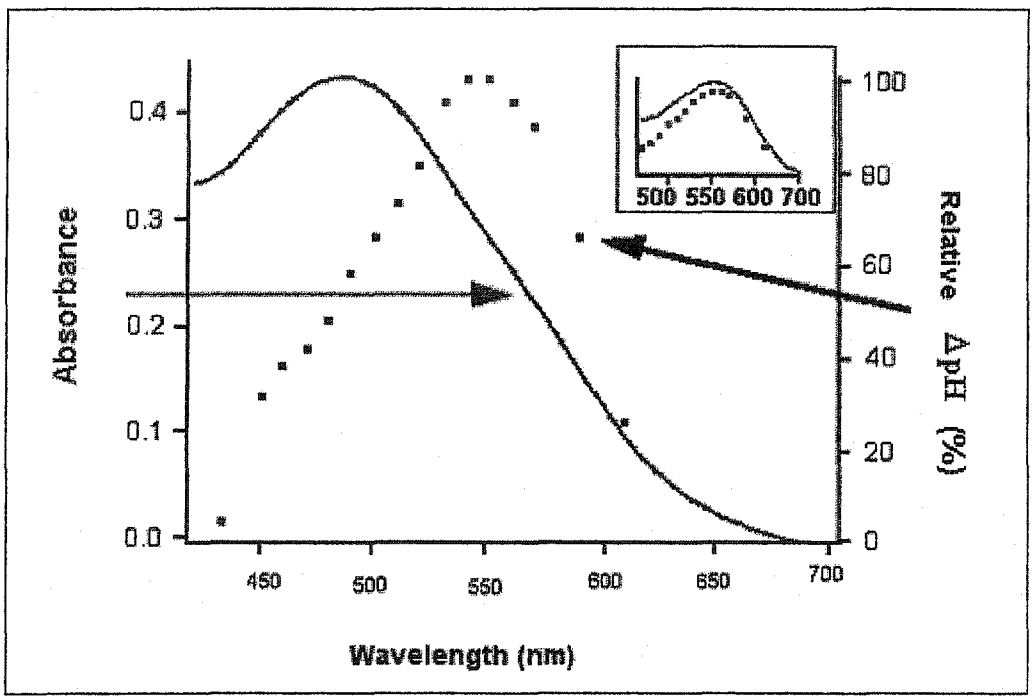

Figure 1. 20 Action spectra for proton pumping across purple membrane vesicles. The solid line is the absorbance (left) of the sample in the presence of 0.3% v/v enflurane. The square black dots are the relative pH change (right) measured as a function of the excitation wavelength in the same sample under the same conditions. The inset shows the same measurements on the sample after enflurane was removed under mild vacuum (Boucher F. et al.[81]).

1.6 REMAINING QUESTIONS AND OBJECTIVE OF THE PROJECT

The above results show different effects of anesthetics on the PM spectral character and bR functionality and these effects are reversible. However, the full reversibility of structural changes in the purple membrane remains to be determined. As mentioned, enflurane affects the bR trimeric structure and the orientation of bR helices. The data from this research did not show whether these changes reverse or not following the removal of general anesthetics. In addition, analysis with differential scanning calorimetry (DSC) shows that some structural features of the purple membrane do not completely recover after anesthetic treatment.

Figure 1. 21 shows the DSC of native purple membranes and of enflurane-treated purple membranes. A DSC thermogram of the native purple membrane contains a main transition near 95 °C and a pretransition at around 75 °C. The main transition corresponds to the denaturation of the apoprotein and the pretransition corresponds to different steps of the intermolecular re-arrangement of the crystalline structure and the intramolecular reorganization of bacteriorhodopsin itself[86]. In comparison to the DSC of the native purple membrane, we found that DSC of the enflurane-treated purple membrane almost lacks the pretransition. Only a very small part of the pretransition remains, suggesting a loss of the original membrane organization after the treatment of enflurane.

The purple membrane consists of a crystalline array of bR trimers. Some irreversible changes may involve different structural levels, from bR configuration to bR trimers and to the crystalline structure. The objective of this project was to investigate to which extent the PM structure recovers its original state after the anesthetic-treatment. Several physical methods have been employed to observe the structure of the purple membrane in the presence of enflurane and after removal of enflurane. At first, we observed the changes in the UV/Vis spectrum upon the addition of the different concentrations of enflurane. In addition to CD spectroscopy in the determination of bR trimers, the DSC of the purple membrane has been

measured after treatment with two different concentrations of enflurane. The crystalline structure has been assessed with X-ray diffraction and atomic force microscopy. Changes in the bR structure was also identified by infrared difference spectroscopy while flash photolysis experiment has been used to examine changes in the kinetics of the intermediate M. Finally, the recovery of simple lipid bilayers after anesthetic treatment has also been examined. This set of physical techniques was used to understand to which extent an anesthetic can induce irreversible changes in the purple membrane and if possible, to precise its mechanism of action.

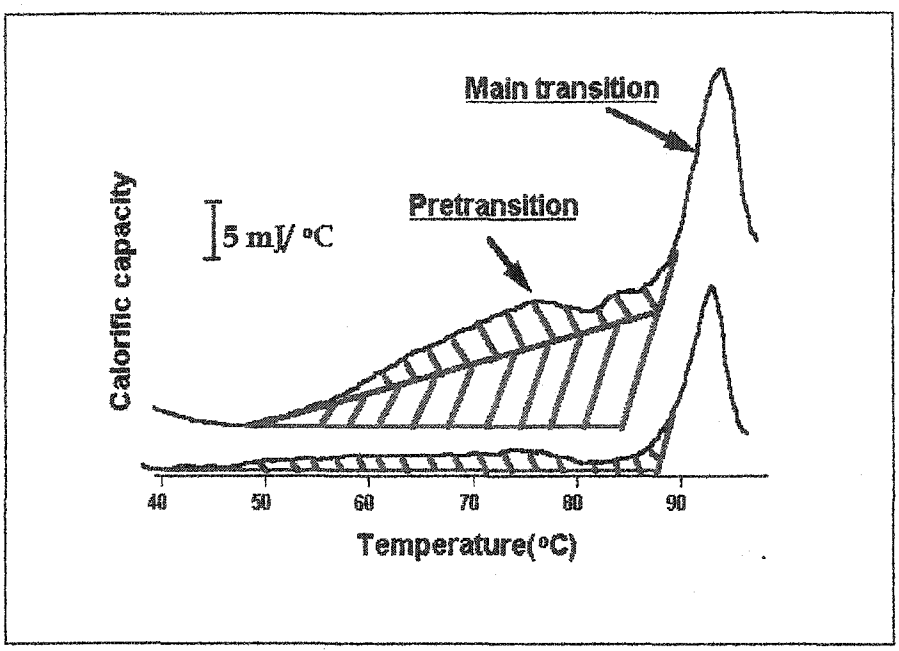

Figure 1. 21 Calorimetric profiles obtained in 100 mM KCl, 50 mM Phosphate buffer for native (upper trace) and enflurane-treated (lower trace) purple membranes. The hachure represents the pretransition. The red part vanishes after enflurane treatment, while the purple part remains.

CHAPTER 2

MATERIALS AND METHODS

2.1 PREPARATION OF PURPLE MEMBRANES

The purple membrane was prepared from cultured cells of *Halobacterium salinarium* strain S_9, obtained from Dr. W. Stoeckenius, at the University of California at San Francisco. It was purified according to the standard procedures found in the literature[48, 87].

2.1.1 Culture of Bacteria

Halobacterium grows in a special high salt culture medium. The following products were added to one liter of distilled water:

1. NaCl 25% w/v
2. KCl 0.2% w/v
3. $Na_3C_6H_5O_7$ $2H_2O$ (Na Citrate) 0.3% w/v
4. $MgSO_4$ $7H_2O$ 2% w/v
5. 1 ml of ferrous sulfate solution containing 0.5g $FeSO_4$ $7H_2O$ in 10 ml distilled water acidified with 3 drops of HCl.
6. The pH of the medium was adjusted with NaOH or HCl to 6.5-6.7.

Autoclave was not necessary since only halobacterium can grow in this high level of salt.

7. Oxoid peptone (bacteriological peptone) 1 % w/v

Peptone was added just before inoculation.

Bacteria were first grown aerobically at 37 °C in 1600 ml of medium contained in an Erlenmeyer of 4000 ml. The Erlenmeyers were installed on a shaker (New Brunswick Scientific Co., Inc.) with speed of rotation at a 180 rpm. When the number of bacteria reached a maximum at the end of the exponential

growth phase, the condition of the culture was changed in order to induce the production of the purple membrane. Lowering the shaking rate to 100 rpm then reduced aeration. The culture was exposed to a series of fluorescent tubes (280 watts in total) for 3 days. After that period of time, the culture was purple. The bacteria were collected for preparation of the purple membranes.

2.1.2 Collection of Purple Membranes

Six 1600-ml cultures were harvested by centrifugation at 10,000 g for 20 minutes with a Sorvall centrifuge RC-5B. Bacteria were washed twice with a basal salt solution. The one-liter basal solution contained:

1. NaCl	25% w/v
2. KCl	0.2% w/v
3. $MgSO_4$ $7H_2O$	2% w/v

The bacterial pellet was weighed, and three times its weight of the basal solution was added. The suspension was stirred for 1 hour in the dark. 10 mg of DNAase was added to reduce the viscosity. The mixture was dialyzed for 16 hours against water with changes after 1.5 hours and 6 hours. The bacteria were then broken, releasing various fragments into the solution.

The dialysate was centrifuged at 10,000 g for 20 minutes. The fragments of the bacterial cells were in the pellet, while the membranes were in the supernatant. The supernatant containing the membranes was centrifuged at 50,000 g for 1.5 hours. The purple membranes were in the pellet and the red membranes were in the supernatant. The cellular membrane of halobacteria is usually red because of the presence of the carotenoid pigment, instead of bacteriorhodopsin. The purple membranes appeared only when the concentration of oxygen was low and light intensity was high. However, some red membranes still remained in the purple patches. The next step included the removal of this red part from the membrane. The "crude" purple membrane was first washed with distilled water, and then recentrifuged at the same rate for 1.5 hours. This step was repeated two or three times until the supernatant showed almost no color.

2.1.3 Purification of Purple Membranes

The pellet containing the purple membranes still contained some amounts of red membranes. It was further purified by ultra-centrifugation on a discontinuous sucrose gradient, prepared by layering 10 ml of a 1.3 M sucrose solution on top of 15 ml of 1.5 M sucrose solution. The samples were suspended in distilled water and added on top of the 1.3 M sucrose layer. Centrifugation was carried out at 50,000 g for 48 hours in a SW28 rotor in a L7-80 Beckman ultracentrifuge at 4 °C. The purple membranes were recovered at the interface of the 1.5 M and 1.3 M sucrose layers, and the red band at the top of the 1.3 M sucrose layer. The purple band was collected and dialyzed against distilled water for 16 hours with a change of water after 1.5 hours and another change after 6 hours for eliminating sucrose. The dialysate was centrifuged at 50,000 g for 1.5 hours to remove sucrose. The purple membranes were resuspended in the basal salt solution for conservation or in a 100 mM KCl and 50 mM phosphate buffer (pH=7.5) for the experiments. The concentration of bR was then calculated taking into account that the extinction coefficient at 570 nm was 63000 $L \cdot cm^{-1} \cdot mol^{-1}$.

2.2 ABSORBANCE SPECTROSCOPY

The stock solution of purple membranes was diluted with a 100 mM KCl and 50 mM phosphate buffer to a bR concentration of 0.5 X 10^{-5} M. The purple membrane suspension was then put into an airtight-stoppered cuvette. The absorption spectrum of purple membranes was recorded from 400 to 700 nm with a UV/Vis Pye Unicam SP 8-100 spectrophotometer (Canlab, Montreal). The 100 mM KCl and 50 mM phosphate buffer (pH=7.5) was as the reference. The color change of purple membranes induced by enflurane or halothane was shown by a shift in the absorbance maximum from 570 to 480 nm, or to 380 nm if a higher concentration of enflurane or halothane was added. This was achieved by injecting microliter amounts of pure enflurane or halothane with a micro-syringe. The sample was then stirred vigorously to allow anesthetic molecules to disperse well in the purple membrane suspension. The

samples for flash photolysis, DSC, AFM and FTIR were assessed by absorption spectroscopy to confirm that the purple membranes had completely changed to the bR_{480} form.

2.3 FLASH PHOTOLYSIS

Bacteriorhodopsin functions as a proton pump. On absorbing a photon, bacteriorhodopsin undergoes a photochemical cycle, accompanying the transportation of the proton from the inside to the outside of the membrane. The intermediate M is the key reaction in this process and concerns the deprotonation and reprotonation of the Schiff base leading to the proton flow across the membrane. The disturbance in proton transportation must reflect the alteration of the kinetics of the intermediate M. Therefore, we can observe the disturbance on the function of bacteriorhodopsin by examining the modification of the intermediate M upon the addition of anesthetics.

2.3.1 Principle

Flash photolysis is a technique that allows us to analyze the kinetic relaxation of a photosensitive molecule as a function of time after a short light excitation. The basic principle of this technique is that two perpendicular luminous radiations are projected by two different luminous sources. The first radiation is an actinic light that induces the photochemical reaction we wish to study. This flash should be intense enough to excite the sample molecules very rapidly. The second radiation, usually called an analyzing beam, is a continuous monochromatic illumination for detecting the chemical transformation of the sample by the first exciting beam. The optical information from the transitory transmission of the analyzing beam is detected by a photodiode. The brief amplitude changes at a given wavelength demonstrate the properties of the photochemical steps of a photoactive molecule. If there is no reaction, there will be no change in the intensity of the transmission beam. The signal of the optical detector is amplified and converted to an electrical voltage with an amplifier and fed to a very rapid oscilloscope. The original kinetics data are transferred to a computer, stored and analyzed.

2.3.2 Experimental Method

The actinic light pulse was provided by the 532-nm, 10-ns, 20-mj pulse of a Q-switched Nd-YAG laser (Laser System 2000; JK Lasers, Rugby, England). The laser beam (4 mm diameter) arrives at the sample at a right angle to the analyzing beam. The analyzing beam is produced by an arc lamp of 150-W Xe (Photon Technology Inc.) dispersed by a monochromator (Photon Technology Inc., N°01-002). Next to the monochromator is a lens that converges the beam so as to make it pass through the sample and arrive at a photodiode detector. Between the monochromator and the sample, there is an electro mechanical shutter (Uniblitz model 225L) that allows the analyzing beam to go through the sample and be detected by the photodiode. After opening the actinic light, the intensity of absorbance detected by the diode changes following the absorbance of the sample. The photodiode is protected from scattered actinic light by a high-attenuation 532-nm Raman holographic filter and a narrow interference filter. The signal is transferred to the oscilloscopes Nicolet 4094 and 4094C. The whole measurement is synchronized by an optical synchronizer (Fig. 2.1).

2.3.3 Sample Preparation

The samples for flash photolysis experiments were the same as those for absorbance spectroscopy. The transient absorbance changes of the native PM sample without enflurane were chosen as a control. Enflurane was added by injecting microliter amounts of enflurane to the PM suspension. This mixture was periodically stirred until there were no more changes in its spectrum. The transition of bR_{570} to bR_{480} was assessed by absorption spectroscopy to confirm the transition before the measurement of flash photolysis. Enflurane was removed by placing the samples under mild vacuum for a few minutes. The recovery of the PM color was seen as the maximal absorbance of the samples recovered to 570 nm. However, completeness of enflurane removal could not be determined at the time of the experiment. The reversibility of the effects of enflurane on the transient absorbance changes of purple membranes was determined at different times – such as 1 hour and 1 day - after the removal of enflurane.

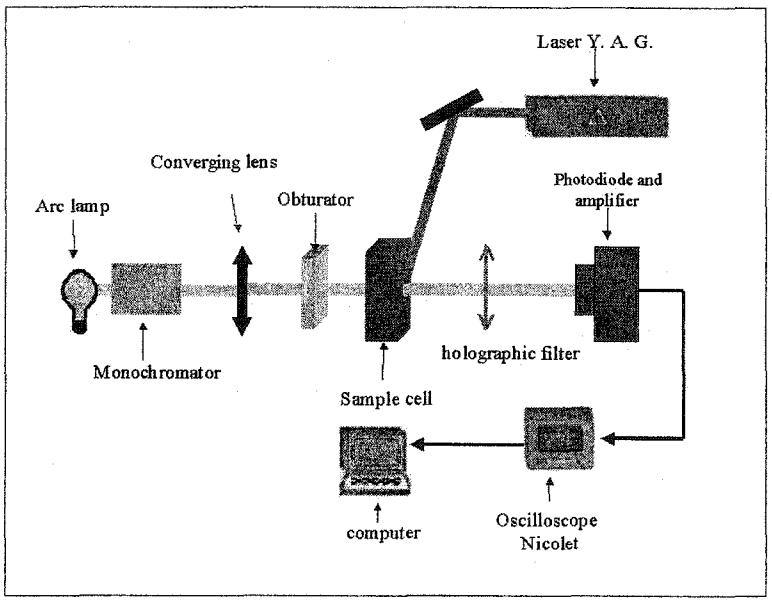

Figure 2. 1 Diagram of measurement of flash photolysis.

2.4 CIRCULAR DICHROISM SPECTROSCOPY

2.4.1 Principle

Circular dichroism (CD) spectroscopy is a form of light absorption spectroscopy that measures the difference in absorbance of right and left-circularly polarized light by a substance. Circular dichroism can only occur within a normal absorption band and thus requires an inherently asymmetric molecule which has neither central symmetry nor planar symmetry. The secondary and tertiary structures of proteins are asymmetric. Circular dichroism spectroscopy has been extensively applied to the structural characterization of peptides including the examination of conformational changes (e.g., monomer-oligomer, substrate binding, denaturation, etc.) and the estimation of secondary structural content. Like the other forms of absorption spectroscopy (UV/Vis, IR, etc.), CD is particularly powerful in monitoring conformational changes. Due to the excitonic coupling between the three retinal chromophores within the trimer, the native purple membranes give rise to two absorption bands in the circular dichroism spectrum,

a positive band at 520 nm and a negative band at 605 nm. The monomeric bacteriorhodopsin shows only a positive band centered near the absorption maximum[84]. This is convenient in that it allowed us to monitor the modification induced by enflurane in the quaternary structure of bacteriorhodopsin.

2.4.2 Sample Preparation

The sample preparation for CD spectroscopy was the same as that for the UV/Vis absorbance spectroscopy. The purple membrane suspension (3.2 $X10^{-5}$ M bR) was put into an airtight cuvette. The spectra were measured for the purple membranes before addition of enflurane, in the presence of enflurane and after removal of enflurane. The measurements were carried out with a Jasco polarimeter at Boston University.

2.5 DIFFERENTIAL SCANNING CALORIMETRY

2.5.1 Experimental Method

The configuration changes of proteins, the phase transition of lipid membranes and even the denaturation of proteins are thermochemical reactions. Differential scanning calorimetry (DSC) was used to determine the thermophysical and thermochemical properties of these processes. The calorimeter measures heat flows into (endothermic) or out of (exothermic) a sample as it undergoes a phase or configuration change.

Figure 2.2 shows a differential scanning calorimeter. It consists of at least two cells: the sample cell and the reference cell. The sample cell was filled with a weight equivalent to that of the buffer conditioned in the reference cell. The sample and the reference were heated or cooled at the same rate and the difference in heat flow between them was recorded.

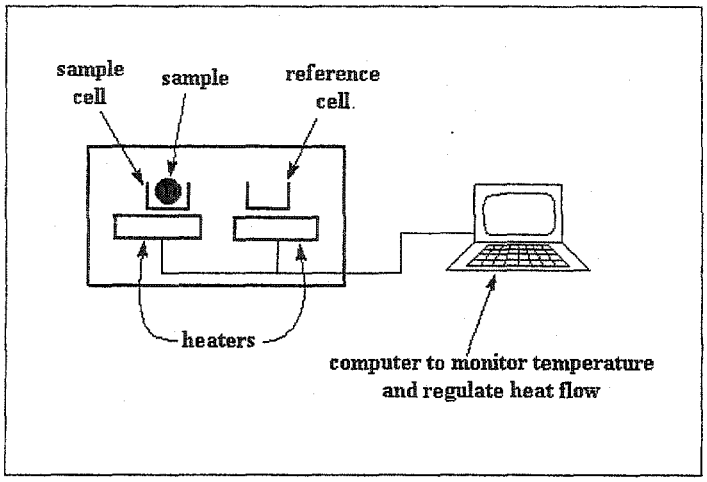

Figure 2. 2 Diagram of a differential scanning calorimeter.

The differential heat flow remained zero or constant until a thermal reaction occurred in the sample. A difference in heat flow was measured as a function of temperature. The direction of the peak indicates whether the transition is endothermic or exothermic. Figure 2. 3 shows an endothermic transition. Tm is the temperature of the midpoint of transition.

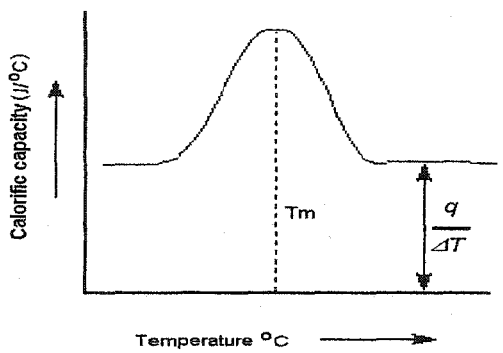

Figure 2. 3 A thermogram of DSC. Tm: the temperature of transition; q: heat flow; ΔT: the change of temperature.

Calorific Capacity

Upon heating the two cells, the computer plots the difference in heat flow from the two heaters against the temperature, that is the heat (q) absorbed or emitted by the sample against the temperature. Calorific capacity is the heat flow in an interval of temperature (ΔT).

$$\frac{q}{\Delta T} = C_p = \text{calorific capacity}$$

2.5.2 Thermal Transition of the Purple Membrane

The thermogram of the purple membrane is composed of a main transition at 95 °C and a large pretransition between 70-80 °C (Fig. 2.4A). Shnyrov et al.[86] interpreted the structural characters of the purple membranes in different temperature ranges by using the annealing procedure. Figure 2.4 demonstrates this technique. Figure 2. 4B illustrates the deconvolution of the thermogram of the purple membrane. This is achieved by heating/cooling cycles on the purple membranes. The structural characters in each temperature range were then analyzed with intrinsic fluorescence spectroscopy and CD spectroscopy. For example, the samples were heated from 20 °C to 66 °C, and one got the curve *a* (Fig. 2. 4B), which represents the thermal change in this temperature range. The samples were cooled to 20 °C and reheated to 82 °C (thick curve *b*, Fig. 2.4B). The samples were again cooled in the cell, and the process was repeated for each transition in succession (thick curve *c* and *d*, Fig. 2.4B). When curve *b* is subtracted from curve *a*, the result shows the initial portion of the curve shape and the temperature of the maximum (Tm) for the first transition. Repeating this procedure gave the data for each transition. The portion of each curve after the maximum was constituted for each transition by assuming a symmetry relative to the corresponding Tm. Thus, the thermogram of the purple membranes is divided into five transitions:

1. The first transition (62 °C) may be related to some molecular rearrangement of the membrane leading to a less compact protein and lipid packing, thus allowing for the exposure of some residues.

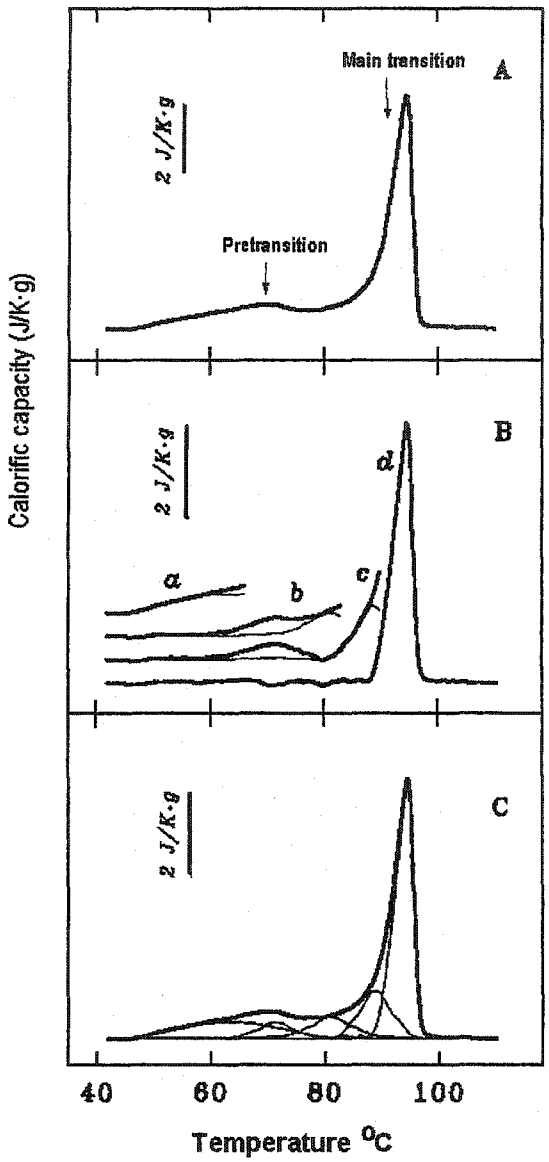

Figure 2. 4 (A) Thermogram of the purple membranes. (B) Demonstration of the successive annealing procedure for the purple membrane. (C) Results of decouvolution of the calorific capacity curve into individual components (thin curves) (Shnyrov L. 1993 [86]).

2. The second reversible transition (70 °C) is due to reversible changes in the bR tertiary structure, which indirectly affect protein-protein interactions with a resulting disorder of the crystal lattice.

3. The third transition (70-85 °C) is the irreversible formation of vesicles.

4. The forth transition (85-95 °C) may correspond to an irreversible conformational change in bR.

5. The fifth annealing transition (>95 °C) would lead the protein to the final denatured state and may also be related to the complete destruction of the membrane.

From this analysis, the pretransition in the thermogram of the purple membrane includes the first, the second and the third transition, transitions which correspond to some molecular rearrangement of the membrane, reversible changes in the bR tertiary structure, as well as some irreversible changes when the temperature is higher than 70 °C. The main transition corresponds to the denaturation of the bR structure. Thus examination of the thermogram of anesthetic-treated purple membranes allowed us to determine how enflurane affects the structure of purple membranes.

2.5.3 Sample Preparation

The concentration of bR for DSC - about 1 X 10^{-4} M - was higher than those used for other experiments. Since this concentration was too high to measure the absorption spectrum for the determination of the transition, the stock PM suspension was diluted with a 100-mM KCl and 50-mM phosphate buffer (pH=7.5) to a final bR concentration of 0.8 X 10^{-5} M. Enflurane was added to induce the transition of the purple membranes. The absorption transition of the purple membranes was assessed by UV/Vis absorption spectroscopy. Next, such enflurane-treated purple membranes were concentrated by ultracentrifugation at 50,000 g, for 1.5 hours. The purple membranes were re-suspended to a bR concentration of 1 X 10^{-4} M. The samples were degassed before DSC measurement. The thermograms were measured at a scanning rate of 1 °C/min with a Hart (4207) differential scanning calorimeter.

2.6 X-RAY DIFFRACTION AND THE PURPLE MEMBRANE

2.6.1 Sample Preparation and X-ray Diffraction Measurement

For X-ray diffraction measurements, the purple membranes were suspended in the buffer containing 10 mM Tris-aminomethane and 100 mM NaCl (pH=8.1) at a bR concentration of 2.5 X 10^{-5} M. The samples (native membranes, membranes added with enflurane and membranes from which the anesthetic had been removed) were added in 1.5 mm capillary tubes, sealed and centrifuged to pellet the membrane. X-ray diffraction was measured at small (SAXS) angles on D43 and D22 stations of the DCI synchrotron facility at the Laboratoire pour l'Utilisation du Rayonnement Electromagnétique (L. U. R. E.) (Orsay, France). A 1.45 Å monochromatic X-ray beam was focused by a Ge (111) crystal. The beam defined by a 500-μm collimator was collected after diffraction using an image-plate, then digitized and analyzed. The diffraction spacing was calibrated using liquid crystalline silver Behenate (d = 53.380 Å). The diagram of diffraction of the samples was corrected with water.

2.7 ATOMIC FORCE MICROSCOPY

2.7.1 Principle

Atomic force microscopy (AFM) is a direct method for observing various surfaces, including biological samples. Since it has a very regular crystalline lattice of trimers, the purple membrane was selected as a model for applying the AFM to the membrane protein. Lewis et al. have observed the dynamic light-induced conformational alterations in bacteriorhodopsin using this technique[88]. It is possible to measure the image of purple membranes before and after anesthetic treatment. Figure 2.5 illustrates the principle of atomic force microscopy. AFM consists of a mica glass sample holder slide and of a piezoelectric crystal stage. The probe tip on the end of a cantilever arm moves up and down as it scans the

surface of the sample. This vertical motion is monitored by a laser and recorded by a photodiode detector. In this way, the sample is scanned with a constant force and the resulting z piezo motion produces a topographical map of the region scanned with a high resolution.

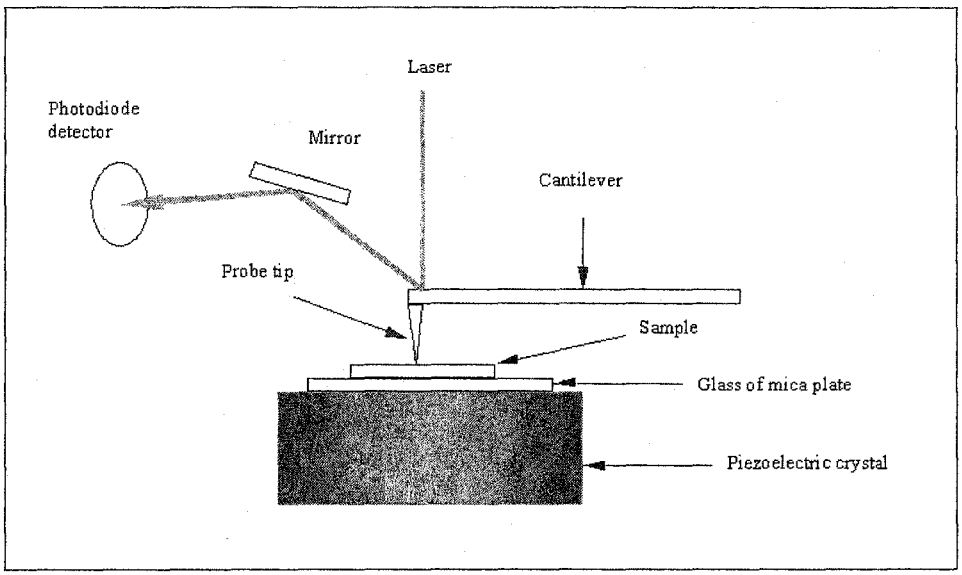

Figure 2. 5 Principle of atomic force microscope.

2.7.2 Sample Preparation

50 μl of purple membrane suspension (10 μg/ml bR) was deposited on mica discs. After 10 to 30 minutes, the sample was gently washed with a buffer to remove membranes that were not firmly attached to the mica substrate. Since enflurane evaporates during the deposit of samples on mica discs, it is impossible to make a measurement in the presence of anesthetics. The AFM images of samples (the native purple membranes and the sample previously treated with 0.5% enflurane or ether) were measured in the scanning mode on the set up of professor Herman Gaub at the Physical Institute in Munich.

2.8 FOURIER TRANSFORM INFRARED SPECTROSCOPY

Infrared spectroscopy is a useful technique for determining the conformation and orientation of membrane-associated proteins and lipids. The technique is especially powerful for detecting conformational changes by recording spectral differences before and after perturbations. The presence of the lipid bilayer does not limit the spectroscopic resolution or sensitivity, and membrane proteins can be studied in their native lipid environment. Since the vibrational modes of lipids and proteins are present in the IR spectrum, the influence of different lipid structures on the protein, and vice versa, can also be investigated by infrared spectroscopy.

2.8.1 Principle

The bands corresponding to the structure of the proteins and lipids in infrared spectroscopy have been widely studied[89, 90]. Tables 2.1 and 2.2 show the assignments of the bands of membrane proteins and lipids.

Table 2. 1 Amide bands of proteins

Designation		Frequency range (cm^{-1})	Description[a, b]
Amide A		~3300	NH_s
Amide B		~3100	NH_s
Amide I	α-helix	1600	CO_s (76%), CN_s, (14%), CCN_d (10%)
	β-sheet	1634,1670	
Amide II		1545	NH_{ib} (43%), CN_s (29%), CO_{ib} (11%), CC_s (9%), NC_s (8%)

[a] The percentages are approximate and refer to the potential-energy distribution calculated for N-methylacetamide (Bandekar, 1992).

[b] s, stretch; d, deformation; ib, in-plane bend.
(Adapted from Krimm and Bandekar[91], 1986)

Table 2. 2 Important infrared absorption bands of membrane lipids

Assignment	Approximate wavenumber (cm^{-1})[a]
CH_3 asymmetric stretching	2956 (s)
CH_2 asymmetric stretching	2920 (s)
CH_3 symmetric stretching	2870 (s)
CH_2 symmetric stretching	2850 (s)
CH_3 asymmetric bend	1640 (m)
CH_3 symmetric bend	1378 (m)
PO_2 asymmetric stretching	1228 (s)
PO_2 symmetric stretching	1085 (m)
CO—O—C symmetric stretch	1070 (m)
[a] s, strong; m, medium; w, weak.	
(Adapted from Krimm and Bandekar[92], 1986)	

These bands are well resolved in the infrared spectrum of purple membranes. With these assignments of bands we can determine the structural changes of purple membranes induced by enflurane.

2.8.2 Preparation of Purple Membrane Films

The purple membrane films were prepared with purple membranes suspended in a low concentration of buffer. The stock purple membrane suspension was centrifuged at 50,000 g for 40 minutes. The pellet was re-suspended in 1 mM KCl and 0.5 mM $phosphate_4$ buffer, pH=7.5 to eliminate buffer interference. A 25-μl purple membrane solution (1 X 10^{-5} M bR) was placed on the CaF_2 window, and the film of the purple membrane was dried at ambient temperature.

2.8.3 Infrared Spectrum Recorded upon Addition and Removal of Enflurane

Infrared spectra of purple membranes were obtained with a Perkin-Elmer spectrum 2000 spectrometer equipped with a MIRTGS detector and continuously purged with N_2 dryer to remove humidity. Each spectrum was an average of 400 scans and was recorded at ambient temperature (roughly 22-23 °C) with a 4 cm^{-1} resolution. The window supporting the purple membrane film was placed on a specially designed support (Fig. 2.6).

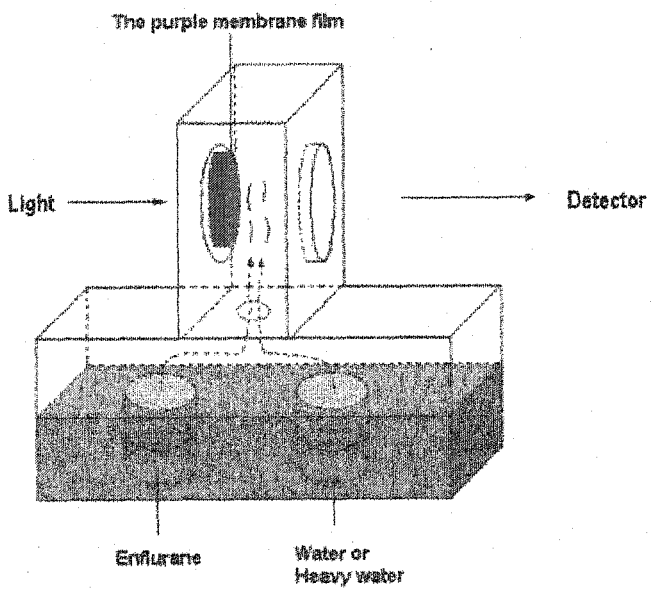

Figure 2. 6 A schematic view of the support used for the enflurane-treated purple membranes.

The window with the samples was placed on one side of the support. The other side of support was closed by another empty window. On the base of the support, there are two wells. 1 ml enflurane was

added to one well and 1 ml H_2O or D_2O was added to the second, depending on the requirement of the experiment. Water or heavy water was put into the well one day before the measurement and the purple membranes were equilibrated with water molecules during the night. This ensured that enflurane induces the transition of the purple membrane to its red form[92]. Enflurane was added on the second day due to its high vapor pressure, it spontaneously evaporated from the well to the purple membrane film on the window, inducing the 570 nm to 480 nm spectral transition. The infrared spectrum of the purple membrane film was recorded as a function of time once enflurane was added into the well while the color transition was assessed by absorption spectroscopy. After such measurements, the empty window was removed. Enflurane thus evaporated and the infrared spectrum was recorded during enflurane evaporation as a function of time.

2.9 ANALYSIS OF PHASE TRANSITION OF DPPC WITH INFRARED SPECTROSCOPY AND FLUORESCENCE SPECTROSCOPY

2.9.1 Principle

Phospholipid bilayers constitute the primary structural element in biological membranes, and their physical properties are of considerable experimental and theoretical interests. Among the properties of lipid membranes, our main focus is on the phase transition. As the temperature increases, the lipid bilayer undergoes a phase transition from a gel to a liquid-crystalline phase at a well-defined temperature Tm. The lipid acyl chains in the gel phase lie on a two-dimensional triangular lattice, and the chains themselves are ordered, being mostly all-*trans*. The phase transition at Tm is characterized by both lattice and chain melting, the latter being characterized by the thermal induction of several gauche bonds. The bilayers in the liquid crystalline phase are two-dimensional fluids in which the lipid molecules laterally diffuse in the plane of the membrane, and their acyl chains are disordered (Fig. 2.7). There are several ways to monitor

the phase transition of lipid membranes. We used infrared spectroscopy and fluorescence spectroscopy to test the changes in Tm induced by enflurane.

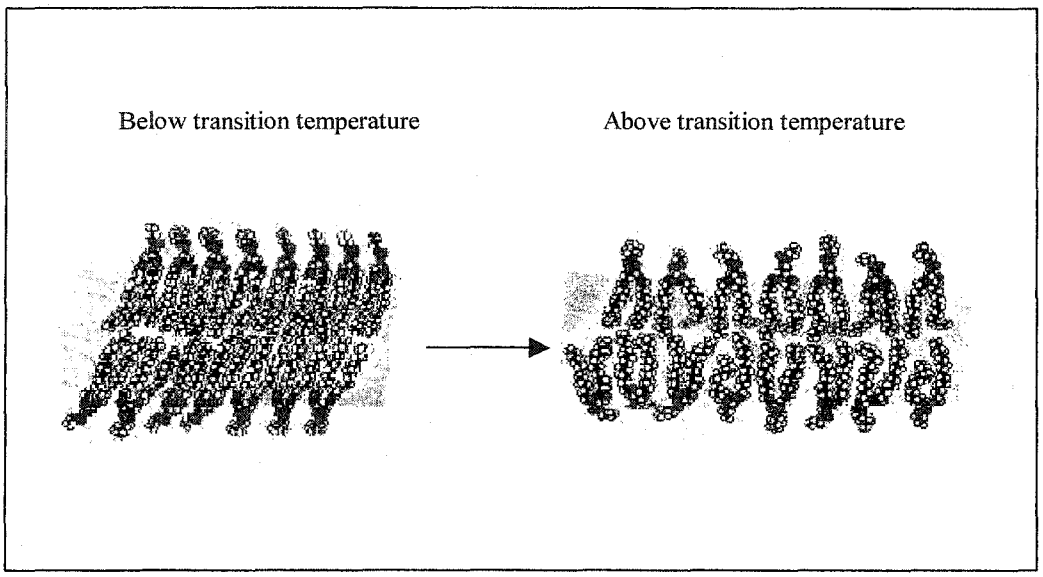

Figure 2. 7 Phase transition diagram of synthetic lipid membranes. Left is the lipid membrane below transition temperature. Right is that above transition temperature.

2.9.2 Infrared Spectrum Record and Preparation of DPPC Films

With an increase in temperature, the DPPC phase changes from a gel to a liquid crystalline phase. In the liquid crystalline phase, the CH group in the acyl chain has more freedom of movement. The frequencies of the CH_2 symmetric stretching modes increase as the temperature rises. Thus, the phase transition of DPPC can be determined by observing the CH_2 stretching modes in the 3000 – 2800 cm^{-1} region. The temperature-dependent infrared spectrum of DPPC was recorded on a Nicolet 4020 spectrometer fitted with a cryostat that enabled accurate temperature control.

The DPPC film was made with a sample containing 10% (w/v) DPPC vesicles. 10 mg DPPC were dispersed in 50 μl H_2O and 50 μl D_2O. DPPC vesicles were heated up to 50 °C, then cooled to room

temperature. This heating and cooling cycle was repeated four to five times to ensure the homogeneity of the DPPC vesicles. For temperature-dependent experiments, 10 μl of the DPPC mixture was dispersed on one of two CaF_2 IR windows, spaced by 0.012 mm spacer placed between them. The temperature of the windows was controlled with an automatic temperature controller (Specac Ltd, UK). Because the samples were closed in the two IR windows, it was possible to measure the spectrum in the presence of enflurane. Enflurane was added by injection through a small hole in one of the IR windows. Measurements in the presence of enflurane were made one day after equilibration of enflurane into DPPC vesicles. Enflurane was removed by exposing the sample to room atmosphere. Spectra were recorded one day after the removal of enflurane.

2.9.3 Fluorescence Spectrum Record and Sample Preparation

The fluorescent dye Laurdan (6-dodecanoyl 2-dimethyl aminonaphthalene) has been widely used for the past seven years to probe lipid membrane dynamics[93, 94, 95]. The probe intercalates between the membrane lipids due to its hydrophobic tail, while its fluorescent head lies in all likelihood below the hydrophilic polar heads of the membrane lipids. The emission spectrum of Laurdan in DPPC vesicles is very sensitive to the physical state of the surface of lipid bilayers. When the temperature is raised from 25 °C to 45 °C, the emission maximum of Laurdan shifts from 435 nm to 490 nm (Fig. 2. 8). The transition temperature for the emission maximum from 439 nm to 490 nm is 42 °C. It therefore provides an easy means of monitoring the physical state of lipid bilayers.

The phase transition of DPPC-Laurdan vesicles was followed by fluorescence measurements. The vesicle suspension was placed in a quartz cuvette in a computer-controlled Fluoromax fluorimeter (Spex Instruments, Jobin Yvon, Longjumeau, FRANCE) equipped with 4 photomultipliers [96]. The cell holder was thermostated using a cryostat (RC6, Lauda, Germany), and a homemade system was used to raise the temperature of the cell holder from 20 °C to 50 °C at a constant rate of 0.5 °C/min. To assess any temperature difference between the sample and the cryostat, blank calibration runs were performed with a

thermocouple immersed in a 2-ml vesicle sample before and after each series of measurements. The emission spectrum of Laurdan between 380 nm and 650 nm (λ_{ex}=360 nm) was continuously recorded during the temperature rise.

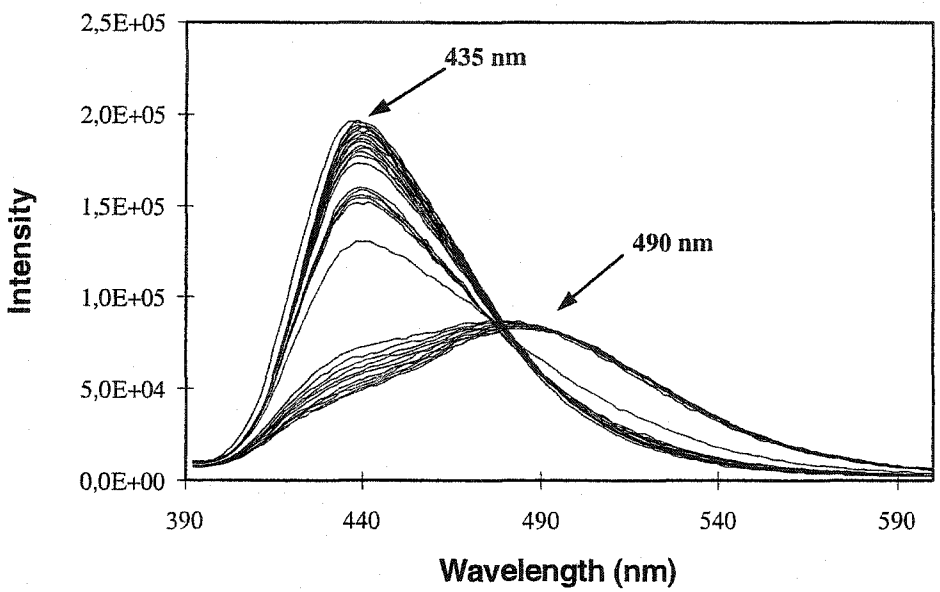

Figure 2. 8 Fluorescence spectrum of Laurdan in DPPC vesicles recorded as the emission maximum shifts from 435 nm to 490 nm upon the rise of temperature from 25 °C to 45 °C.

DPPC, solubilized in chloroform, was added with Laurdan (final Laurdan to lipid ratio: 0.1 mol %). The lipids were dried under nitrogen and lyophilized overnight. The dry lipids were hydrated in a buffer (10 mM Tris, 150 mM KCl, pH=8) at 50 °C to a concentration of 10% and vortexed to form a suspension of lamellar phase. The lamellar suspension was sequentially extruded at 45 °C through Nucleopore filters (pore diameters of 0.8, 0.4, 0.2, 0.1 and 0.05 μm) to finally obtain large homogeneous unilamellar vesicles, about 150 nm in diameter, as estimated from the light scattering measurement.

2.10 CHEMICALS

Chemicals used were from the Sigma or Aldrich company. They were of the finest grade available. More specific reactants are described here below.

Enflurane: Company Anaquest

$C_3H_2ClF_5O$,

F. W.:184.4932

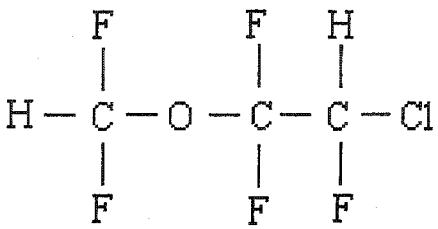

Halothane: Hoescht Canada Inc. Québec.

$C_2HBrClF_3$

F. W. :197.38

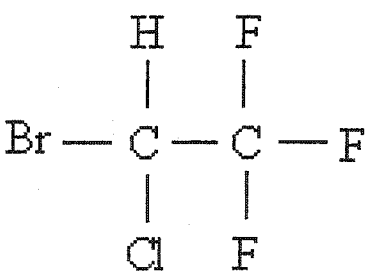

Laurdan: Molecular Probes, Inc.

6-dodecanoyl-2-dimethylaminonaphthalene

F. W.: 354

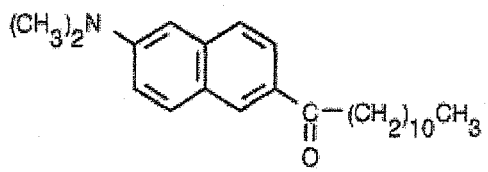

CHAPTER 3

RESULTS AND DISCUSSION

3.1 ANESTHETICS AND THE SPECTRAL PROPERTIES OF PURPLE MEMBRANES

3.1.1 The Characteristic Spectrum of Purple Membranes in the Presence of Anesthetics

In the presence of enflurane, as with any other halogenated anesthetic, there exists an equilibrium between two spectral forms of bacteriorhodopsin. As the anesthetic is added, the original absorption band located at 570 nm progressively disappears at the expense of a new band at 480 nm. Figure 3.1 shows the spectra of the purple membrane upon the addition of 0.06, 0.09, 0.12, 0.15, and 0.18% (v/v) enflurane respectively. The absorption change is reversible. About 92% of the absorption at 570 nm recovers when enflurane evaporates from the sample under a mild vacuum. The maximal absorbance at 480 nm disappears (Fig. 3.1, dotted line). The absorbance difference spectra recorded for this conversion between bR_{570} and bR_{480} are shown in Figure 3.2. It can be clearly seen that the absorbance decreases at 570 nm and increases at 480 nm with increasing concentrations of enflurane.

The change in absorbance induced by anesthetics is pH dependent. Figure 3.3 shows the percentage of bR converted to the red 480 form by enflurane as a function of pH. The concentration of bacteriorhodopsin is the same as that shown in Figure 3.1. The concentration of enflurane is 0.1% (v/v). At this concentration, the purple membrane does not change completely to its red form, but the change of bR absorption still shows an acid-base equilibrium between the red and purple forms. The apparent pKa is 7.3. When the pH is lower than 7.3, the maximal absorbance remains at 570 nm unless very high concentrations of enflurane are used. When the pH is higher than 7.3, the red form of bR appears at a relatively low concentration of enflurane. We have chosen pH=7.5 in the following experiments to examine the structural and functional changes of the purple membrane.

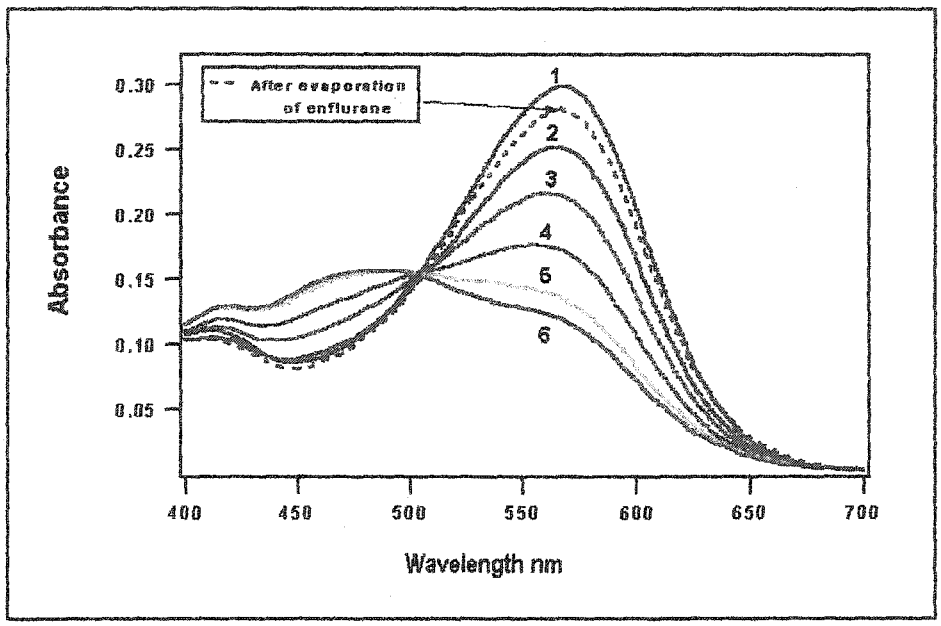

Figure 3. 1 Spectral shift of purple membranes (0.5 X 10^{-5} M in bR) suspended in 100 mM KCl, 50 mM phosphate buffer (pH=7.5) upon the addition of enflurane. Spectra 1 to 6 correspond to 0, 0.06, 0.09, 0.12, 0.15, and 0.18% (v/v) enflurane, respectively. The dotted line represents the spectrum of purple membranes after the evaporation of enflurane.

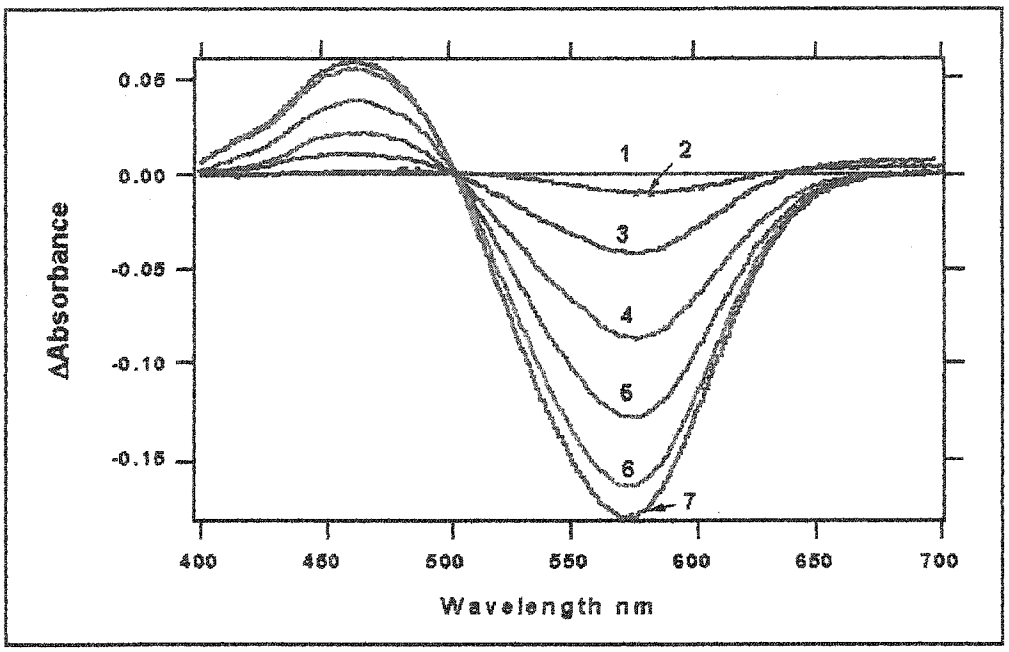

Figure 3. 2 Absorbance difference spectra of the purple membrane in 100 mM KCl, 50 mM phosphate buffer (pH=7.5) recorded after the addition of the sample with 0, 0.03, 0.06, 0.09, 0.12, 0.15, and 0.18 % (v/v) enflurane represented by spectra 1 to 7.

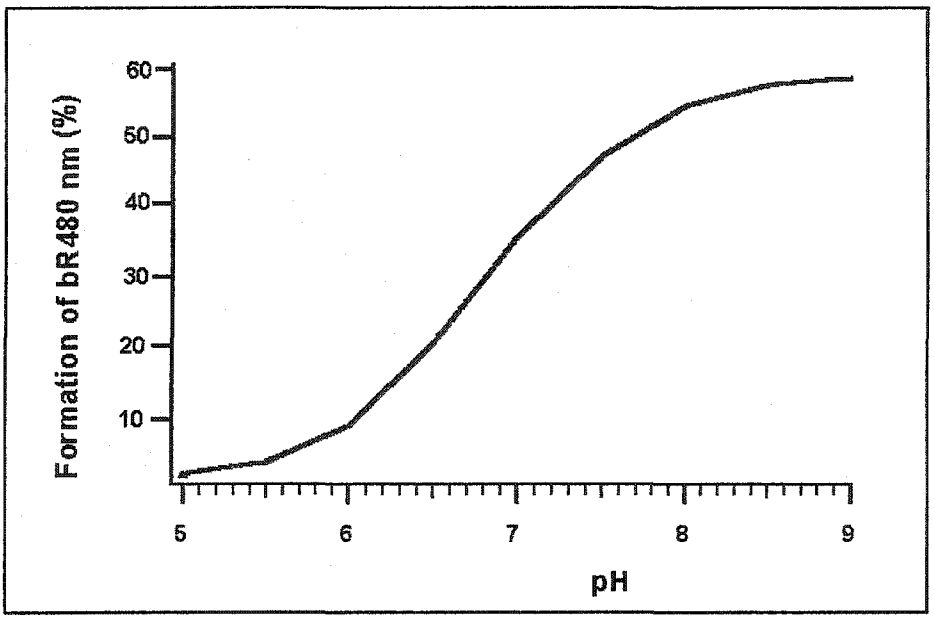

Figure 3. 3 Percentage of formation of bR_{480} as a function of pH in the presence of 0.1 % (v/v) enflurane.

3.1.2 Effects of Anesthetics on the Absorption Spectrum of Purple Membranes: the Dose-Response Curves

The dose–response curve for conversion of bR_{570} to bR_{480} is not simple. In Figure 3.4, we show the result of the measurement of this conversion upon the continuous addition of enflurane into the sample. For that particular experiment, the sample in a 3 ml cuvette was installed on a syringe pump. Enflurane was injected into the sample at a speed of 0.08 μl per minute for 3 hours. The curve in this figure is expressed as the fraction of the maximal absorbance change at 570 nm and it clearly indicates a cooperative transition where most of the bR absorbance change occurs between 0.2 and 0.3% enflurane.

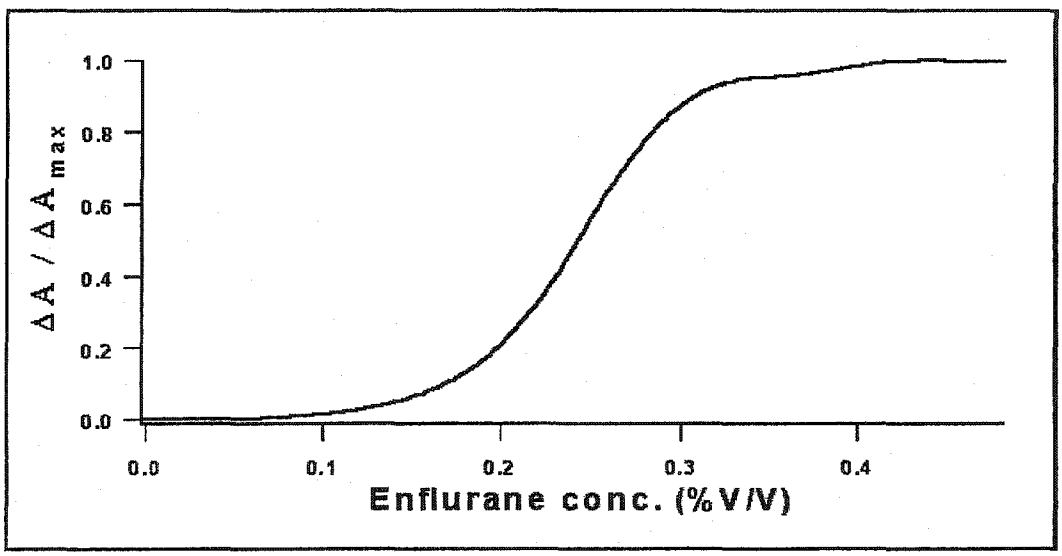

Figure 3. 4 Fraction of maximal absorbance changes at 570 nm upon continuous injection of enflurane in the purple membrane sample at pH=7.5.

This 0.2 – 0.3% (v/v) concentration range is much higher than that observed in the previous experiments. Indeed, in Figure 3.1, we can see that most bR_{570} is converted to bR_{480} near 0.1% (v/v) enflurane. The explanation for such a discrepancy might well be that in the first measurements, the sample were vigorously shaken after each addition of enflurane and the spectra were recorded after a few minutes of equilibration time. On the other hand, when enflurane was added continuously, the high-density enflurane might not mix well with the sample and the curve in Figure 3.4 might not represent equilibrium data.

To check this discrepancy, we have repeated the experiment but with stepwise anesthetic addition, each followed by vigorous sample shaking. The result is shown in Figure 3.5. We can still observe the cooperative behavior of the transition but in a much lower enflurane concentration range: 0.06 to 0.15% (v/v).

Finally the question of reversibility of the phenomenon remains. It is known for a while that if samples are left open to the ambient atmosphere or maintained under a mild vacuum after treatment with anesthetics, the anesthetic evaporates rapidly and bacteriorhodopsin recovers its characteristic purple color. Such so-called "anesthetic-treated" samples were tested for their ability to respond to a second treatment with an anesthetic. In this experiment, the sample was treated with enflurane, converted to bR_{480}, submitted to vacuum to remove enflurane and, after it had recovered its maximal absorbance at 570 nm, we added enflurane for the second time and measured its response to the anesthetic. Figure 3.6 shows the absorbance changes at 570 nm and 480 nm upon the second addition of enflurane to such a sample. Most of the transition occurs between 0.03 and 0.09% (v/v) enflurane, which are still lower than that shown in Figure 3.5.

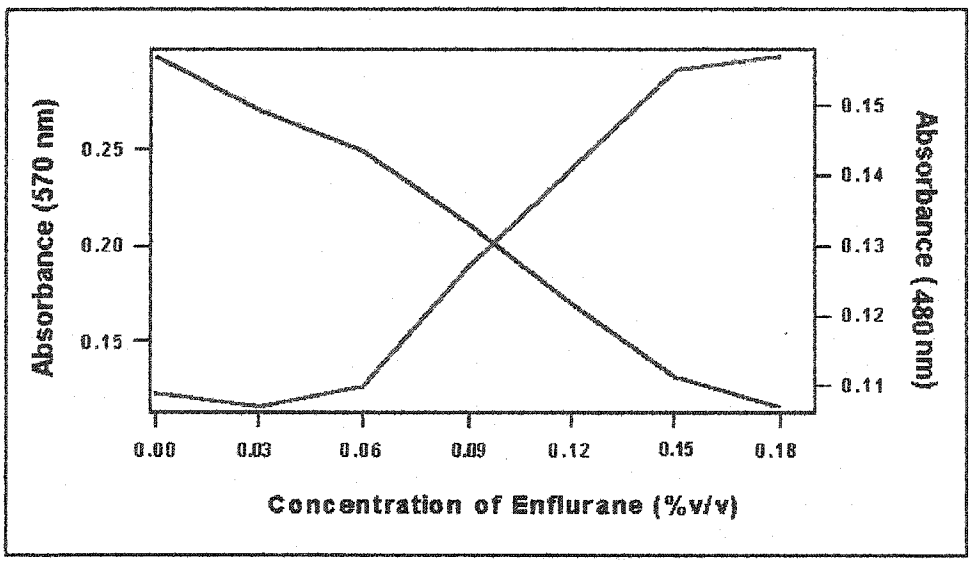

Figure 3. 5 Absorbance changes of the native purple membrane at 570 nm (purple) and 480 nm (red) as a function of the concentration of enflurane.

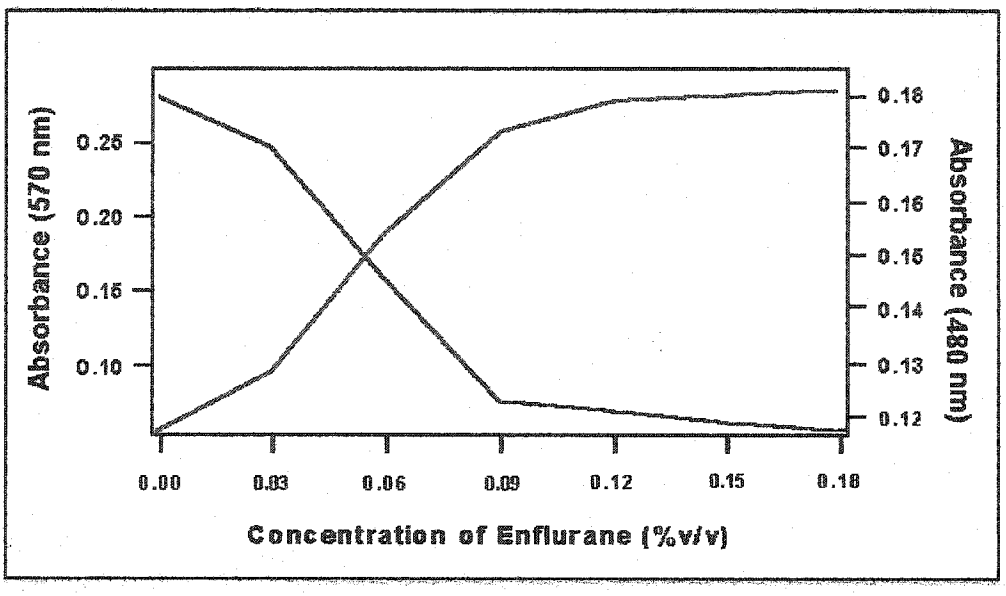

Figure 3. 6 Absorbance changes of the purple membrane at 570 nm (purple) and 480 nm (red) as a function of the concentration of enflurane for the second enflurane treatment.

The cooperativity is preserved in the second anesthetic addition but the transition occurs at a still lower anesthetic concentration. It may indicate that some enflurane remained in the sample after evaporation or that some permanent structural change has occurred during the first anesthetic addition.

3.1.3 Analogy between High Temperatures and Anesthetic Effects

In addition to delipidation or the addition of xenobiotics, a rise in temperature from 20 to 70 °C is also known to reversibly produce the same red bacteriorhodopsin spectral form[97]. As the temperature increases, the absorbance progressively decreases at 570 nm and increases at 480 nm (Fig. 3. 7). The maximal absorbance at 570 nm recovers when the sample is cooled down to room temperature.

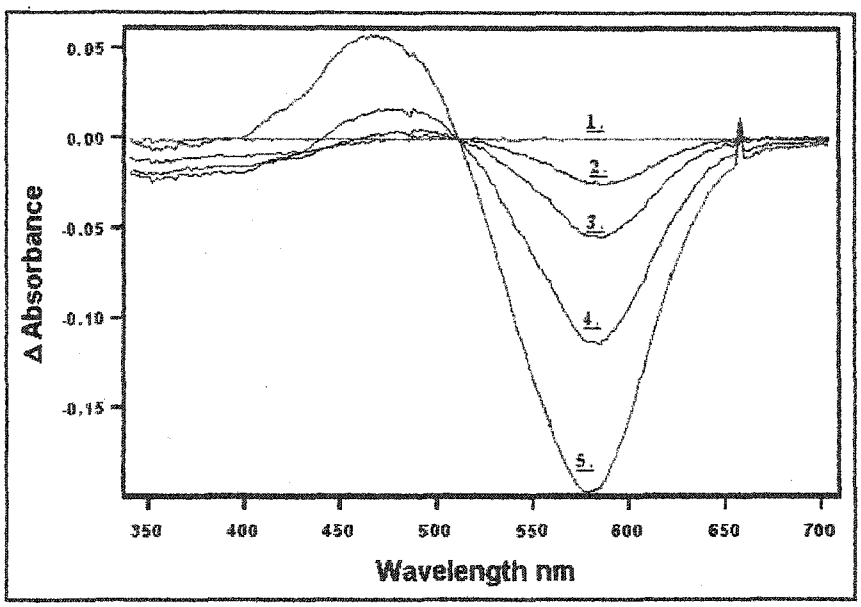

Figure 3. 7 Absorption difference spectra of purple membranes in 100 mM KCl and 50 mM phosphate buffer (pH=7.5) upon heating. Spectra 1 to 5 correspond to differences observed at 20, 40, 50, 60 and 70 °C, respectively.

The $bR_{570} \Leftrightarrow bR_{480}$ equilibrium induced by high temperatures is also pH dependent and shows the same apparent pKa as that observed in the presence of enflurane. Figure 3.8 shows the percentage of formation of the bR red form as a function of pH. The solid line represents the percentage of formation of the red form in the presence of 0.1% (v/v) enflurane, and the triangles correspond to the percentage of formation of the red form at 70 °C.

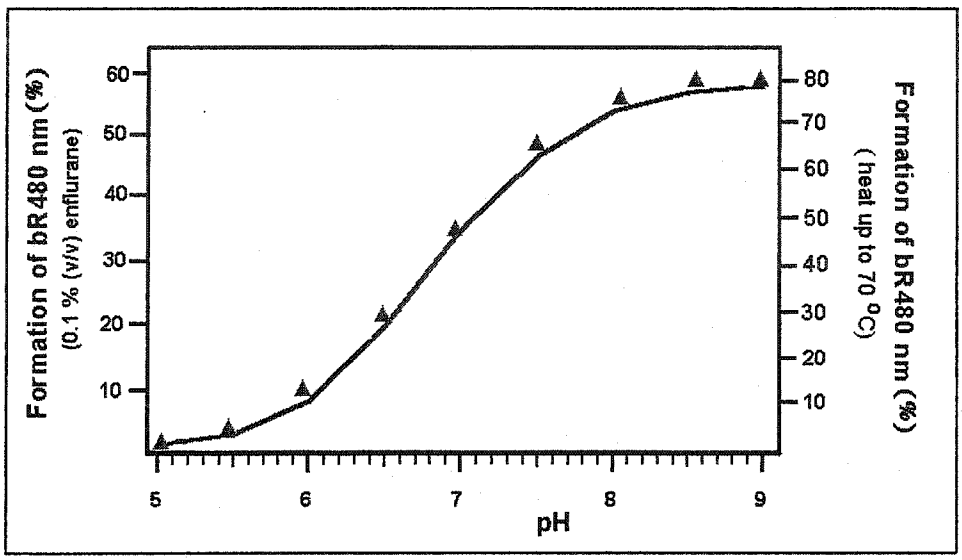

Figure 3. 8 Percentage of bR_{480} formed at different pH in the presence of 0.1% enflurane (solid line) or upon heating to 70 °C (Triangle dots).

The similarity between high temperatures and enflurane is also found in the thermal characteristics of the purple membrane. Shnyrov and Mateo observed two transitions in the thermogram of the purple membrane: one is the pretransition, representing the organization of the purple membrane; the other is the main transition, which corresponds to the structure of bR helices. Heating samples to 70 °C removes the pretransition of purple membranes, because a high temperature disturbs the organization of the purple membrane[86]. If a high temperature (up to 70°C) changes the membrane organization and eliminates the

pretransition, the question arises as to whether or not enflurane has the same effect on the purple membrane. Consequently, we examined the calorimetric properties of purple membranes after a 0.2% (v/v) enflurane treatment at room temperature. We added enflurane into the sample and shook it well. The absorbance spectrum shows a full transition of the $bR_{570} \Rightarrow bR_{480}$ (Fig. 3.9). After enflurane was removed, the sample recovered its purple form. It was then degassed and submitted to calorimetric measurement.

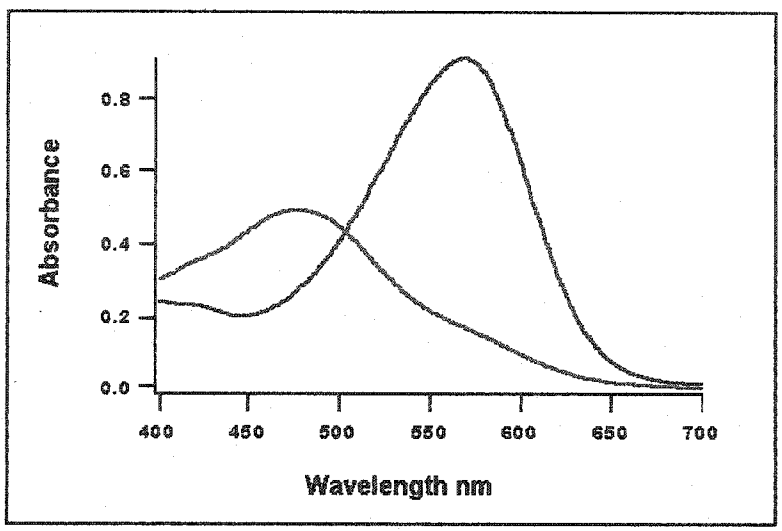

Figure 3. 9 Absorbance transition of the native purple membrane (purple) to its red form (red) in the presence of 0.2% (v/v) enflurane.

Figure 3.10 illustrates the calorimetric thermogram of native purple membranes (upper trace) and enflurane-treated purple membranes (lower trace). There are two transitions for the native purple membrane - a pretransition and a main transition. The pretransition is shown with two hachure areas - one purple, the other red. After enflurane treatment, the red part disappears, and only the purple part remains (lower trace). Enflurane eliminates most of the pretransition. The result shown here thus compares with that induced by high temperatures[97].

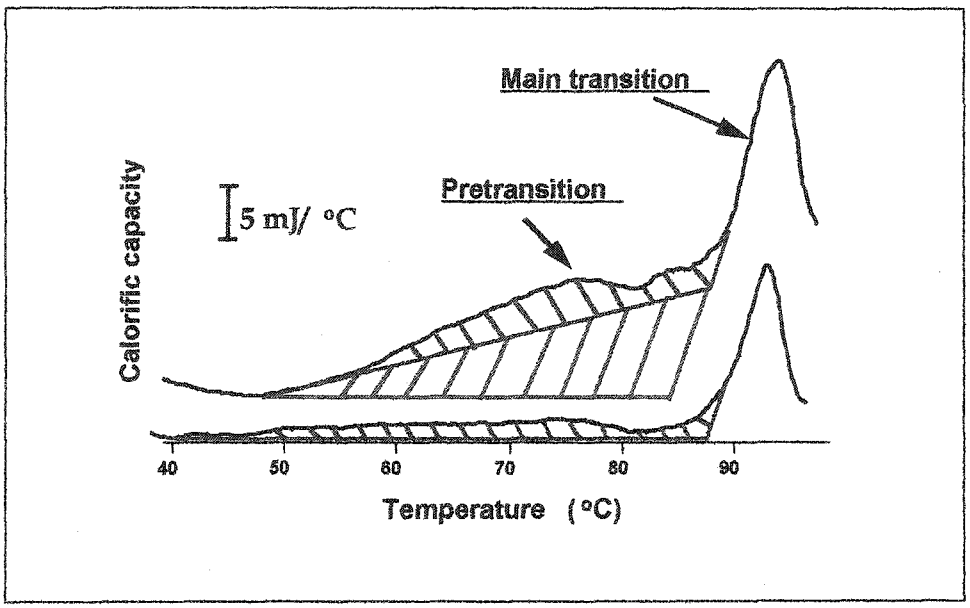

Figure 3. 10 Differential calorimetric scanning profiles of purple membranes (150 μM bacteriorhodopsin) suspended in 100 mM KCl and 50 mM phosphate buffer (pH=7.5) observed for native membranes (upper trace) and anesthetic-treated membranes (lower trace).

From a physiological point of view, there is little interest in comparing the effects of enflurane and high temperatures. From a molecular point of view, however, a comparison of these effects may prove useful. Similar effects between high temperature and enflurane make it possible to interpret the changes induced by enflurane in the purple membrane. If the high temperature disturbs the original membrane organization, enflurane has the same effect on the purple membrane. The structural change induced by enflurane does not recover after removal of enflurane. More importantly, at room temperature enflurane induces an apparently irreversible structural change that otherwise occurs only at rather high temperatures.

3.1.4 Conclusion

These results lead us to conclude that:

1. One should be extremely careful when establishing a dose for an anesthetic effect. Indeed, when we compare a dose-response relationship on comparable samples, a midpoint effect may be observed at a concentration that depends on the procedure. Of course, both Figures 3.4 and 3.5 show cooperative transitions at different concentrations. The difference between them may depend on the fact that in the continuous addition experiment (Fig. 3.4), the measurement was not made under equilibrium conditions.

2. From the results shown in Figures 3.5 and 3.6, we find that samples that have previously been in contact with an anesthetic seem to undergo a permanent structural change. This structural change may also account for the incomplete recovery of absorption after enflurane treatment (Fig. 3.1). They are thus likely to keep some memory of the anesthetic. At this point, one cannot rule out the possibility that this memory has the form of a trace amount of enflurane.

3. On the other hand, the permanent structural change induced by an anesthetic may well be subtle since the absorbance transition retains its cooperative character, even under conditions where the pretransition in the thermogram disappears almost completely.

As a result, we may tentatively conclude that enflurane may severely affect the organization of purple membranes, but that a local structural feature immediately appears to recover after enflurane is removed, thereby maintaining the cooperativity of the absorbance transition. The local structure may involve the trimers of bacteriorhodopsin. The following experiments will show which local structure recovers after enflurane treatment.

3.2 ANESTHETICS AND THE PHOTOCHEMISTRY OF THE PURPLE MEMBRANE

Bacteriorhodopsin transports a proton across the membrane by absorbing a photon. The proton transport cycle of bR is triggered by the deprotonation and reprotonation of the retinal. These deprotonation and reprotonation steps are accompanied by a large spectral change - the formation and decay of the intermediate M_{412}. Upon the flash excitation of bR, it is possible to follow the kinetics of M rise and decay during the photocycle with a time resolution spectrophotometer.

No proton is pumped across the membrane in the presence of enflurane, but the bR photocycle still has its unprotonated intermediate M. The curves in Figure 3.11 show the absorbance changes during M rise (Fig. 3.11, upper panel) and decay (lower panel) as a function of time. The different curves were recorded in the presence of increasing enflurane concentrations in the purple membrane sample. As the enflurane concentration increases, the half-time for the M-rise kinetics decreases from 250 μs to about 20 μs. The M-decay kinetics shows a more complicated behavior. Indeed, careful examination of the curves in Figure 3.11 indicates that at an enflurane concentration as low as 0.03% (v/v), the first part of the kinetics is faster, while its last part slows down in comparison with the intact membrane sample. This M decay corresponds to chromophore reprotonation and was analyzed in greater detail.

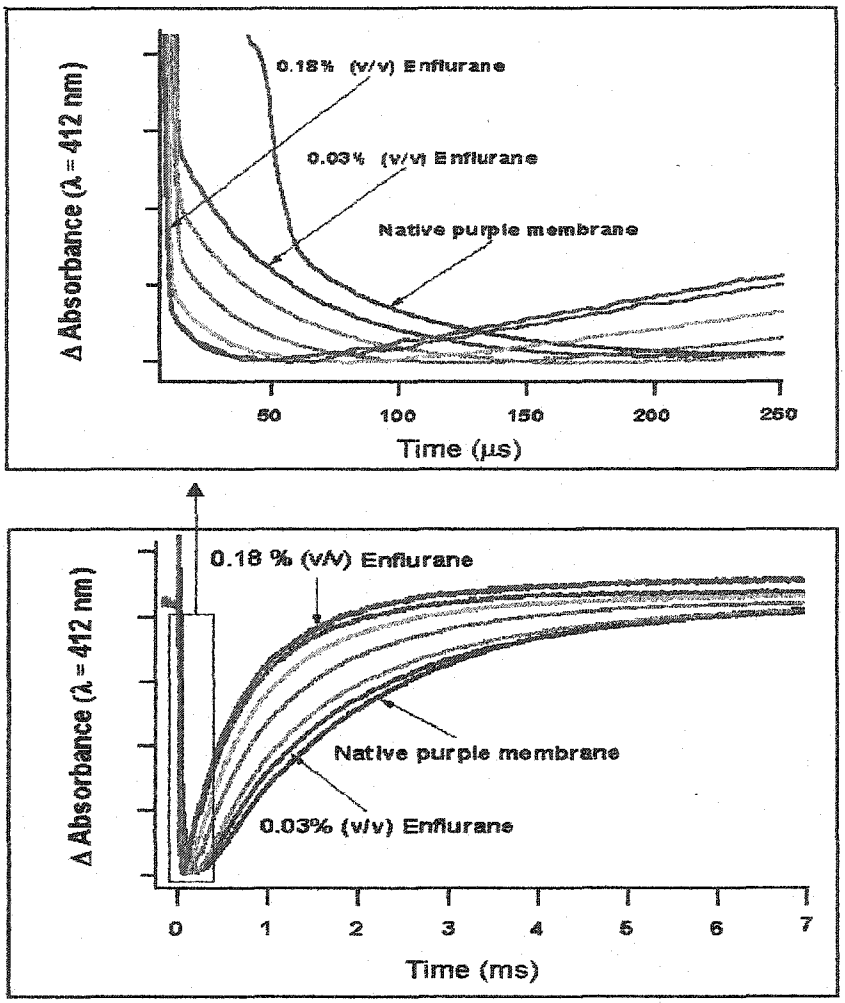

Figure 3. 11 Absorbance changes during rise (upper panel) and decay (lower panel) of the intermediate M of bacteriorhodopsin (0.5×10^{-5} M) as a function of time. Enflurane concentrations are at 0, 0.03, 0.06, 0.09, 0.12, 0.15, 0.18% (v/v), respectively. Measurement was made at pH=7.5.

3.2.1 Reprotonation Steps of the Chromophore at Different Enflurane Concentrations

For purposes of comparison, the M decay curves were fitted with a double exponential decay by a curve fitting analysis system under Igor Pro 3.12. The double exponential curve can be written as:

$$\mathbf{Y = K0 + K1*exp(-K2*X) + K3*exp(-K4*X)} \qquad (1)$$

Where K0 is the initial value of absorbance, K1 and K3 are the relative quantities (amplitudes) of the two components of the decay, and K2 and K4 are the time constants of two components. X stands for the time axis; thus, the unit of time constant is s^{-1}. When the decay has only one phase, K2 must be close to K4. When a two-phase decay appears, K2 differs greatly from K4. Time constant values thus reflect changes in the M decay rate. The time constant K represents the rate of absorbance change. According to two-exponential expression (1), a high time constant (K2 or K4) signifies a high rate of absorbance change.

Both single and double exponentials express well the M decay before addition of enflurane because the M decay of the native bR has only one phase. This is represented by one time constant in a single exponential fitting or by two equivalent time constants in a double exponential fitting. In the presence of enflurane, only double exponential fittings match the M decay represented by two different time constants.

Table 3.1 shows the time constants and amplitudes of the M decay of bacteriorhodopsin as a function of enflurane concentration according to Figure 3.11. As explained, the K2 and K4 values are very close before enflurane treatment because M decay contains only one phase. When enflurane is added, the M decay splits into two phases. K4 represents the fast component in the M decay, which increases as the concentration of enflurane increases. When the amount of enflurane reaches 0.18% (v/v), K4 is ~ 4 times as high as that of the native sample, and its amplitude is about 50-60% of the total signal. The slow phase is represented by K2. After the addition of enflurane, K2 decreases at a low concentration of enflurane, such as 0.03% and 0.06% (v/v), then reaches ~ 700 s^{-1} when the concentration of enflurane is 0.18% (v/v).

However, this is not to suggest that the slow phase speeds up when we notice the difference between K2 and K4. At this enflurane concentration, K2 is about one-third of K4. The amplitude of K2 is about 40 – 50%. Thus, in the presence of a high enflurane concentration, the M decay is characterized by a very fast phase followed by a slow one.

Table 3. 1 Time constants (s^{-1}) and amplitudes for the decay of the intermediate M of bacteriorhodopsin.

Concentration of enflurane (%v/v)	0	0.03	0.06	0.09	0.12	0.15	0.18
Time constant (K2) (Amplitude)	555 (47%)	373 (44%)	336 (35%)	590 (48%)	699 (40%)	806 (40%)	732 (39%)
Time constant (K4) (Amplitude)	550 (53%)	947 (56%)	1054 (65%)	1653 (52%)	1861 (60%)	2115 (60%)	2220 (61%)

The two different components of the M decay of bR_{480} represent two recovery pathways from the intermediate M to bR: a direct way from 'M' to bR and an indirect way of bR recovery through the intermediate O. As has been shown in 1.5.3, these two recovery cycles occur at the same rate for the native bR. We see that K2 is very close to K4. When bR_{570} changes to bR_{480}, the direct pathway becomes very fast, which corresponds to a high K4, and the indirect way becomes very slow, which corresponds to a relatively low K2.

According to the analysis of the absorption of the purple membrane after enflurane removal, purple membranes recover to their characteristic spectral form. To see if the two-phase M decay recovers its native one-phase characters, we examined the kinetics of M decay after enflurane removal.

3.2.2 Recovery of the bR Photokinetics after Enflurane Removal

After enflurane removal under a vacuum, the color of bacteriorhodopsin returns to purple and the proton transportation recovers[81]; the kinetics of the M decay, however, does not fully recover. Indeed, Figure 3.12 shows the kinetics of M decay one hour after enflurane has been removed under a vacuum and again one day after the samples have been left exposed at room temperature. There are always differences between the enflurane-treated sample and the native sample one hour after the removal of enflurane, and a difference can still be observed one day after the removal of enflurane.

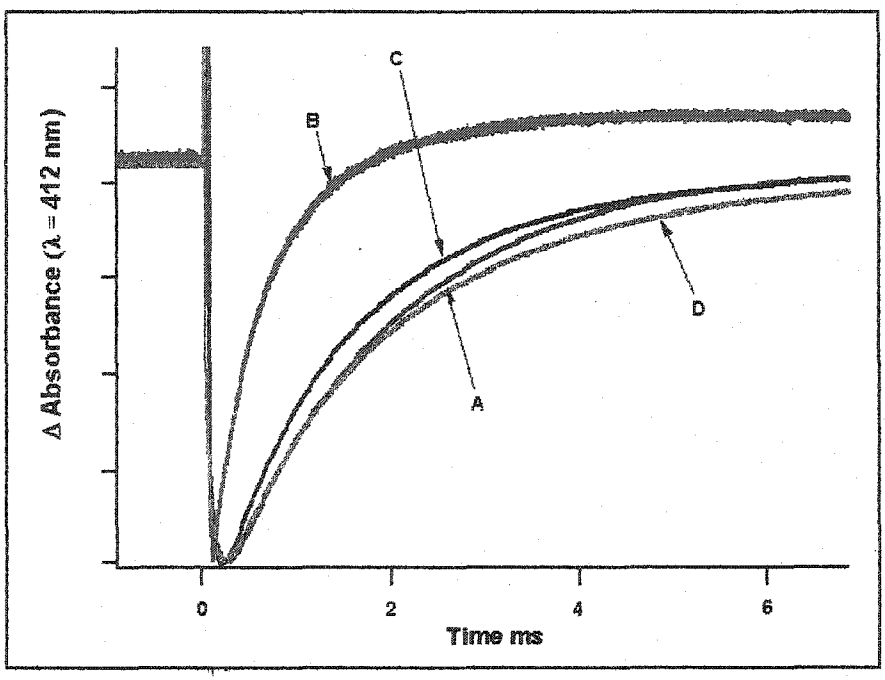

Figure 3. 12 Decay of the intermediate M of bacteriorhodopsin. A. Before enflurane treatment; B. Sample with 0.18% (v/v) enflurane; C. One hour after removal of enflurane; D. One day after removal of enflurane. Measurement was done under the same conditions as for Figure 3.11.

Table 3.2 illustrates the time constants and amplitudes of M decay corresponding to the results in Figure 3.12. In the presence of enflurane, the M decay is represented by a high K4 and a low K2. One hour after enflurane has been removed, both K2 and K4 decrease and approach values for the native membranes. One day after enflurane removal, K4 almost recovers its native value, while K2 (the slow component) becomes very low with an amplitude of about 25%.

Table 3. 2 Time constants (s^{-1}) and amplitudes for the decay of the intermediate M of bacteriorhodopsin after enflurane removal

Treatment	0% (v/v) enflurane	0.18% (v/v) enflurane	Recovery for 1 hour	Recovery for 1 day
Time constant (K2) (Amplitude)	555 (47%)	735 (38%)	408 (39%)	145 (25%)
Time constant (K4) (Amplitude)	550 (53%)	2230 (62%)	828 (61%)	632 (75%)

In the above experiments, we used amounts of enflurane that were high enough to induce a complete spectral transition of bacteriorhodopsin. However, since the remaining effects of enflurane on the purple membrane may be the result of such a high enflurane concentration and since flash photolysis is very sensitive to anesthetics, we examined the effects of a small amount of anesthetic on the M decay.

Figure 3.13 compares the absorbance changes of samples before enflurane treatment, in the presence of 0.03% (v/v) enflurane and one hour after the removal of enflurane. This experiment was performed at pH=6.5, since such a low pH favors the purple form of bR. In the presence of a small concentration of enflurane at pH=6.5, bR remains purple, and the structure of purple membranes is not significantly changed. Under these conditions, the M decay before the addition of enflurane contains one phase (curve

A). After a small amount of enflurane is added, the M decay changes (curve B). Curve C represents the M decay after the evaporation of enflurane.

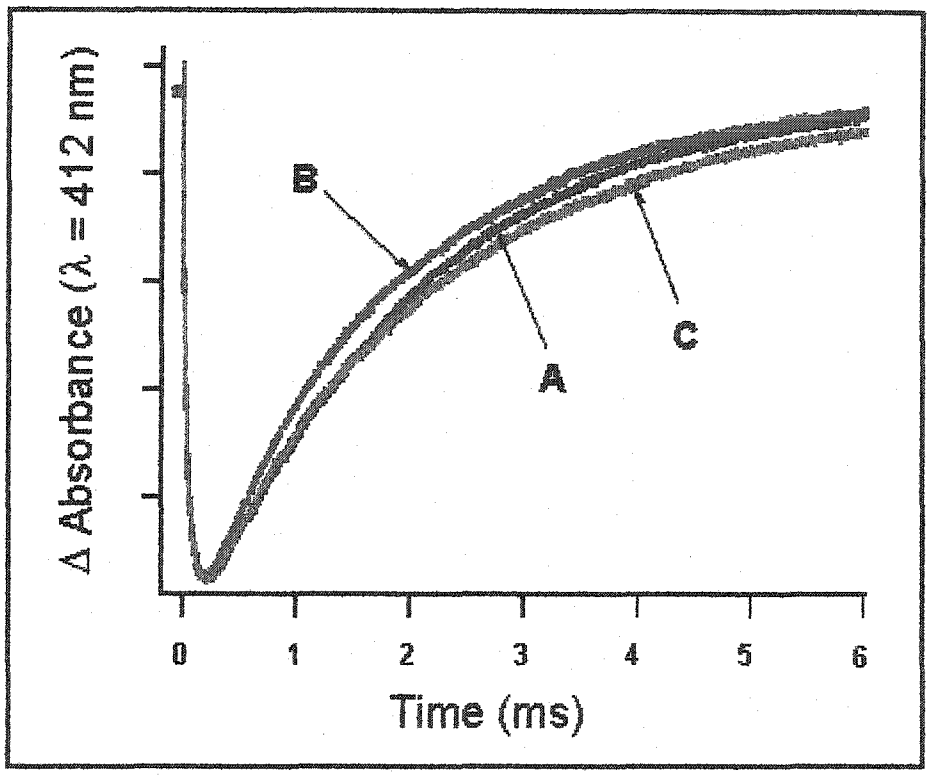

Figure 3. 13 M decay of bR in 100 mM KCl and 50 mM PO_4 buffer pH=6.5. Enflurane concentration is 0.03% (v/v). Curve A: Native samples; Curve B: Purple membranes in the presence of 0.03% (v/v) enflurane; Curve C: Purple membranes one hour after removal of enflurane.

Table 3.3 illustrates the time constants and amplitudes for the M decay. In the presence of 0.03% (v/v) enflurane, K2, which represents the slow phase of decay, does not change very much, and its amplitude is about 70%. K4, which represents the fast phase, is higher than that of the native sample, and its amplitude is about 30%. After removal of enflurane, the M decay still consists of two different phases. Although both values are close to that of the native sample, K4 is still ~ 2 times as high as K2. Obviously, the M decays do not recover completely after the removal of enflurane, whatever the amount of enflurane previously used.

Table 3. 3 Time constants (s^{-1}) and amplitudes for the M decay of sample before enflurane treatment, with 0.03% (v/v) enflurane and one hour after removal of enflurane

Treatment	0% (v/v) enflurane	0.03% (v/v) enflurane	Recovery for one hour
Time constant (K2) (Amplitude)	515 (46%)	490 (70%)	333 (52%)
Time constant (K4) (Amplitude)	504 (54%)	819 (30%)	693 (48%)

Although we cannot state conclusively whether or not the remaining effects of enflurane are due to the small amount of enflurane left in the membrane, the experiments show that full recovery does not occur even when a small amount of enflurane is added and under the pH conditions where bR absorption is not changed. Thus, recovery does not depend on the enflurane concentration.

3.2.3 Conclusion

From an analysis of the kinetics of M decay, we conclude that:

1. In the presence of enflurane, M decay consists of two phases, a fast one and a slow one. After the removal of enflurane, the kinetics of M decay does not recover completely. The M decay still consists of two phases.

2. Incomplete recovery of bR photochemistry occurs when a full absorption transition is induced by enflurane, but it also occurs when a very low concentration of enflurane is added to the sample. At this concentration, no color transition is observed, but the kinetics of M decay changes and does not completely recover. We conclude that the residual effects of enflurane are not the result of the excessive amount of enflurane used in the procedure.

3. Incomplete recovery is observed when enflurane is removed under a vacuum. Since we cannot rule out the possibility that a trace amount of enflurane remains in the sample after evaporation, incomplete recovery may be due to this small amount of enflurane left in the sample.

3.3 ANESTHETICS AND QUATERNARY AND HIGHER ORDER STRUCTURAL CHANGES IN THE PURPLE MEMBRANE

In previous sections we examined the effect of the anesthetic enflurane on the spectral and photochemical properties of bacteriorhodopsin. These properties mainly probe changes in the retinal moiety of the protein, its immediate molecular surroundings and the key residues involved in proton pumping. However, the purple membrane has a complex macromolecular architecture, namely, a crystalline array of bacteriorhodopsin trimers that can be probed by a variety of physical techniques. It thus appears important to examine whether such macromolecular structural organization is affected by the presence of enflurane and to which extent the changes can be reversed.

The crystalline structure of bacteriorhodopsin can be examined by several techniques including differential scanning calorimetry, X-ray diffraction and atomic force microscopy. On a smaller scale,

trimeric organization is better revealed with circular dichroism spectroscopy. The effects of enflurane on purple membranes and its reversibility have been analyzed with the aid of these techniques.

3.3.1 Circular Dichroïsm (CD) Spectroscopy

In its native membrane, the trimeric structure of bacteriorhodopsin gives rise to excitonic coupling between the three retinal chomophores within the trimer. It is generally admitted that this phenomenon is responsible for the bilobed aspect of the circular dichroism spectrum of the retinal, since monomeric bacteriorhodopsin shows only a positive band centered near the absorption maximum[84]. Accordingly, we expect that any modification in the quaternary structure of bacteriorhodopsin should be reflected in its CD properties.

Figure 3.14 illustrates the CD spectra of the purple membrane in the spectral region of retinal absorbance. As we have just mentioned, strong negative and positive bands are seen near 600 and 520 nm respectively (Fig. 3.14, 1). This is the characteristic spectrum of bacteriorhodopsin trimers. At the pH of 8.5 used in this measurement, addition of the sample with a high enflurane concentration (0.6% v/v) rapidly converts all bR_{570} to the bR_{480} form. The high pH and the high concentration of enflurane assure a complete transition from bR_{570} to bR_{480}. At the same time, the characteristic bilobed aspect of the CD spectrum disappears, and there remains only a much smaller band near 470 nm (Fig. 3.14, 2). When the very same sample is submitted to a mild vacuum, or when it is equilibrated with room temperature, enflurane rapidly evaporates. The purple color of bR_{570} is immediately restored under such conditions and the bilobed CD spectrum also reappears.

This simple experiment strongly suggests that the trimeric organization of bacteriorhodopsin is completely lost in the presence of enflurane at a concentration high enough to induce the spectral $bR_{570} \rightarrow bR_{480}$ transition. Recovery of the purple color after enflurane removal is accompanied by the immediate reformation of the trimers. However, the CD spectrum of the trimer does not recover its original intensity even after extensive enflurane evaporation. This indicates that some residual enflurane molecules may

remain trapped in the membrane or that a significant fraction of the purple membrane does not recover - at least not instantaneously - its trimeric structure.

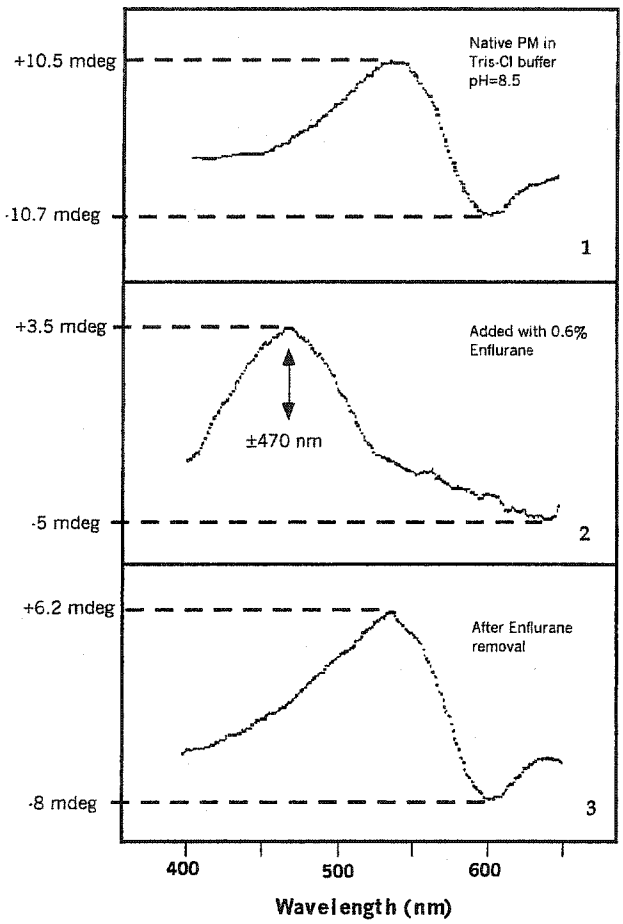

Figure 3. 14 Circular dichroism spectra of the native purple membranes (1), in presence of 0.6% enflurane (2) and after rapid enflurane evaporation under a mild vacuum (3).

3.3.2 Thermal Behavior of the Purple Membrane

Normally, calorimetric analysis does not provide direct structural information on the sample studied. The case of the purple membrane, however, is somewhat peculiar. Indeed, as expected for a membrane containing a unique protein, the thermogram of the purple membrane shows a main transition near 95 °C

corresponding to the irreversible denaturation of bacteriorhodopsin. This principal transition is preceded by a wide pretransition which spreads from 45 to 80 °C. Shnyrov and Mateo[86] showed by thermal annealing that this wide pretransition corresponds to the progressive disruption of the crystalline lattice of the membrane (Section 2.5.2). Thus, it is relevant to probe enflurane-induced structural changes in the purple membrane by this technique.

Since enflurane is highly volatile, we did not measure the calorimetry of the purple membrane in the presence of enflurane. Enflurane evaporates upon degassing before measurement and upon heating during measurement. Nevertheless, if some irreversible changes are induced by enflurane, it should remain measurable even after enflurane removal during sample degassing. Accordingly, we incubated purple membranes (1.4 $X10^{-4}$ M, 100 mM KCl and 50 mM PO_4 buffer, pH=7.5) in the presence of 0.03 or 0.2% v/v enflurane. For these two concentrations, the amount of change in the bacteriorhodopsin spectrum is shown in Figure 3.15. In the first case, enflurane has little effect except for a small hypsochromic spectral shift and absorbance decrease, whereas for the higher enflurane concentration, almost all bacteriorhodopsin is transformed to the bR_{480} spectral form.

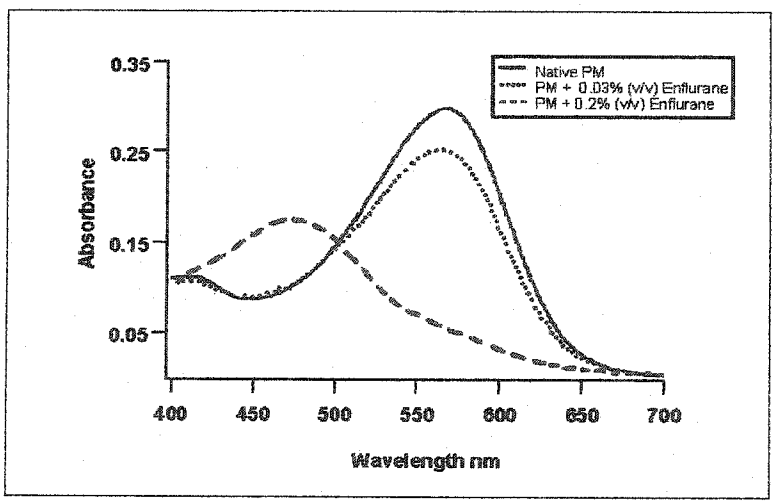

Figure 3. 15 Absorption spectra of the native purple membrane (——), purple membranes in the presence of 0.03 % (v/v) (.....) and 0.2 % (v/v) (------) enflurane.

Incubation of purple membranes in the presence of enflurane prior to calorimetric measurement has a drastic effect on their thermogram (Fig. 3.16). At a smaller enflurane concentration, the pretransition has already almost completely vanished, while the main denaturation transition peak is smaller and occurs at a slightly lower temperature. At a higher enflurane concentration, the pretransition has completely vanished and the main transition has continued its decrease in intensity and temperature.

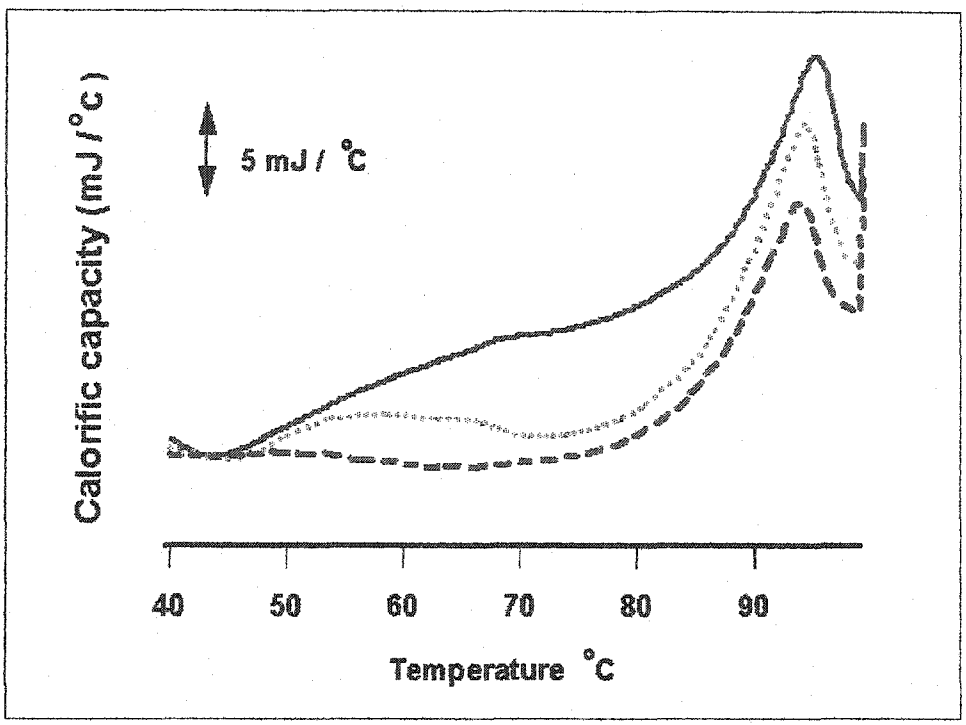

Figure 3. 16 Calorimetric profiles obtained for the native purple membranes (——) and purple membranes previously incubated with 0.03% (v/v) (.....) and 0.2% (v/v) (-----) enflurane.

Because its crystalline structure, the DSC profile of the purple membrane has an asymmetric transition with a large pre-transition. The part of the transition occurring below 65 °C is related to some rearrangement of the membrane without destruction of the secondary structure. After disturbance of the

molecular organization of the membrane, around 70 °C, bR tertiary structure changes reversibly, indirectly affecting protein-protein interactions and the order of the crystal lattice. The denaturation of bacteriorhodopsin is centered at 85 - 90 °C. The last peak at 95 °C is related to the complete destruction of the membrane[86].

Treatment with a low concentration of enflurane (0.03% (v/v)) leads to the loss of the pretransition around 70 - 80 °C and the decrease of the main transition at 95 °C. The lower temperature part of the pretransition (around 50 - 65 °C) remains. This suggests that most of the tertiary structural changes occur at a low enflurane concentration, resulting in a less stable form of bacteriorhodopsin. At the higher enflurane concentration, the complete disappearance of the pretransition indicates that the membrane must have lost most of its structural features (trimeric and hexagonal patterns), leaving the bacteriorhodopsin in a less stable form. It should be noted that because of the time needed for preparation of the samples and for the calorimetric measurement itself, almost two hours (sometimes much more) elapsed between the time the samples were in contact with enflurane and the time of measurement. Thus, the changes reflected by the thermograms must have a strong irreversible character. The organization of the purple membrane is not the same as that of the native sample.

As made clear in Sections 3.1 and 3.2, the properties of the purple membrane do not recover completely following the evaporation of enflurane from the purple membrane. Here, results show that the organization of the purple membrane is irreversibly changed by enflurane. Since the structure of the purple membrane is characterized by the crystalline array of trimers, we examined the crystalline structure of the purple membrane with X-ray diffraction and atomic force microscopy before and after enflurane treatment.

3.3.3 X-ray Diffraction

If, as previous experiments suggest, enflurane induces important changes - including large-scale membrane organization - at different structural levels, then X-ray diffraction would appear to be an

appropriate tool for estimating the extent of membrane structural reorganization or disorganization. Figure 3.17 shows the intensity profile of small angle X-ray diffraction by pelletted purple membranes sealed in a quartz capillary. Although it was possible to measure several diffraction orders, we show only the peaks corresponding to the first order, since higher order peaks contain essentially the same information. The abscissa of those graphs, q, represents $2\pi/d$, where d is the inter-reticular distance. The upper trace, that of the native membrane, is the characteristic diffraction pattern of the purple membrane and confirms the *ca* 65 Å dimension of the unit hexagonal cell of bacteriorhodopsin trimers array.

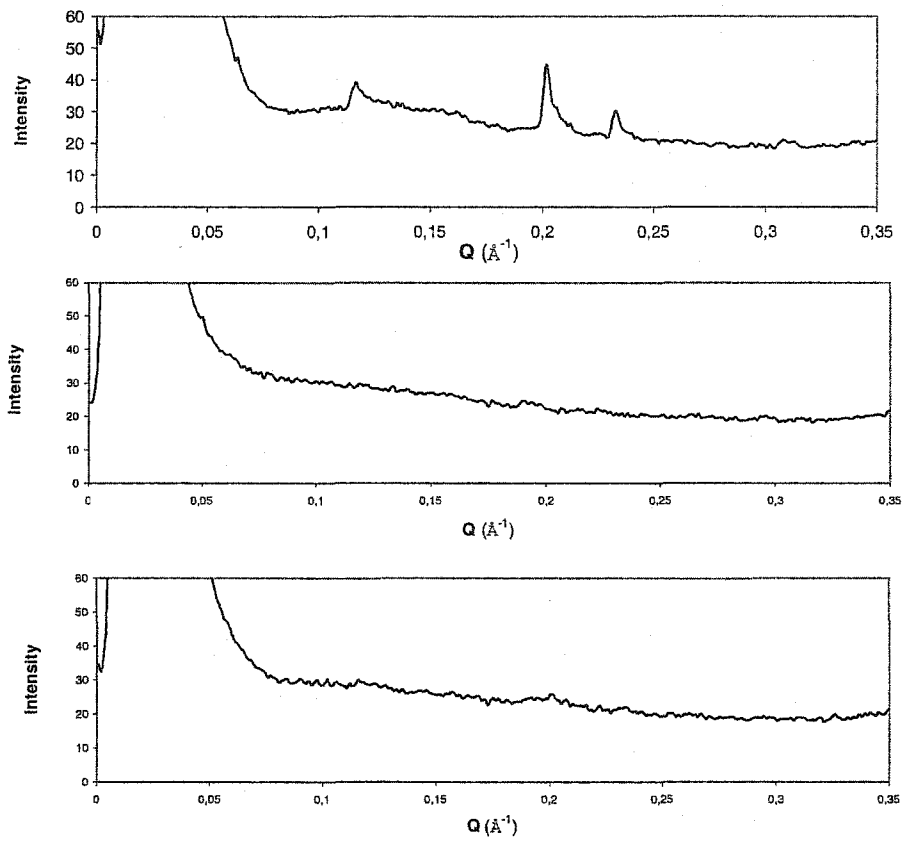

Figure 3. 17 Diagram of small angle X-ray diffraction by purple membrane pellets. Upper and lower curves were obtained for native membranes and membranes from which enflurane had been removed. Middle curve was obtained in the presence of 0.5% (v/v) enflurane.

Since the samples used in these experiments are in the form of sedimented membranes contained in a sealed capillary, measurements can be made in the presence of enflurane. The middle curve of the diffraction patterns shown in Figure 3.17 is that of membranes in the presence of 0.5% (v/v) enflurane. More than 90% of this sample is in the form of bR_{480}. This curve makes it obvious that the hexagonal organization of bacteriorhodopsin trimers no longer exists in the sample. On the other hand, the lower curve was obtained with a sample that had been transformed to bR_{480} and then reversed to bR_{570} under a vacuum before pelletting it in the capillary, five days before measurement. Somewhat surprisingly, it showed very small, if any, diffraction peaks.

The obvious conclusion to be drawn here is that the formation of the red form of bacteriorhodopsin by enflurane is accompanied by a complete disruption of the crystalline character of the membrane and that the original crystallinity is very poorly recovered within a time frame of several days.

3.3.4 Atomic Force Microscopy

Atomic force microscopy (AFM) is a direct method for observing various surfaces, including biological samples. Since it has a very regular crystalline lattice of trimers, the purple membrane is selected as a model for applying the AFM to membrane protein[98]. Thus, it may provide unique clues to the understanding of the apparently irreversible loss of crystallinity of the purple membrane observed during previous measurements.

Thanks to the kind collaboration of a former colleague who was completing a postdoctoral training on AFM in Munich (Dr. Michel Grandbois), it was possible to obtain AFM images of purple membranes before and after treatment with enflurane. These are shown in Figure 3.18. Here again, it is not possible to make measurements in the presence of enflurane, because enflurane evaporates from the sample placed on the mica plate used as a support for AFM.

In the left part of the panel, the hexagonal array of trimers is clearly visible. This is the standard AFM picture of the purple membrane. The right panel shows the image obtained with the sample after the removal of enflurane. The image is fuzzy and the crystal clearly appears as small fragments of the much larger one that exists in the native sample. In addition, unlike the native sample, the sample after the removal of enflurane does not present a regular crystal-like structure. Clearly, some structure does exist but it has the appearance of striated small patches.

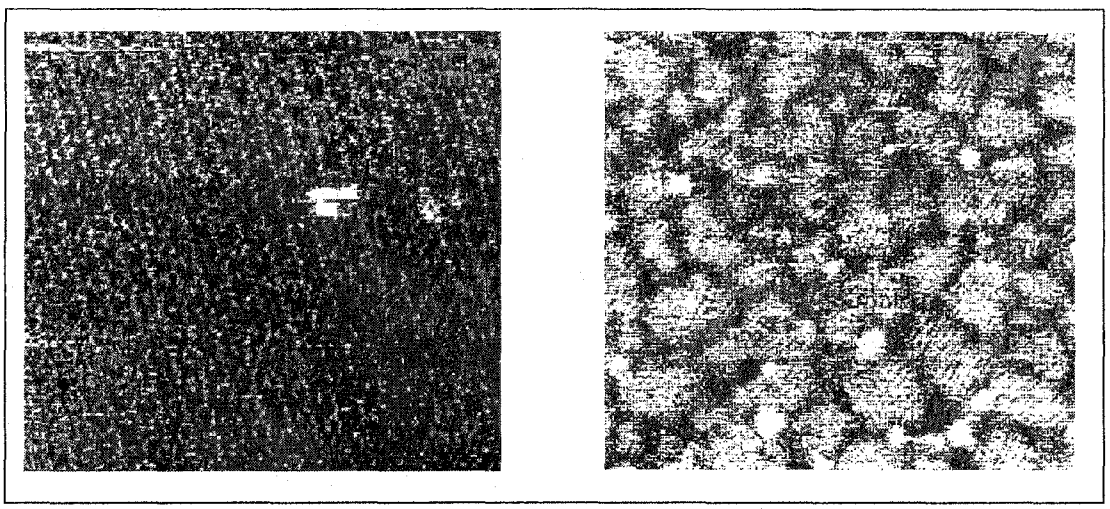

Figure 3. 18 Atomic force microscopy of the native purple membranes (left panel) and the purple membranes after removal of enflurane (right panel) (scanning range 25 x 25 nm left and 50 x 50 nm right).

The important modification of the large-scale organization of the membrane after treatment with enflurane makes it possible to understand certain previously obtained data and to outline the main events that occurred after enflurane was removed. Only two features recover their native characteristics quickly when enflurane is removed – the absorption and the circular dichroism spectral characters. This indicates that the protein structure in the close vicinity of the retinal chromophore and the trimeric organization of the bacteriorhodopsin monomers are reversibly changed by the xenobiotic. Thus, it is likely that the fuzzy image observed after removal of enflurane is that of aggregates of bacteriorhodopsin trimers. For the

moment, we prefer to call them aggregates instead of crystals. We found no indication of a crystalline form. Indeed, the differential calorimetric measurements show no indication of the lattice organization, the X-ray diffraction shows only very weak peaks that probably account for less than 5% recovery of the initial crystalline structure, and atomic force microscopy here clearly shows the membrane with a completely different appearance. Thus, it is obvious that enflurane modifies the large-scale organization of the purple membrane patches irreversibly.

We cannot, however, completely eliminate the possibility that the fragmented aggregates observed after enflurane removal contain some form of crystalline bacteriorhodopsin. If this were so, we would normally observe some diffraction peaks, but when we consider the random orientation of the small-striated patches in that sample, it is obvious they would hardly be able to generate strong interference patterns in an X-ray beam. Finally, the lower stability revealed by the thermogram of the purple membranes after enflurane removal may well account for the fuzziness of their AFM image, since a less rigid structure is likely to be deformed by the microscope tip.

3.3.5 Conclusion

Based on results obtained from the different physical techniques used, the conclusion is rather straightforward. The local and small-scale organization of the bacteriorhodopsin experiences significant and reversible structural changes in the presence of enflurane. The space scale of such reversible changes extends to the size of bacteriorhodopsin trimers. Over this range, important changes also occur, including loss of crystallinity and of a strong interaction between trimers. However, the character of these changes is for the most part irreversible. Given the high degree of cooperativity in the membrane, it is possible they may account for the decreased stability of individual bacteriorhodopsin monomers.

3.4 ANESTHETICS AND THE STRUCTURAL MODIFICATION OF BACTERIORHODOPSIN

From the results shown above, we know that the effects of enflurane on the purple membrane are not fully reversible. Indeed, X-ray diffraction demonstrates that enflurane irreversibly affects the crystalline structure of the purple membrane. Although the trimeric structure almost recovered, the images from AFM show that the large-scale structure of the purple membrane is broken after treatment with enflurane. The proteins aggregate into small pieces. The bR photochemistry is changed as well. The decay of the intermediate M clearly changes from a mono- to a biphasic decay after enflurane treatment. These changes may reflect certain structural modifications in the protein or the lipids around it. Thus, a more precise examination of the events that occur in the structure of the purple membrane appears relevant. Among other things, infrared spectroscopy makes it possible to probe the structural features in proteins. We therefore attempted to characterize the effect of enflurane on bacteriorhodopsin using this technique. It is likely that, upon entering the membrane, enflurane induces significant structural changes in the protein that may affect its vibrational properties. Accordingly, we examined the FTIR spectra of purple membrane films upon addition of enflurane and after evaporation of enflurane, looking for reversible as well as irreversible modifications.

3.4.1 Fourier Transform Infrared Spectrum of the Native Purple Membrane

Figure 3.19 displays the infrared spectrum of the native purple membrane film dried under ambient atmosphere. The native purple membrane films were prepared from the sample suspended in 1 mM KCl and 0.5 mM phosphate buffer (pH=7.5) in order to remove the interference of the buffer. The bands in the spectrum are well resolved and consistent with those reported in the literature[34]. The assignments of these bands are listed in Table 3.4.

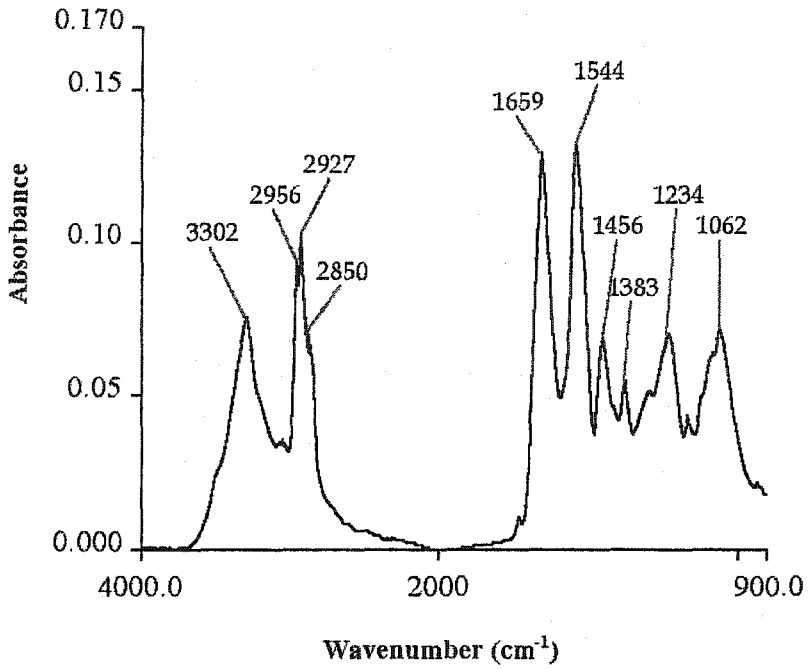

Figure 3. 19 Infrared spectrum of the native purple membrane film prepared from the sample suspended in 1 mM KCl and 0.5 mM phosphate buffer, pH=7.5.

Table 3. 4 Assignments of the native purple membrane bands in the 3600-900 cm^{-1} spectral region.

Wavenumber (cm^{-1})	Assignment
3302	Amide A
2956	CH_3 asymmetric stretching
2927	CH_2 asymmetric stretching
2850	CH_2 symmetric stretching
1659	Amide I
1544	Amide II
1464 1456 1446	CH_2 deformation, CH_3 asymmetric deformation
1383	CH_3 symmetric deformation
1234	$(PO_2)^-$ asymmetric stretching
1062	C-O-C asymmetric stretching: PGP, GLS
	S. M. Barnett, 1996 [34]

Among these bands, the amide A band at 3302 cm^{-1} corresponds to the N-H stretching mode in the structure of the protein. The bands at 2956 cm^{-1}, 2927 cm^{-1}, 2850 cm^{-1} arising from lipids and are assigned to the asymmetric methyl stretching modes ($\nu_{as}[CH_3]$), asymmetric methylene stretching modes ($\nu_{as}[CH_2]$), and symmetric methylene stretching modes ($\nu_s[CH_2]$), respectively.

The protein amide I and amide II modes appear at 1659 cm^{-1} and 1544 cm^{-1} respectively. The amide I band arises principally from the C=O stretching vibration of the peptide group. The amide II band comes primarily from the N-H stretching vibration. The secondary structure of bR is composed primarily of α_I- and α_{II}-helices. As mentioned in Section 1.5.2.2, the amide I band in the α_{II}-helix locates at 1659 cm^{-1} instead of 1655 cm^{-1} for the normal α-helices. Because of the photoselection effect, the tilted N-H bond gives rise to an amide II band as intense as the amide I band.

The spectral region below 1500 cm^{-1} contains bands from vibrational modes arising mainly from the purple membrane lipids. The important feature centered at 1456 cm^{-1} corresponds to overlapping bands at 1464, 1456 and 1446 cm^{-1}. These modes arise from methylene deformation modes ($\delta[CH_2]$) and asymmetric methyl deformation modes ($\delta_{as}[CH_3]$). The band at 1383 cm^{-1} corresponds to the symmetric methyl deformation modes ($\delta_s[CH_3]$). The band at 1234 cm^{-1} is attributed to the asymmetric phosphate stretching mode ($\nu_{as}[PO_2]^-$). The band at 1062 cm^{-1} is assigned to C-O and C-C stretching modes.

3.4.2 Infrared Difference Spectra of the Purple Membrane upon Addition and Removal of Enflurane

To best observe the changes induced by the entrance of enflurane into the membrane, we recorded infrared spectra of the hydrated purple membrane film in the presence of a saturated enflurane atmosphere. This was achieved in an airtight cell where the purple membrane layer was on the inside of a window. Two wells on the bottom of the cell, containing water and enflurane respectively (see Section 2.8.3), maintained a high concentration of enflurane vapors and sufficient humidity to allow the 570 to

480 nm spectral transition, which is very slow in dry films[93]. The infrared spectra were also measured upon removal of enflurane. Enflurane evaporated very rapidly after we opened the airtight cell. The color of the purple membrane film changed from red to purple.

The UV-Vis spectra were measured to assess the transition from the purple form, bR_{570} to the red form, bR_{480} and then the recovery from bR_{480} to bR_{570}. Figure 3.20 illustrates the UV-Vis spectra of the purple membrane 1, 3 and 6 hours after addition of enflurane and 1 hour after evaporation of enflurane. We see that the transition of purple to red is not complete: almost half of the bR is transformed to bR_{480} within the first hour and little change occurs after that time. In fact, the full transition never occurs, even 24 hours after addition of enflurane, where not more than 50% of bR changed to its red form. Upon enflurane evaporation, the maximal absorbance at 570 nm also recovered within the first hour. Even if recovery is incomplete after 1 hour, longer periods of waiting did not improve the recovery. In any case, the amount of bR transformed in the process should be sufficient for our purpose.

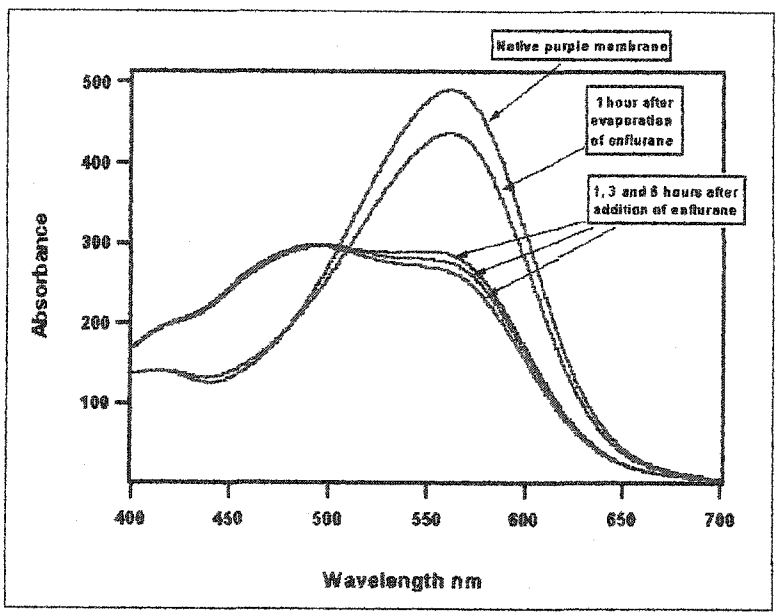

Figure 3. 20 Absorption spectra of the purple membranes, 1, 3 and 6 hours after addition of enflurane and 1 hour after evaporation of enflurane.

On the other hand, enflurane has a strong absorption around 3000 cm^{-1} and in the region below 1400 cm^{-1}. Figure 3.21 shows the infrared spectrum of enflurane from 4000 – 900 cm^{-1}. A strong absorption of enflurane appears at 3033 and 3004 cm^{-1}, and the region below 1400 cm^{-1} is totally covered by the absorption of enflurane. Some spectral features also appear at 1735, 1652, 1546 and 1457 cm^{-1}. To remove enflurane interference in this region when we produced the difference spectra, we subtracted the spectrum of enflurane from the infrared spectrum of the purple membrane in the presence of enflurane.

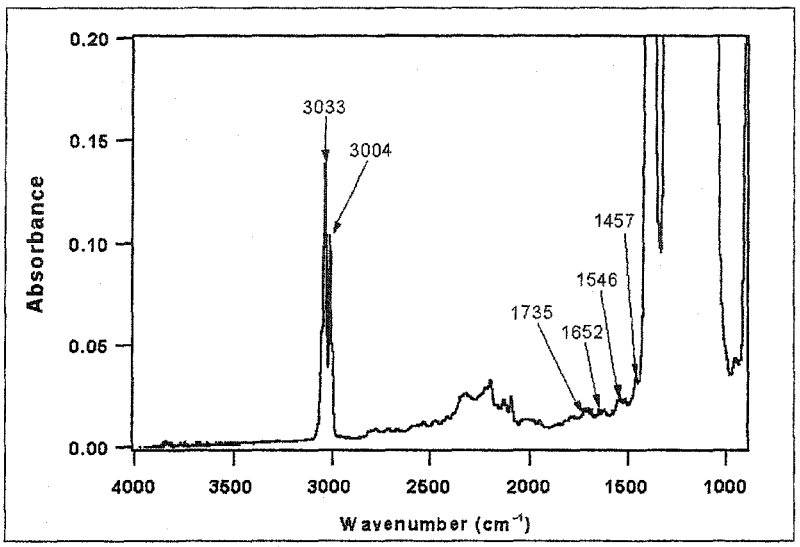

Figure 3. 21 Infrared spectrum of enflurane from 4000 to 900 cm^{-1}.

3.4.2.1 Structural Changes in Bacteriorhodopsin upon Addition of Enflurane

The difference spectra were produced by subtracting the spectrum of the native purple membranes under 100% humidity from the spectrum of the purple membranes in the presence of enflurane [(PM + enflurane) - native PM]. Under such conditions, the region around 3000 cm^{-1} is covered by the absorption of water, and the region below 1400 cm^{-1} is covered by the absorption of enflurane. Thus, we show only the difference spectra in the region from 1700 cm^{-1} to 1430 cm^{-1}. As mentioned, enflurane also has absorption in this region. Therefore, the spectrum of enflurane was also subtracted to remove any

interference from enflurane. In such difference spectra, a positive band or positive feature indicates an increase in the intensity of a certain band upon addition of enflurane in this region, and a negative band suggests a reduction in the intensity or absorption of a band.

Figure 3.22 illustrates the infrared difference spectra of the sample 1, 3 and 6 hours after the addition of enflurane. In the spectra, amide I and amide II bands are observed as negative bands at 1659 cm^{-1} and 1542 cm^{-1}. Another negative band is found at 1528 cm^{-1}, which is assigned to the ethylene bond in the retinal. The positive features are found at 1688 and 1624 cm^{-1}. They are attributed to β-turn and β-sheet in bacteriorhodopsin. The shoulder at 1644 cm^{-1} most likely comes from α_I-helices and random coils [99]. A small negative band is also found at 1460 cm^{-1}. This band corresponds to the methyl and methylene deformation modes. These changes occurred just 1 hour after the addition of enflurane. After that time, there were no more changes in the intensity of these bands, which is consistent with the changes found in the UV-Vis absorption spectrum.

The bands at 1660 and 1542 cm^{-1} correspond to the amide I and amide II bands for α-helices. The bands at 1688 and 1624 cm^{-1} correspond to the β-turn and β-sheet. The increase in the intensity of bands at 1680 and 1624 cm^{-1} and the decrease in the intensity of the amide I and II bands suggest that enflurane affects the α_{II}-helices structure in bacteriorhodopsin. This seems to be reflected as an increase in β-structure, in α_I-helices or even in random structure since their characteristic bands increase simultaneously. The band at 1528 cm^{-1} can be attributed to the decrease in the intensity of ethylene modes in the retinal. This band appears as a negative feature when the bR color changes from purple to red. The negative band at 1460 cm^{-1} is normally attributed to CH_2 and CH_3 asymmetric deformation modes. Change in such a mode is also likely when one recalls that anesthetic molecules primarily dissolve in the lipid bilayer.

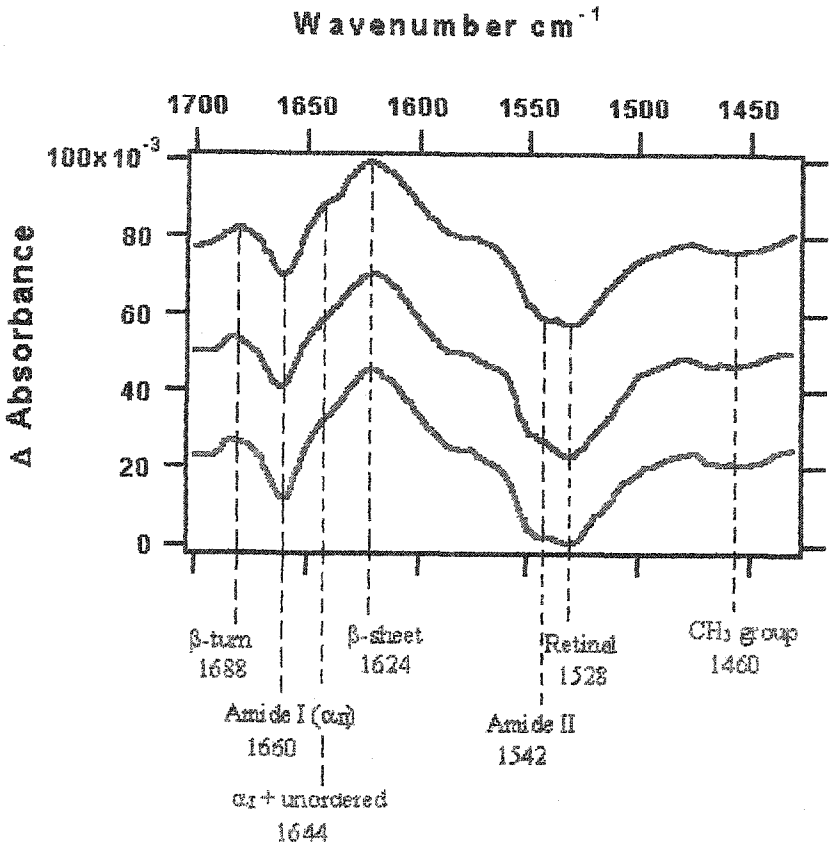

Figure 3. 22 Infrared difference spectra of purple membranes in the region 1700 - 1400 cm^{-1} upon addition of enflurane after 1, 3 and 6 hours (from top to bottom).

3.4.2.2 Recovery of the bR Structure after Removal of Enflurane

The infrared spectra of the purple membranes were measured 1, 3 and 6 hours after the removal of enflurane. During that time, enflurane evaporated and the color of the film on the window recovered to purple. We examined these enflurane-out difference spectra [(recovered PM – (PM + enflurane)) to look for reversible as well as irreversible changes in the membrane. Figure 3.23 shows these infrared difference spectra in the region 1700 – 1400 cm^{-1}.

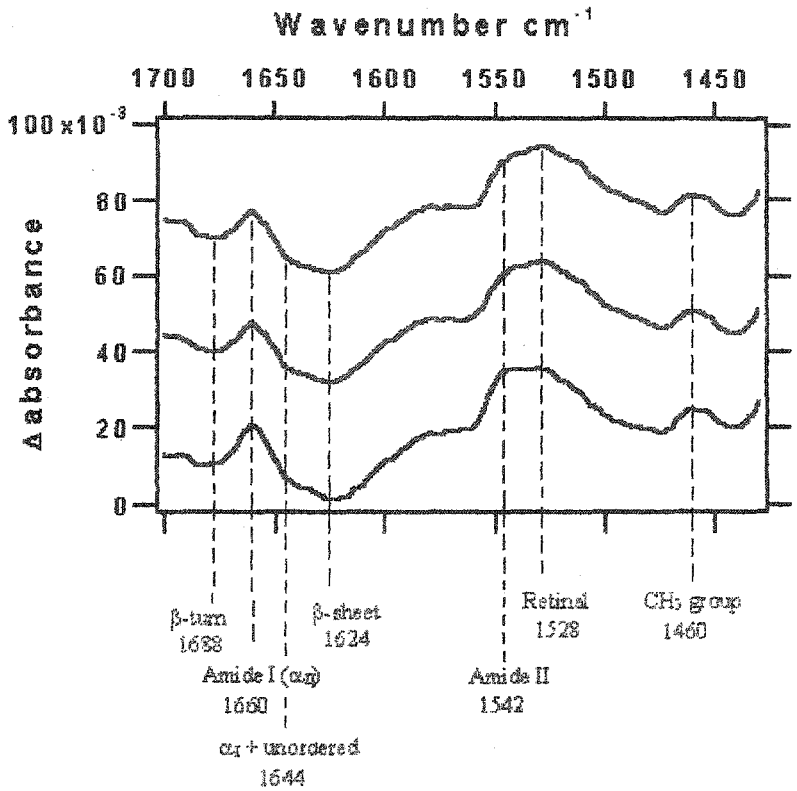

Figure 3. 23 Infrared difference spectra of purple membranes in the region 1700 – 1400 cm^{-1} 1, 3 and 6 hours after opening the cell of sample (from top to bottom).

First, we notice that the intensities of the bands in the spectra that were measured 1, 3 and 6 hours after removal of enflurane are almost the same. This is consistent with the observation on the UV-Vis absorption spectrum; the absorption properties of the purple membrane recover very rapidly upon evaporation of enflurane. When we examine the changes in each band, we find that the difference spectra after evaporation of enflurane are almost inverted with respect to the enflurane-in spectra shown in Figure 3.22. This suggests strongly the reversible feature of the structural changes in the membrane. The decrease in the intensity of the bands at 1688, 1644 and 1627 cm^{-1} and the increase in the intensity of the bands at 1659 and 1542 cm^{-1} indicate that bR α_{II}-helices recover their original state from the β-structures or unordered structures, including the recovery of the α_I-helices to the α_{II}-helices. The increase in band

intensity at 1528 cm^{-1} reflects the recovery of the color of the retinal. The changes in the lipid bilayer also recover as indicated by the increase in the intensity of the band at 1460 cm^{-1}. However, the increase in the intensity of this band is larger than its decrease in intensity in the presence of enflurane. This may indicate some incompletely reversible feature of the structural changes in the lipid bilayer. Table 3.5 summarizes the enflurane-induced changes in the bR structure and the recovery of these changes.

Table 3. 5 Reversibility of enflurane-induced structural changes in bacteriorhodopsin.

Infrared bands (assignments)	Upon addition of enflurane	During evaporation of enflurane [a]	Reversible (R) or Not Reversible (NR)
1688 cm^{-1} (β-turn)	+	–	R
1660 cm^{-1} (the amide I of α_{II}-helices)	–	+	R
1644 cm^{-1} (the amide I of α_{I}-helices and random)	+	–	R
1624 cm^{-1} (β-structure)	+	–	R
1542 cm^{-1} (the amide II)	–	+	R
1527 cm^{-1} (ethylene mode of the retinal)	–	+	R
1460 cm^{-1} (CH_2 and CH_3 groups)	–	+	R[b]

[a] +: Positive band; -: negative band
[b] incompletely reversible

It is worth mentioning here that in the present experiments, we did not observe the large increase of the amide I previously reported in Messaoudi's experiments. Indeed, in their analysis of the same phenomenon, Messaoudi et al.[85] observed much more important changes in the amide I and II bands upon conversion of bacteriorhodopsin by enflurane and concluded that the phenomenon was mainly due to a

reorientation of helices with respect to each other. Their sample films, however, were prepared after the purple membrane solution had been treated with the anesthetic. Under those conditions, we showed that the purple membrane was seriously modified into small patches that are unlikely to orient on the infrared window. Accordingly, large intensity changes may occur in the ratio of amide I to II band, owing to the loss of photoselection effect. Such a bias does not exist in our procedure. Since the purple membranes are transformed once the films are cast, the intact membrane may be broken, but they retain their orientation on the infrared window (Fig.3.24). Accordingly, we must be not surprised to observe a much less important structural change with conversion between the purple and red forms of bacteriorhodopsin.

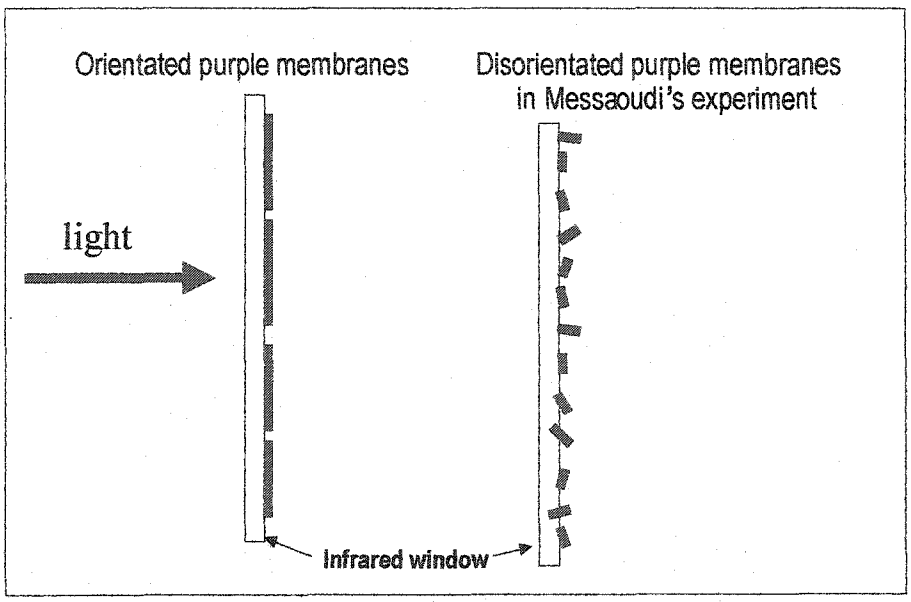

Figure 3. 24 Comparative membrane orientation on infrared window. On the left, the purple membrane stays in order in the presence of enflurane vapor (our experiment). On the right, the small pieces of the purple membrane cast disorder on the infrared window after enflurane treatment (Messaoudi's experiment).

3.4.3. Tertiary Structure of Bacteriorhodopsin

In bR, only peripheral regions are accessible to the H/D exchange of backbone amide peptide groups, but the backbone amide peptide groups in the core region are largely inaccessible to H/D exchange[100, 101].

Polarized FTIR spectroscopy combined with H/D exchange has shown that this core region consists primarily of α-helical structure that is, for the most part, oriented perpendicular to the membrane plane and buried largely within the lipid bilayer[102].

A major effect of H/D exchange on the infrared absorption of the native bacteriorhodopsin is to lower the absorption of the amide II band at 1544 cm^{-1} and increase the absorption in the region near 1445 cm^{-1} (the amide II' mode). This effect occurs because of the NH → ND exchange of peptide backbone groups, which causes a downshift in the frequency of the amide II vibration by approximately 100 cm^{-1} [103]. In bacteriorhodopsin, the effect is relatively small because of the existence of a core region which is inaccessible to H/D exchange. When detergents denature the purple membranes, the core structure of bacteriorhodopsin becomes accessible to the H/D exchange. Complete H/D exchange only occurs when denatured purple membranes are reconstituted/regenerated in the D_2O buffer [104].

In the presence of enflurane, purple membranes turn to red, even yellow, in color if halothane is used instead of enflurane. Infrared spectroscopy combined with H_2O/D_2O exchanges may reveal whether the changes occur in the periphery region or in the core region of bacteriorhodopsin. Indeed, if hydrogen bonds in the helical structure of bacteriorhodopsin are broken by enflurane or halothane, the H/D exchange will occur and may be detected by infrared spectroscopy.

To verify this possibility, infrared spectra were measured 30 minutes, 1 hour, 24 hours and 48 hours after exposing the purple membrane in the D_2O to enflurane. As expected, the band of the amide II decreased as the band corresponding to the amide II' increased. There was a very small decrease in the intensity of the amide II band 2 days after the sample was exposed to enflurane. At the 3rd day, we added halothane into the above sample until the maximal absorbance turned to 380 nm. The band for the amide II in the FTIR spectra decreased again, suggesting more H/D exchange in the α-structure of bacteriorhodopsin. Figure 3.25 illustrates the changes in the region of the amide II in the spectra of D_2O-exposed purple membranes in the presence of enflurane and halothane. All the spectra are normalized to

the amide I mode. The intensities of the amide I and amide II bands and the percentage of the amide II band change in the presence of D_2O are shown in Table 3. 6.

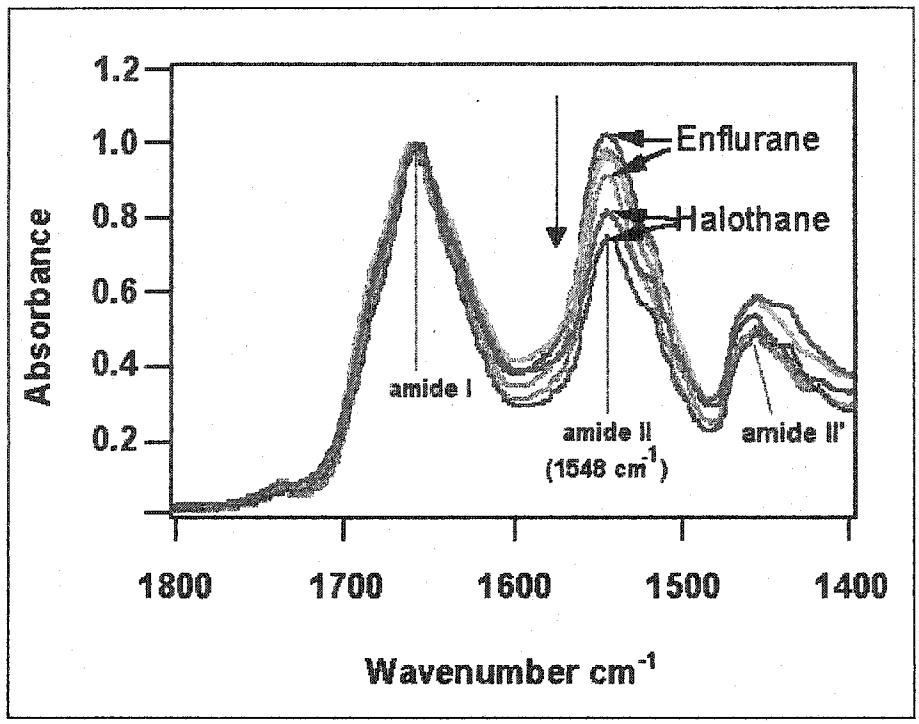

Figure 3. 25 Intensities of amide I and amide II bands in the spectra of purple membranes in D_20 30 minutes, 1 hour, 24 hours and 48 hours after the samples were exposed to enflurane and 24 hours and 48 hours after addition of the same sample with halothane (from top to bottom).

It is clear that enflurane does not induce complete exchange. Only about 20% amide protons are exchanged 2 days after exposing purple membranes in D_2O to enflurane. No observable exchange continues in the next 2 days. Addition of halothane on the 3rd day turns bR_{480} to bR_{380}; at this time, H/D exchange restarts and the change of the amide II reaches 41% on the 5th day. Halothane is stronger than enflurane. It can induce the transition of the purple membrane to red and yellow very rapidly. It also induces a much important H/D exchange in the purple membrane. However, the fact that enflurane

induces a limited H/D exchange after 2 days confirms the localized and reduced character of the protein structural changes by enflurane.

Table 3. 6 Frequencies of the amide I and amide II bands and the percentage of the amide II band change 30 minutes, 1 hour, 24 hours and 48 hours after the purple membrane in D_2O was exposed to enflurane, and 24 and 48 hours after the sample was exposed to halothane.

Time		Amide I 1659 cm^{-1}	Amide II 1645 cm^{-1}	Δ Amide II %
enflurane	30 minutes	0.976	1.000	0
	12 hours	1.001	0.908	10
	24 hours (1st day)	1.000	0.815	19
	48 hours (2nd day)	0.976	0.774	22
Addition of halothane on the 3rd day				
halothane	24 hours (4th day)	0.961	0.711	29
	48 hours (5th day)	0.970	0.585	41

3.4.5 Conclusion

The present infrared spectral data show that the enflurane-induced changes in bacteriorhodopsin recover to their original spectral properties. Enflurane appears to induce changes in α_{II}-helices. Part of α_{II}-helices changes to α_{I}-helices, and to β-structure, or unordered structures. These changes recover after evaporation of enflurane. The changes observed in the environment of lipids are not fully reversible, suggesting incompletely reversible changes in the lipid bilayer. However, these changes must be rather limited since no large absorption change is observed. The small scale of the structural modification is confirmed by the H/D exchange measurements which indicate that, in the presence of enflurane for up to 12 hours, not more than 10% of amide protons become accessible to the solvent. Thus, the structural

modification of bacteriorhodopsin by enflurane must occur locally and in all likelihood at the surface of the membrane.

3.5 TESTING THE REVERSIBILITY OF ANESTHETIC EFFECTS ON A SIMPLE LIPID BILAYER

The physical state of lipids in the membrane is important to the function of membranous proteins. Anesthetics modify the structural, thermodynamic, and dynamic properties of the lipid bilayer, properties which in turn modify the behavior of membranous proteins[105]. In addition, several recent experimental studies have been done on anesthetic binding sites in membranes. These sites include the acyl chain domain, various locations in the headgroup region, and the water/lipid interface [106, 107, 108]. In order to get some insight in the origin of the irreversible effects of enflurane, we have examined its effect on the phase transition temperature of pure DPPC vesicles as measured by infrared spectroscopy and fluorescence spectroscopy.

3.5.1 Infrared Spectroscopy

In the spectrum of DPPC vesicles, the band at 2850 cm^{-1} corresponds to the symmetric stretching modes of CH_2 groups on the acyl chain. During the gel to liquid-crystalline phase transition, this band shifts from 2850 to 2852 cm^{-1}. Figure 3.26 shows that the transition occurs near 40 °C for pure DPPC vesicles. In the presence of saturating amounts of enflurane, the phase transition drops to 32 °C. This was achieved by injecting 1 µl of enflurane into the DPPC vesicle suspension. A few hours after enflurane removal and equilibration, the original transition temperature recovers at 40 °C, although it occurs on a wider temperature range (Fig. 3.26, green line). Since the CH_2 groups are located on the hydrophobic tail of the lipid, the results of FTIR reveal that the effect of enflurane is easily removed from the hydrophobic core of the membrane. The changes in this region of the membrane are thus reversible.

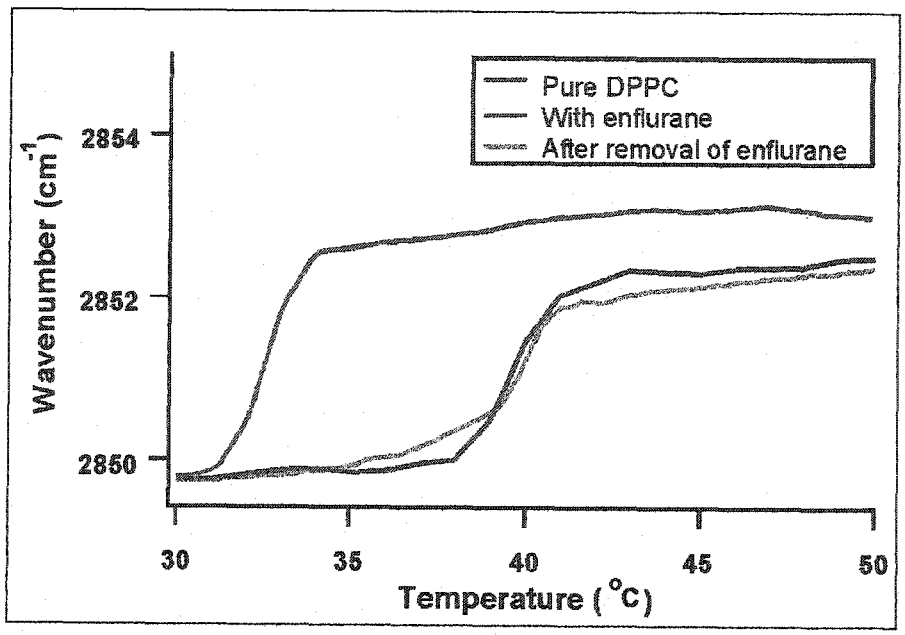

Figure 3. 26 Frequency shift of the CH_2 groups on the acyl chains of pure DPPC vesicles (purple line), in the presence of enflurane (red line) and after removal of enflurane (green line) during the phase transition.

3.5.2 Fluorescence Spectroscopy

As we have mentioned in Section 2.9.3, the emission maximum of Laurdan is sensitive to the physical state of the lipid bilayer. The emission maximum of Laurdan in DPPC vesicles (DPPC/L) shifts from 435 nm to 490 nm upon the rise of temperature from 25 to 50 °C. Figure 3.27 shows the ratio of the fluorescence intensity at 490 nm to that at 435 nm as the function of temperature. Before enflurane treatment, the emission maximum of Laurdan is at 435 nm when the temperature is lower than 41°C. As temperature rises, the emission maximum of Laurdan shifts to 490 nm; the ratio of the fluorescence intensity of Laurdan at 490 to that at 435 nm increases. The transition temperature (Tm) is at 42 °C. The transition temperature decreases as a function of the concentration of enflurane in the sample. For

example, in the presence of 0.1% (v/v) enflurane, the transition temperature is approximately 36 °C. When the concentration of enflurane is 0.15% (v/v), the transition temperature is at 35 °C. When the concentration of enflurane reaches 0.3% (v/v), the transition temperature is at 33 °C. This effect is not easily removed. Indeed, the transition temperature is approximately 36 - 37 °C after evaporation of enflurane. It never recovers to 42 °C. Since the emission spectrum of Laurdan is related to the change near the surface of the membrane, this result indicates that the physical state of the membrane surface does not completely recover after enflurane-treatment.

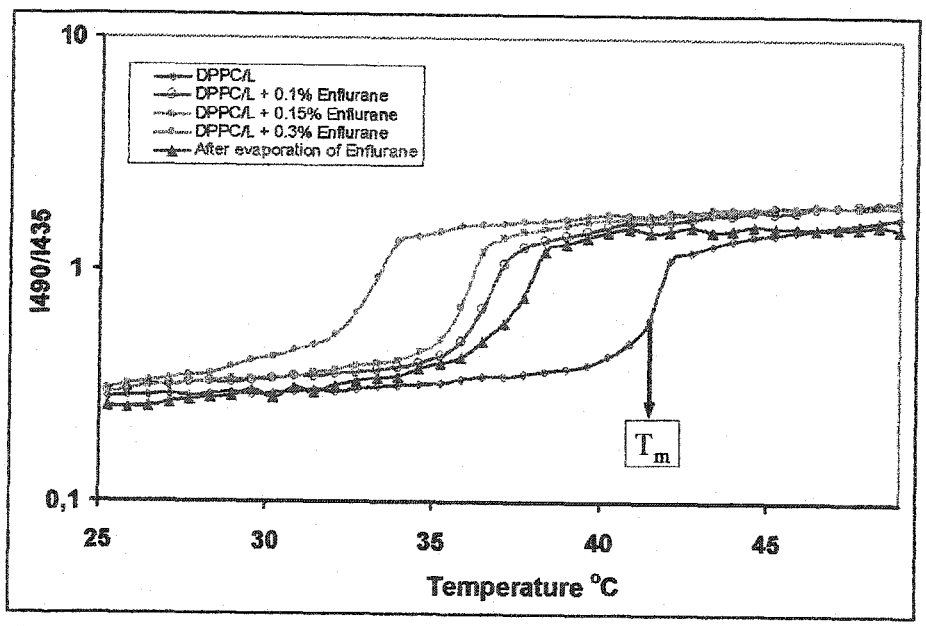

Figure 3. 27 Ratio of the fluorescence intensity of Laurdan at 490 to that at 435 nm for pure DPPC vesicles (DPPC/L) (the right last curve), in the presence of enflurane 0.1, 0.15 and 0.3% (v/v) (Three left curves, from right to left), and after evaporation of enflurane (line with triangles).

Attempts to remove enflurane have been achieved in different manners (Fig. 3. 28). First, we simply bubbled nitrogen gas over the aqueous suspension. With respect to the purple membrane color, this is sufficient to rapidly restore the original spectral characteristics of bacteriorhodopsin. Enflurane

evaporation under the mild vacuum of a water trump is also effective for removing enflurane. Finally, we can also perform complete lyophilisation and vesicle reconstitution.

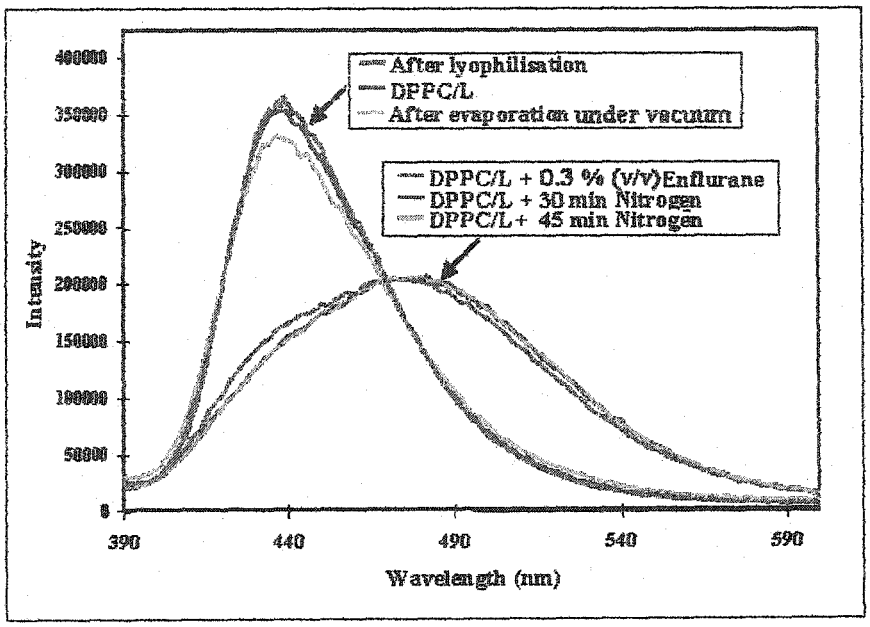

Figure 3. 28 Emission spectra of Laurdan in DPPC vesicles (DPPC/L) vesicles, with 0.3% (v/v) enflurane, after removal of enflurane with nitrogen gas, under vacuum and after lyophilization. The spectra were measured at 35 °C.

As seen in Fig. 3.28, the emission maximum is still indicative of a liquid-crystalline phase, at 35 °C after passing nitrogen gas for evaporation of enflurane, which means that DPPC vesicles do not recover their initial state. After enflurane has been removed under vacuum, the maximum emission returns to 435 nm, but the band magnitude is still low. The complete recovery of the DPPC physical state is observed only after lyophilization and resuspension of the DPPC vesicles. DPPC vesicles can completely recover their physical state only under two conditions: first, if enflurane is completely removed during this procedure and second, if the damage in the DPPC vesicles induced by enflurane is corrected during the reconstitution of DPPC vesicles. This set of experiments shows us that the recovery of changes in the surface of membrane is not easy to obtain unless a drastic method is used, which is not easily applicable

for biomembrane system, such as the purple membrane. Thus, small amounts of enflurane are possibly left in the purple membrane, and/or the properties of the purple membrane cannot be restored.

3.5.3 Conclusion

Although the lipid bilayer used in the experiments is different from the lipids of the purple membrane, we were able to analyze the effects of enflurane on the different parts of the membrane, namely, the hydrophobic core of the membrane and the water/lipid interface at the surface of the membrane. These experiments make it clear that enflurane effects are not fully reversible even in a simple experimental model. If we look deep in the hydrophobic core of lipid bilayers, as with the CH_2 stretching modes, it appears easy to recover the original physical properties as evaporation of enflurane brings back the original transition temperature. However, when we look at the interfacial region of the bilayer, as with Laurdan fluorescence, only a drastic method like lyophilization makes it possible to recover the original physical state. The changes in the DPPC vesicles are thus not fully reversible.

CHAPTER 4

GENERAL CONCLUSIONS

The effects of anesthetics on the purple membrane have been extensively studied for more than ten years. These researches mostly showed the effects of anesthetics on the structure and function of bacteriorhodopsin[37, 81], as well as the reversibility of these effects[36, 81]. The reversible effects of anesthetics include, namely, the spectral changes and the proton-pumping activity. They are related to changes around the chromophore and in the surroundings of the proton transportation pathway. However, in the present work we have also examined structural features of higher order and we found that some changes did not completely recover. It then becomes worthwhile to see to which extent some of the purple membrane structural and functional properties could recover after anesthetic-treatment. Our most significant conclusions are as follows:

1. Reversible changes occur locally in the purple membrane, within the bR trimeric structure. When enflurane enters the purple membrane, bacteriorhodopsin switches from a trimeric organisation to a monomeric form. This quaternary structural change accompanies the spectral shift of the chromophore whose maximal absorbance goes form 570 to 480 nm. At the same time, the proton pumping activity is reversibly abolished. With respect to the secondary structure of bR, part of its α_{II} helices change to α_{I} helices, or even to a random structure. These changes occur most likely in a region near the surface of the membrane. The D/H exchange experiment shows that only 20% of amide protons can be exchanged during purple membranes exposure to enflurane. After removal of enflurane, the changes in the secondary structure of bR recover as indicated by FTIR difference spectra. Together with its native maximal absorbance and its proton pumping ability, bR also recovers its trimeric organization as indicated by the bilobed CD spectrum.

2.The crystalline structure of the purple membranes does not recover. The evidences come from results of X-ray diffraction and atomic force microscopy.

3.Some other properties of purple membranes appear to be not completely reversible. First, the cooperativity among bacteriorhodopsin molecules is different before and after enflurane-treatment. Second, the kinetics of the M decay in bR photocycle changes from one phase to two phases and then this change does not complete recover. An incompletely reversible change also occurs in the band at 1640 cm^{-1} in the infrared difference spectrum of bR, the band which corresponds to methylene deformation modes ($\delta[CH_2]$) and asymmetric methyl deformation modes ($\delta_{as}[CH_3]$) of lipids.

4.The function of bR is strongly related to the structure of the purple membrane. In the presence of enflurane, the crystalline organization of the bR trimers is lost. There is no proton transportation[81]. After removal of enflurane, the crystalline lattice of the purple membrane does not reappear, only bR trimers recover. Proton pumping is recovered but bR photochemistry kinetic features do not fully recover. Therefore, the function of bR depends on the trimeric structure and incomplete reversible changes in bR photocycle can be related to the changes in crystalline structure.

5.The fluorescence spectrum of a probe located in artificial membrane made of DPPC reveals that the effects of enflurane on the surface of a membrane are not easily reverted. There are multiple reports on the effects of anesthetics on the lipid membrane. Chiou[109] et al. revealed that alcohols induce dehydration of the phosphate moiety and of the sn-2 C=O moieties of the hydrophilic head. Alcohols seem to bind only to the phosphate group. It might also be the case for enflurane. The difficulty in removing the effects of enflurane from the surface of membrane may be due to a strong interaction between enflurane and the hydrophilic region of the membrane. With respect to reversibility of anesthetic effects, the change near the membrane surface is not reversible. If anesthetics also induce the same effects on the purple membrane, it

is thus likely that an irreversible change of the crystalline organization of purple membrane result from the strong interaction of enflurane with polar groups on the surface of membrane.

6. The concentration of anesthetics is important when we discuss their side effects. A too low concentration of anesthetics do not induce anesthesia while a too high concentration of anesthetics results in the loss of consciousness after removal of anesthetics or even death. The MAC of enflurane is about 0.60 mM. The concentration of enflurane in our experiments is about 8 mM (0.09% v/v), the concentration that induces the maximal absorbance shift to 480 nm and hinders the proton transportation. It may be too high comparing with its MAC, but effects of enflurane on the maximal absorbance and proton transportation in this concentration is comparable to the one that affects ligand-gated ion channels in nerve membranes. In fact, the irreversible changes in the purple membrane occur even at very low concentrations of enflurane as shown by DSC thermograms. Interestingly, the kinetics of M decay after the sample treated with different concentrations of enflurane also shows the same phenomenon. Therefore, from our results, irreversible effects of enflurane on the purple membrane do not depend on the excess concentration of enflurane used in the experiments. However, it is not rule out that residue effects of enflurane on the purple membrane might be due to a trace amount of enflurane remaining in the samples after enflurane evaporates under mild vacuum, which may be the point to be researched in the further.

The recovery of structural changes in the purple membrane after enflurane treatment involves regeneration of the native structure of an integral membrane protein. Observation of some irreversibility in the disorganizations of bR by anesthetics may thus reflect some critical step in the biogenesis. These results are thus interesting not only in terms of anesthetic action but also in terms of membrane protein assembly.

Much work on their mechanism of action focuses on anesthetic-induced structural changes in the membrane but very few works have addressed the issue of their reversibility. Our researches add a new

point in this field. It is well known that clinical general anesthesia has long term or permanent effects. The reason for this remains unknown. Observation of irreversible effects of anesthetics in the purple membrane might open the way to some molecular explanation of this effect.

Recovery of enflurane-induced structural changes in the purple membrane is similar to membrane protein assembly from individual protein molecules. With respect to the purple membrane, the most important role in membrane assembly is bR-lipid interaction[110]. It is mostly because not only many of the lipid hydrocarbon tails are highly ordered and fit into cavities lined with apolar residues on the membrane-embedded surface of bR, but also because of special binding between the headgroups of lipids with some amino acid residues near the surface of the membrane. Lipids may mediate interaction between trimers and within the trimers. One of the examples for this is that lipids are not easily removed for the purple membrane. The changes in lipids can affect the lattice assembly of the purple membrane. In our experiments, asymmetric distribution in the intensity of band at 1460 cm^{-1} may indicate an incomplete recovery of the bR-lipid interaction which results in an irreversible change in the crystalline lattice of the bR trimers.

Besides bR-lipid interaction, the bR trimeric structure is also important to lattice assembly. Moller[111] et al. observed reversible loss of crystallinity of the purple membrane after photobleaching in the presence of hydroxylamine; provided that the bR trimers remain intact. In the presence of enflurane, the bR trimers are changed into monomers. After removal of enflurane, the trimers recover, but the crystalline lattice does not recover.

It is evident that the bR-lipid relationship is important to purple membrane crystallinity but the role of bR trimers in the formation of crystalline structure is ambiguous. Although bR is generally assumed to form trimers prior to lattice assembly, there is little evidence that the trimer exists as a stable entity or as an intermediate in lattice assembly in vivo. Thus the crystalline structure forms once bR monomers cluster

into trimers. However, while we observed the bilobed CD spectrum after removal of enflurane, we could not see any X-ray diffraction peak. What does prevent the formation of crystals? Are the trimers after anesthetic-treatment the same as those in the native purple membrane? AFM image after enflurane treatment shows some aggregation of bR molecules, but trimeric structure is not very clear. Furthermore, bR trimers are stabilized by interactions mainly between helices B and D[112]. If bR trimeric structure is changed after enflurane treatment, is it due to the changes in bR helices? Here are number of questions that will wait further work in order to be answered.

References

1. Karlin A., Akabas M. H. (1995) Toward a structural basis for the function of nicotinic acetylcholine receptors and their cousins. *Neuron.* 15, 1231-1244.

2. Ortells M.O., Lunt G. G. (1995) Evolutionary history of the ligand-gated ion-channel superfamily of receptors. *Trends Neurosce.* 18, 121-127.

3. Hucho F. L., Tsetlin V. (1996) Structural biology of key nervous system proteins. *J. Neuron.* 16, 1781-1792.

4. Jones O. T., McNamee M. G. (1988) Annular and nonannular binding sites for cholesterol associated with the nicotinic acetylcholine receptor. *Biochemisry* 27, 2364-2374

5. Ellena J. F., Blazing M. A., McNamee M. G. (1983) Lipid-protein interactions in reconstituted membranes containing acetylcholine receptor. *Biochemistry* 22, 5523-5535.

6. Jones O. T., Eubanks J. H., Earnest J. P., McNmee M. G. (1988) Annular and nonannular binding sites for cholesterol associated with the nicotinic acetylcholine receptor. *Biochemistry* 27, 2364-2374.

7. Dreger M., Krauss M., Herrmann A., Hucho F. (1997) Interactions of the nicotinic acetylcholine receptor transmembrane segments with the lipid bilayer in native receptor-rich membranes. *Biochemistry* 36, 839-47.

8. Jones M. V., Westbrook G. L. (1996) The impact of receptor desensitization on fast synaptic transmission. *Trends Neurosci.* 19, 96-101.

9. Miller K. W. (1985) The nature of the site of general anesthesia. *Int. Rev. Neubiol.* 270, 1-61.

10. Franks N. P., Lieb, W. R. (1994) Molecular and cellular mechanism of general anesthesia. *Nature* 367, 607-614.

11. Meyer H. H. (1899) Theorie der alkoholnarkose. *Arch. Exp. Pathol. Pharmakol.* 42, 109-118.

12. Overton E. (1901) Studien über die Narkose zugleich ein Betrag zur Allgemeinen Pharmakologie. Jena: Verlag von gustav Fisher.

13. Pang K. Y. Y., Braswell L. M., Chang L., Sommer T. J., Miller K. W. (1980) The perturbation of lipid bilayers by general anesthetics: A quantitative test of the disordered lipid hypothesis. *Mol. Pharmacol.* 18, 84-90.

14. Trudell M. K., Rastogi S. K., Hubbell W, L., Cohen E. N. (1973) The effect of two inhalation anesthetics on the order of spin-labeled phospholipid vesicles. *Biochim. Biophys. Acta* 291, 321-327.

15. Franks N. P., Lieb, W. R. (1981) Is membrane expansion relevant to anesthesia *Nature* 292, 248-251.

16. Franks N. P., Lieb W. R. (1985) Mapping of general anaesthetic target sites provides a molecular basis for cutoff effects. *Nature* 316, 349-51.

17. Miller K. W., Firestone L. L., Alifimoff J. K., Streicher P. (1989) Nonanesthetic alcohols dissolve in synaptic membranes without perturbing their lipids. *Proc Natl Acad Sci U S A* 86, 1084-7.

18. Koblin D. D., Chortkoff B. S., Laster M.J., Eger E. I. 2nd., Halsey M.J., Ionescu P. (1994) Polyhalogenated and perfluorinated compounds that disobey the Meyer-Overton hypothesis. *Anesth. Analg.* 79, 1043-8.

19. LaBella F. S. (1981) Is there a general anesthesia receptor? *Can.. J. Physiol. Pharmacol.* 59, 432-442.

20. Evers A. S., Berkowitz B. A., d'Avignon D, A. (1987) Correlation between the anesthetic effect of halothane and saturable binding in brain. *Nature* 328, 157-160.

21. Franks N. P., Lieb W. R. (1988) Volatile general anesthetics activate a novel neuronal K^+ current. *Nature.* 310, 599-601.

22. Howard F. M. Jr., Lennon V. A., Finley J., Matsumoto J., Elveback L. R. (1987) Clinical correlations of antibodies that bind, block, or modulate human acetylcholine receptors in myasthenia gravis. *Ann. N Y Acad Sci.* 505, 526-38.

23. Belelli I., Pistis I., Peters J. A., Lambert J. J., (1999) General anesthetic action at transmitter-gated inhibitory amino acid receptors. *Trends Pharmacol Sci.* 20, 496-502.

24. Eckenhoff R. G., Tanner J. W. (1998) Differential halothane binding and effects on serum albumin and myoglobin. *Biophys. J.* 75, 477-83.

25. Changeux J. P., Devillers T. A., Chemouilli P. (1984) Acetylcholine receptor: an allosteric protein. *Science* 225, 1335-1345.

26. Lechleiter J., Wells M., Gruener R. (1986) Halothane-induced changes in acetylcholine receptor channel kinetics are attenuated by cholesterol. *Biochim. Biophys. Acta* 856(3), 640-645.

27. Haupts U., Tittor J., Oesterhelt, D. (1999) Closing in on bacteriorhodopsin: progress in understanding the molecule. *Annu. Rev. Biophys. Biomol. Struct.* 28, 367-399.

28. Lanyi J. K. (1999) Progress toward an explicit mechanistic model for the light-driven pump, bacteriorhodopsin. *FEBS Lett.* 464, 103-7

29. Heberle J. (2000) Proton transfer reactions across bacteriorhodopsin and along the membrane. *Biochim. Biophys. Acta* 1458, 135-47

30. Stephen H. W., William C. W. (1999) Membrane protein folding and stability: physical principles. *Annu. Rev. Biophys. Biomol. Struct.* 28, 235-268.

31. Tajkhorshid E., Baudry J., Schulten K., Suhai. S. (2000) Molecular dynamics study of the nature and origin of the twisted structure of the retinal chromophore in bacteriorhodopsin. *Biophys. J.* 78, 683-693.

32. Pomerleau V., Harvey-Girard E., Boucher F. (1995) Lipid-protein interactions in the purple membrane: structural specificity within the hydrophobic domain. *Biochim. Biophys. Acta* 1234, 221-224.

33. Joshi M. K., Dracheva S., Mukhopadhyay A. K., Bose S., Hendler, R. W. (1998) Importance of specific native lipids in controlling the photocycle of bacteriorhodopsin. *Biochemistry* 37, 14463-70.

34. Barnett S. M., Dracheva S., Hendler R., Levin I. W. (1996) Lipid-induced conformational changes of an integral membrane protein: an infrared spectroscopic study of the effects of Triton X-100 treatment on the purple membrane of Halobacterium halobium ET1001. *Biochemistry* 35, 4558-4567.

35. Nishimura S., Mashimo T., Hiraki K., Hamanaka T., Kito Y., Yoshiya I. (1985) Volatile anesthetics cause conformational changes of bacteriorhodopsin in purple membrane. *biochim. Biophys. Acta* 818, 421-424.

36. Messaoudi S., Lee K-H., Beaulieu D., Baribeau J., Boucher F. (1992) Equilibria between multiple spectral forms of bacteriorhodopsin effect of delipidation, anesthetics and solvents on their pH dependence. *Biochim. Biophys. Acta* 1140, 45-52.

37. Uruga T., Hamanaka T., Kito Y., Uchida I., Nishimura S., Mashimo T. (1991) Effects of volatile anesthetics on bacteriorhodopsin in purple membrane, Halobacterium halobium cells and reconstituted vesicles. *Biophysical Chemistry.* 41, 157-168.

38. Oesterhelt D., Stoecknius W. (1971) Rhodopsin-like protein from the purple membrane of Halobacterium halobium. *Nature New Biol.* 233, 149-152.

39. Racker E., Stoeckenius W. (1974) Reconstitution of purple membrane vesicles catalyzing light-driven proton uptake and adenosine triphosphate formation. *J. Biol. Chem.* 249, 662-663.

40. Unwin P. N. T., Henderson R. (1975) Molecular structure determination by electron microscopy of unstained crystalline specimens. *J. Mol. Biol.* 94, 425-440.

41. Henderson R., Unwin P. N. T. (1975) Three-dimensional model of purple membrane obtained by electron microscopy. *Nature* 257, 28-32.

42. Pebay-Peyroula E., Rummel G., Rosenbusch J. P., Landau E. M. (1997) X-ray structure of bacteriorhodopsin at 2.5 angstroms from microcrystals grown in lipidic cubic phases. *Science* 277, 1676-1681.

43. Stoeckenius W., Bogomolni R. A. (1982) Bacteriorhodopsin and related pigments of halobacteria. *Annu. Rev. Biochem.* 51, 587-616.

44. Walker J. E., Carne A. F., Schmitt H. W. (1979) The topography of the purple membrane. *Nature* (London), 278, 653-654.

45. Grigorieff N., Ceska TA, Downing K. H., Baldwin J. M., Henderson R. (1996) Electron-crystallographic refinement of the structure of bacteriorhodopsin. *J. Mol. Biol.* 259, 393-421.

46. Kates M. (1988) Biological membranes: aberrations in the membrane structure & function. Karnovsky, M. L., Leaf, A., & Bolis, L. C., Eds. Alan R. Liss, Inc., New York, pp 357-384.

47. Kates M. (1993) Biology of halophilic bacteria, Part II. Membrane lipids of extreme halophiles: biosynthesis, function and evolutionary significance. *Experientia* 49, 1027-1036.

48. Kates M., Kushwaha S. C., Sprott G. D. (1982) Lipids of purple membrane from extreme Halophiles and methanogenic bacteria. *Methods Enzymol.* 88, 98-111.

49. Glaeser R. M., Jubb J. S., Henderson R. K^+ is conducted to the outside of the cell (1985) Structural comparison of native and deoxycholate-treated purple membrane. *Biophys. J.* 48, 775-780.

50. Edholm O., Berger O., Jahnig F. (1995) Structure and fluctuations of bacteriorhodopsin in the purple membrane: a molecular dynamics study. *J. Mol. Biol.* 250, 94-111.

51. Tsujimoto K., Yorimitsu S., Takahashi T., Ohashi M. (1989) Revised structure of a phospholipid obtained from Halobacterium halobium. *J. Chem. Soc., Chem. Commun.* 17, 668-670.

52. Taneva S. G., Petkanchin I. B., Todorov G., Stoylov S. P. (1992) Influence of cation binding on the electro-optically determined electric moments of purple membranes. *Adv. Colloid Interface Sci.* 23, 299-317.

53. Mukhopadhyay A. K., Dracheva S., Bose S., Hendler R. W. (1996) Control of the integral membrane proton pump, bacteriorhodopsin, by purple membrane lipids of Halobacterium halobium. *Biochemistry* 35, 9245-9252.

54. Joshi M. K., Dracheva S., Mukhopadhyay A. K., Bose S., Hendler R.W. (1998) Importance of specific native lipids in controlling the photocycle of bacteriorhodopsin. *Biochemistry* 37, 14463-70.

55. Lanyi J. (1999) Progress toward an explicit mechanistic model for the light-driven pump, bacteriorhodopsin. *FEBS Letters.* 464, 103-107.

56. Luecke H., Schobert B., Richter H. T., Cartailler J. P., Lanyi J. K. (1999) Structure of bacteriorhodopsin at 1.55 A resolution. *J. Mol. Biol.* 291, 899-911.

57. Hwang S. B., Korenbrot J. I., Stoeckenius W. (1977) Structural and spectroscopic characteristics of bacteriorhodopsin in air-water interface films. *J. Membr. Biol.* 36, 115-135.

58. Keszthelyi L. (1988) Primary charge motions and light-energy transduction in bacteriorhodopsin *Biophys. Chem.* 29, 127-136.

59. Dobler B. J., Zinth W., Kaiser W., Oesterheld D. (1988) Excited-state reaction dynamics of bacteriorhodopsin studied by femtosecond spectroscopy. *Chem. Phys. Lett.* 144, 215-220.

60. Groma G. J., Raksi F., Szabo G., Varo G. (1988) Picosecond and nanosecond components in bacteriorhodopsin light-induced electric response signal. *Biophys. J.* 54, 77-80.

61. Hofrichter J., Henry E. R., Lozier R. A. (1989) Photocycles of bacteriorhodopsin in light- and dark-adapted purple membrane studied by time-resolved absorption spectroscopy. *Biophys. J.* 56, 693-706.

62. Lozier R. H., Bogomolni R. A., Stoeckenius W. (1975) Bacteriorhodopsin: a light-driven proton pump in Halobacterium Halobium. *Biophys. J.* 15, 955-962.

63. Trissl H.W. Photoelectric measurements of purple membranes. (1990) *Photochem. Photobiol.* 51, 793-818.

64. Roepe P., Herzfeld J., Lugtenburg J., Rothschld K. Conformationally dependent chromophore/protein coupling in bacteriorhodopsin: typsine protonation state in BR_{570} BR_{548}, K_{630} and C_{610}. (1987) *Biophys. J.* 51, 134a.

65. Lanyi L. K. (1993) Proton translocation mechanism and energetics in the light-driven pump bacteriorhodopsin. *Biochim. Biophys. Acta* 1183, 241-261.

66. Balashov S. P., Ebrey T. G. (1994) Bacteriorhodopsin: molecular mechanisms of transmembrane proton transfer. *The Spectrum* 7, 1-9.

67. Mathies, R. A., Line, S. W., Ames J. B., Pollard W. T. (1991) From femtoseconds to biology: mechanism of bacteriorhodopsin's light-driven proton pump. *Annu. Rev. Biophys. Chem.* 20, 491-518.

68. Balashov S. P., Imasheva E. S., Govindjee R., Sheves M., Ebrey T. G. (1996) Evidence that aspartate-85 has a higher pK(a) in all-*trans* than in 13-*cis* bacteriorhodopsin. *Biophys. J.* 71, 1973-1984.

69. Richter H. T., Needleman R., Lanyi J. K. (1996) Perturbed interaction between residues 85 and 204 in Try-185→Phe and Asp-85→ Glu bacteriorhodopsin. *Biophys. J.* 71, 3392-3398.

70. Nagel G., Kelety B., Mockel B., Buldt G., and Bamberg E. (1998) Voltage dependence of proton pumping by bacteriorhodopsin is regulated by the voltage-sensitive ratio of M1 to M2. *Biophys. J.* 74, 403-412.

71. Subramaniam S., Lindahl M., Bullough P., Faruqi A. R., Tittor J., Oesterhelt D., Brown L., Lanyi J., Henderson R. (1999) Protein conformational changes in the bacteriorhodopsin photocycle. *J. Mol. Biol.* 87, 145-61.

72. Kamikubo H., Kataoka M., Varo G., Oka T., Tokunaga F., Needleman R., Lanyi J. K. (1996) Structure of the N intermediate of bacteriorhodopsin revealed by X-ray diffraction. *Proc. Natl. Acad. Sci. USA.* 93, 1386-90.

73. Han B. G., Vonck J., Glaeser R. M. (1994) The bacteriorhodopsin photocycle: direct structural study of two substrates of the M-intermediate. *Biophys. J.* 67(3), 1179-86.

74. Tavan P., Schulten K., Oesterhelt D. (1985) The effect of protonation and electrical interaction on the stereochemistry of retinal Schiff bases. *Biophys. J.* 47, 415-430.

75. Luecke H., Schobert B., Richter H. T., Cartailler J. P., Lanyi J. K. (1999) Structural changes in bacteriorhodopsin during ion transport at 2 angstrom resolution. *Science.* 286, 2552-2561.

76. Richter H. T., Needleman R., Kandori H., Maeda A., Lanyi J. K. (1996) Relationship of retinal configuration and internal proton transfer at the end of the bacteriorhodopsin photocycle. *Biochemistry* 35(48), 15461-6.

77. Kandori H., Yamazaki Y., Hatanaka M., Needleman R., Brown L. S., Richter H. T., Lanyi J. K., Maeda A. (1997) Time-resolved fourier transform infrared study of structural changes in the last steps of the photocycles of Glu-204 and Leu-93 mutants of bacteriorhodopsin. *Biochemistry* 36, 5134-41.

78. Royant A., Edman K., Ursby T., Pebay-Peyroula E., Landau E. M., Neutze R. (2000) Helix deformation is coupled to vectorial proton transport in the photocycle of bacteriorhodopsin. *Nature* 406, 645-648.

79. Kuhlbrandt W. (2000) Bacteriorhodopsin--the movie. *Nature* 406, 569-570.

80. Pande C., Callender R., Baribeau J., Boucher F., Pande A. (1989) Effect of lipid-protein interaction on the color of bacteriorhodopsin. *Biochim. Biophys. Acta* 973, 257-62.

81. Boucher F., Taneva S. G., Elouatik S., Dery M., Messaoudi S., Harvey-Girard E., Beaudoin N. (1996) Reversible inhibition of proton release activity and the anesthetic-induced acid-base equilibrium between the 480 and 570 nm forms of bacteriorhodopsin. *Biophys J.* 70, 948-61.

82. Henry N., Beaudoin N., Baribeau J., Boucher F. (1988) Further characterization of anesthetic-treated purple membranes. *Photochem. Photobiol.* 47, 85-90.

83. Baribeau J. (1987) Les interactions lipides-protéines dans la membrane pourpre : une approche analytique. *Thèse de doctorat,* Université du Québec à Trois-Rivières.

84. Ebrey T. G., Becher B., Mao B., Kilbride P., Honig B. (1977) Exciton interactions and chromophore orientation in the purple membrane. *J. Mol. Biol.* 112(3), 377-97.

85. Messaoudi S., Daigle I., Boucher F. (1993) Structural features underlying the anesthetic-induced equilibrium between three spectral species of bacteriorhodopsin: bR_{570}, bR_{480} and bR_{380}. *J. Mol. Struct.* 297, 19-27.

86. Shnyrov V. L., Mateo P. L. (1993) Thermal transitions in the purple membrane from Halobacterium halobium. *FEBS.* 324, 237-240.

87. Baribeau J., Boucher F. (1984) Isolation, purification and partial characterization of stable forms of monomeric bacteriorhodopsin in lauryl sucrose. *Can. J. Biochem. Cell Biol.* 63, 305-312.

88. Lewis A., Rousso I., Khachatryan E., Brodsky I., Lieberman K., Sheves M. (1996) Directly probing rapid membrane protein dynamics with an atomic force microscope: a study of light-induced conformational alterations in bacteriorhodopsin. *Biophys. J.* 70(5), 2380-2384.

89. Tamm L. K., Tatulian S. A. (1997) Infrared spectroscopy of protein and peptides in lipid bilayer. *Quarterly Reviews of Biophysics* 30, 365-429.

90. Bandekar J. (1992) Amide modes and protein conformation. *Biochem. Biophys. Acta* 1120, 123-143.

91. Krimm S., Bandekar J. (1986) Vibrational spectroscopy and conformation of peptides, polypeptides, and proteins. *Adv Protein Chem.* 38, 181-364.

92. Messaoudi S. (1991) Phénoménologie et aspect structural de l'équilibre entre quatre formes spectrales de la bactériorhodopsine tel qu'influencé par les anesthésiques et les solvants. *Mémoire de maîtrise,* Université du Québec à Trois-Rivières.

93. Viard M., Gallay J., Vincent M., Paternostre M. (2001) Origin of laurdan sensitivity to the vesicle-to-micelle transition of phospholipid-octylglucoside system: a time-resolved fluorescence study. *Biophys. J.* 80(1), 347-59.

94. Bagatolli L. A., Maggio B., Aguilar F., Sotomayor C. P., Fidelio G. D. (1997) Laurdan properties in glycosphingolipid-phospholipid mixtures: a comparative fluorescence and calorimetric study. *Biochim. Biophys. Acta* 1325(1), 80-90.

95. Zeng J., Chong P. L. (1995) Effect of ethanol-induced lipid interdigitation on the membrane solubility of Prodan, Acdan, and Laurdan. *Biophys. J.* 68(2), 567-73.

96. Paternostre M., Meyer O., Grabielle-Madelmont C., Lesieur S., Ghanam M., Ollivon M. (1995) Partition coefficient of a surfactant between aggregates and solution: application to the micelle-vesicle transition of egg phosphatidylcholine and octyl beta-D-glucopyranoside. *Biophys. J.* 69(6):2476-88.

97. Brouillette C. G., Muccio D. D., Finney T. K. (1987) pH dependence of bacteriorhodopsin thermal unfolding. *Biochemistry* 26(23), 7431-7438.

98. Muller D. J., Schabert F. A., Buldt G., Engel A. (1995) Imaging purple membranes in aqueous solutions at sub-nanometer resolution by atomic force microscopy. *Biophys. J.* 68, 1681-1686.

99. Cladera J., Sabes M. And Padros E. (1992) Fourier transfrom infrared analysis of bacteriorhodopsin secondary structure. *Biochemistry* 31, 12363-12368.

100. Downer N. W., Bruchman T. J., Hazzard J. H. (1986) Infrared spectroscopic study of photoreceptor membrane and purple membrane. Protein secondary structure and hydrogen deuterium exchange. *J. Biol. Chem.* 261(8), 3640-7.

101. Earnest T. N., Roepe P., Braiman M. S., Gillespie J., Rothschild K. J. (1986) Orientation of the bacteriorhodopsin chromophore probed by polarized Fourier transform infrared difference spectroscopy. *Biochemistry* 25, 7793-8.

102. Earnest T. N., Herzfeld J., Rothschild K. J. (1990) Polarized Fourier transform infrared spectroscopy of bacteriorhodopsin. Transmembrane alpha helices are resistant to hydrogen/deuterium exchange. *Biophys. J.* 58(6), 1539-1546.

103. Taneva S. G., Caaveiro J. M. M., Muga A., Goni F. M. (1995) A pathway for the thermal destabilization of bacteriorhodopsin. *FEBS Lett.* 367:297-300

104. Kluge T., Olejnik J., Smilowitz L., Rothschild K. J. (1998) Conformational changes in the core structure of bacteriorhodopsin. *Biochemistry* 37(28):10279-85.

105. Cantor R. S. (1999) Lipid composition and the lateral pressure profile in bilayers. *Biophys. J.* 76, 2625–2639.

106. Eckenhoff R. G. (1996) An inhalational anesthetic binding domain in the nicotinic acetylcholine receptor. *Proc. Natl. Acad. Sci. USA.* 93, 2807-2810.

107. North C., Cafiso D. S. (1997) Contrasting membrane localization and behavior of halogenated cyclobutanes that follow or violate the Meyer-Overton hypothesis of general anesthetic potency. *Biophy. J.* 72, 1754-1761.

108. Xu Y., Tang P. (1997) Amphiphilic sites for general anesthetic action? Evidence from ^{129}Xe-^{1}H intermolecular nuclear overhauser effects. *Biochim. Biophys. Acta* 1323, 154-162.

109. Chiou J. S., Krishna P. R., Kamaya H., Veda I. (1992) Alcohols dehydrate lipid membranes: an infrared study on hydrogen bonding. *Biochim. Biophys. Acta* 1110(2), 225-33.

110. Krebs M. P. and Isenbarger T. A. (2000) Structural determinants of purple membrane assembly. *Biochim. Biophys. Acta* 1460,15-26.

111. Moller C., Buldt G., Dencher N. A., Engel A. and Muller D.J. (2000) Reversible loss of crystallinity on photobleaching purple membrane in the presence of hydroxylamine. *J. Mol. Biol.* 301(4):869-79.

112. White S. H. and Wimley W. C. (1999). Membrane protein folding and stability: physical principles. *Annu. Rev, Biophys. Biomol. Struct.* 28, 319-365.